www.coinweb.no

SINTEF Building and Infrastructure Øyvind Bjøntegaard (Norwegian Public Roads Administration)

Basis for and practical approaches to stress calculations and crack risk estimation in hardening concrete structures – State of the art

COIN Project report 31 – 2011

SINTEF Building and Infrastructure

Øyvind Bjøntegaard (Norwegian Public Roads Administration)

Basis for and practical approaches to stress calculations and crack risk estimation in hardening concrete structures – State of the art

FA 3 Technical performance

SP 3.1 Crack free concrete structures

COIN Project report 31 – 2011

COIN Project report no 31
Øyvind Bjøntegaard (Norwegian Public Roads Administration)
Basis for and practical approaches to stress calculations and crack risk estimation in hardening concrete structures
– State of the art
FA 3 Technical performance
SP 3.1 Crack free concrete structures

Keywords:
Hardening phase, curing technology, stress simulations, crack-risk assessment

Photo, cover: The Norwegian Public Roads Administration (Statens vegvesen)

Project no.: 3D005930

ISSN 1891–1978 (online)
ISBN 978-82-536-1236-2(pdf)
ISBN 978-82-536-1237-9 (printed)

Address: Forskningsveien 3 B
POBox 124 Blindern
N-0314 OSLO
Tel: +47 22 96 55 55
Fax: +47 22 69 94 38 and 22 96 55 08

www.sintef.no/byggforsk
www.coinweb.no

Cooperation partners / Consortium Concrete Innovation Centre (COIN)

Aker Solutions
Contact: Jan-Diederik Advocaat
Email: jan-diederik.advocaat@akersolutions.com
Tel: +47 67595050

Saint Gobain Weber
Contact: Geir Norden
Email: geir.norden@saint-gobain.com
Tel: +47 22887700

Norcem AS
Contact: Terje Rønning
Email: terje.ronning@norcem.no
Tel: +47 35572000

NTNU
Contact: Terje Kanstad
Email: terje.kanstad@ntnu.no
Tel: +47 73594700

Rescon Mapei AS
Contact: Trond Hagerud
Email: trond.hagerud@resconmapei.no
Tel: +47 69972000

SINTEF Building and Infrastructure
Contact: Tor Arne Hammer
Email: tor.hammer@sintef.no
Tel: +47 73596856

Skanska Norge AS
Contact: Sverre Smeplass
Email: sverre.smeplass@skanska.no
Tel: +47 40013660

Spenncon AS
Contact: Ingrid Dahl Hovland
Email: ingrid.dahl.hovland@spenncon.no
Tel: +47 67573900

Norwegian Public Roads Administration
Contact: Kjersti K. Dunham
Email: kjersti.kvalheim.dunham@vegvesen.no
Tel: +47 22073940

Unicon AS
Contact: Stein Tosterud
Email: stto@unicon.no
Tel: +47 22309035

Veidekke Entreprenør ASA
Contact: Christine Hauck
Email: christine.hauck@veidekke.no
Tel: +47 21055000

Preface

This study has been carried out within COIN - Concrete Innovation Centre - one of presently 14 Centres for Research based Innovation (CRI), which is an initiative by the Research Council of Norway. The main objective for the CRIs is to enhance the capability of the business sector to innovate by focusing on long-term research based on forging close alliances between research-intensive enterprises and prominent research groups.

The vision of COIN is creation of more attractive concrete buildings and constructions. Attractiveness implies aesthetics, functionality, sustainability, energy efficiency, indoor climate, industrialized construction, improved work environment, and cost efficiency during the whole service life. The primary goal is to fulfil this vision by bringing the development a major leap forward by more fundamental understanding of the mechanisms in order to develop advanced materials, efficient construction techniques and new design concepts combined with more environmentally friendly material production.

The corporate partners are leading multinational companies in the cement and building industry and the aim of COIN is to increase their value creation and strengthen their research activities in Norway. Our over-all ambition is to establish COIN as the display window for concrete innovation in Europe.

About 25 researchers from SINTEF (host), the Norwegian University of Science and Technology - NTNU (research partner) and industry partners, 15 - 20 PhD-students, 5 - 10 MSc-students every year and a number of international guest researchers, work on presently 5 projects:

- Advanced cementing materials and admixtures
- Improved construction techniques
- Innovative construction concepts
- Operational service life design
- Energy efficiency and comfort of concrete structures

COIN has presently a budget of NOK 200 mill over 8 years (from 2007), and is financed by the Research Council of Norway (approx. 40 %), industrial partners (approx 45 %) and by SINTEF Building and Infrastructure and NTNU (in all approx 15 %).

For more information, see www.coinweb.no

Tor Arne Hammer
Centre Manager

Summary

Temperature- and stress simulation programs are used to calculate the cracking tendency of hardening concrete structures. If cracking is likely to occur, the simulations can be used to find the necessary countermeasures to avoid cracking. The subject area is often denoted stress-based curing technology, or advanced curing technology. The "technology" can also be used in the production planning with regard to for more traditional curing technology considerations, such as how to avoid freezing of fresh concrete, determination of temperature gradients, earliest time of form removal, earliest time of post-tensioning, etc.

The report is an introduction to the understanding of advanced curing technology. The governing properties and mechanisms behind stress development and cracking tendency of hardening concrete structures are dealt with, and illustrated by experimental examples.

Propositions on how to approach simulations with experiments and data implementation are presented, showing materials models and strategies that reflects Norwegian traditions. The presented approaches should however have rather general validity since the choice of a given materials model is often of secondary importance as long as good experimental data is available. Simplified calculation methods are presented to illustrate the interplay between the different concrete properties. Simulation programs based on the finite-elements method are discussed briefly. The main scope here is to give a basis for the understanding of such programs.

The content is based on experience and knowledge from various national and international projects (with Norwegian participation) during the last two decades, in addition to a more general literature study.

Acknowledgements

The proof reading of the report, pieces of advice and comments by Erik J. Sellevold are greatly appreciated. Appreciated is also the contribution from Steinar Helland on chapter 2, and for the pictures in chapter 1.

Table of contents

PREFACE 3

SUMMARY 4

TABLE OF CONTENTS 5

1 INTRODUCTION 7

2 CURING TECHNOLOGY - HISTORICAL REVIEW 9

2.1 DAMS 9
2.2 EXTERNAL RESTRAINT AND STRESS-MEASUREMENTS 10
2.3 STRUCTURAL BEHAVIOUR 12
2.4 COMPUTER-BASED CURING TECHNOLOGY 13
2.5 THERMAL DILATION AND AUTOGENOUS SHRINKAGE 15
2.6 CONFERENCES AND RESEARCH PROJECTS 16
2.7 NORWEGIAN DEVELOPMENTS 17

3 THE HARDENING PHASE AND DEFINITION OF T_0 21

4 INTERNAL AND EXTERNAL RESTRAINT 23

5 STRESS DEVELOPMENT AND "CRACK INDEX" 28

6 MATURITY TIME – THE "STATE PARAMETER" 30

7 THE DRIVING FORCES TO STRESS GENERATION 33

7.1 GENERAL 33
7.2 AUTOGENOUS SHRINKAGE 33
7.3 HYDRATION HEAT AND THERMAL DILATION 35
7.4 THERMAL DILATION AND AUTOGENOUS SHRINKAGE IN STRUCTURES 41

8 CONCRETE PROPERTIES INPUT DATA FOR SIMULATIONS 49

8.1 GENERAL 49
8.2 HYDRATION HEAT 49
8.3 COEFFICIENT OF THERMAL EXPANSION 51
8.4 AUTOGENOUS SHRINKAGE 51
8.5 COMPRESSIVE STRENGTH, TENSILE STRENGTH AND E-MODULUS 51
8.6 UNIAXIAL TENSILE STRENGTH VERSUS SPLITTING STRENGTH 54
8.7 CREEP 55

9 SIMULATION PROGRAMS AND INPUT 57

9.1 SIMULATION PROGRAMS 57
9.2 INPUT DATA FOR 2D AND 3D PROGRAMS, BRIEF OVERVIEW 58

10 SIMPLIFIED SIMULATION METHODS 61

10.1 GENERAL 61
10.2 HAND METHOD – AGE ADJUSTED EFFECTIVE E-MODULUS (AEM) METHOD 61
10.3 HAND METHOD (AEM), CALCULATION EXAMPLE 64
10.4 THREE-STEP ENGINEERING METHOD 67
10.5 THREE-STEP ENGINEERING METHOD, CALCULATION EXAMPLE 69

11 EXAMPLE OF A 2D CALCULATION 74

12 VARIABILITY AND CRACK RISK CRITERIA 75

13 EFFECT OF REINFORCEMENT 79

14 IMPORTANCE OF INPUT PARAMETERS 80

15 MINIMUM TEST PROGRAM AND SIMULATION STRATEGY 81

15.1 MINIMUM TEST PROGRAM 81
15.2 SIMULATION STRATEGY 83

REFERENCES 84

List of appendices

APPENDIX 1 Thermal Dilation-Autogenous Shrinkage: How to separate? 91
APPENDIX 2 CTE of Cem. Paste and Concrete: Mechanisms of Moisture Interaction 105
APPENDIX 3 Verification of three different calculation methods for early age concrete. 113
APPENDIX 4 The Nor-Crack project: Project information, results and materials data base 125
APPENDIX 5 Complete list of IPACS-reports 135

1 Introduction

Concrete is a strong, robust construction material and it is one of the most used building materials to day on a worldwide basis. Reinforced concrete has many favourable properties as a building material: structural properties, durability, fire-resistance, energy-carrying capacity (indoor climate), forming properties and aesthetics. It has also a competitive price and it often involves local suppliers.

The volume instability of concrete is however an unfavourable "property", and the volume instability is particularly active during the hardening phase. This may cause cracks where water (and frost) and aggressive ions may penetrate, leading to functionality-, durability- and esthetical problems. In addition, hardening phase cracking often sadly cause costly repair of newly built concrete structures. And, not infrequently, cracking is a source of dispute in building projects. Figure 1 shows two illustrative pictures of through-cracks in walls that have developed during the hardening phase.

The volume instability and cracking tendency is magnified in massive structures built with high concrete qualities (low w/b-ratios, high cement contents), and it is caused by temperature- and autogenous shrinkage effects. This type of cracking is often denoted "thermal cracking". The effect of drying shrinkage is normally not considered in this context, since the concrete is often covered by formwork etc and the fact that drying shrinkage is a surface effect with minor significance in massive concrete structures.

The main focus here is on the materials behaviour resulting in stresses in hardening concrete structures due to external restraint from adjoining structural parts (due to casting joints). When cracking occur the result of external restraint is often large "through-cracks", with variable width, which go through the entire thickness of the structure. Smaller cracks may be clogged over time due to "self-healing" mechanisms (for instance due to precipitation of calcite), while wider cracks may represent a permanent problem.

Pre-calculations of stresses for hardening concrete structures are performed to minimize/avoid cracking in the sense that they state the required mix design or countermeasures on-site (or the combination of the two) to achieve this for relevant field conditions. Prior to calculations the relevant (transient) concrete properties must be measured and expressed by the models that are used by the given simulation program.

The report intends to give a basic understanding of hardening phase cracking tendency of concrete (commonly denoted "thermal cracking"). The report gives the state-of-the-art understanding of the basic mechanisms and their interplay. Experimental examples are given. The principles of structural behaviour are discussed as well as the main principles of "modern curing technology", i.e. stress calculations and crack risk evaluation. A historical review of the subject area is given first.

The emphasis is on the understanding of the topic and not particularly on the influence of mix design and part materials. Plastic shrinkage cracking in fresh concrete is a different, though related, area which is not dealt with either.

The appendices of the report (articles, papers) are given as an orientation/taste of Norwegian work and projects (from mid 1990's) with Norwegian participation. The last appendix is a list of reports from the large European project IPACS (1997-2001), also with Norwegian participation. All to make possible an easy start of own literature studies on the topic.

Literature references are generally given in brackets [ ], but in the literature review in Chapter 2 references are also specified with author's name and publication year.

(a)

(b)

Figure 1 Examples of through-cracking in walls due to external restraint. Note that Figure (a) shows two restraint cases; first the main wall was cast on the base, then the shorter top wall was cast on the main wall; both situations gave through-cracking in this case.

Photos: Steinar Helland, Skanska Norge AS

2 Curing technology - historical review

The following literature review was carried out to set the present state of knowledge in a historical perspective. The gradually increasing understanding of the "driving forces" to cracking and the simultaneous structural behaviour, as well as "crack control" may serve as keywords. The scope has been to present central milestones from the international scene, as well as in Norway and within the Nordic countries.

2.1 Dams

Challenges with regard to cracking of hardening concrete structures caused by hydration heat have been recognized for a long time; probably as long as the "history of concrete". During building of massive dams this was particularly noticed in the early days. The building of dams in Norway started around 1900. The state of a large number of these dams was evaluated by the Norwegian Engineering Association (Den Norske Ingeniørforening) in 1930 [1]. Here drying shrinkage and internal temperature differences were judged to be some of several harmful mechanisms (frost was naturally also one of them) in the way that surface cracks were formed, representing openings for water. Reportedly, some "internal shrinkage cracks" was also observed, but no explanation on the mechanism behind was given.

With regard to strategies for limitation of thermal cracking, an embedded cooling pipe system was introduced during the construction of the Hoover (Boulder) Dam (between Arizona and Nevada) in the early 1930ies [3]. In addition the dam was built in a sequential manner to allow more heat to escape during building, as well as with contraction joints. The dam is 220 m high and 379 m long, the bottom thickness is 200 m and the top thickness 15 m, totally 3.3 million m^3 concrete was used [4], see Figure 2.

Figure 2 Hoover Dam from the air [4]

It appears that the main motive for using cooling pipes was to lower the maximum temperatures and to shorten the entire cooling period, and in this way to shorten the period with possible harmful temperature differences. In the Hoover Dam more than 900 km of cooling pipes were used, and, for long-term monitoring, around 400 thermometers were embedded. Blanks et al. [2] reported in 1938 that most US dams built up till then developed cracking to a smaller or larger extent, but claimed that the cooling pipe system in the Hoover dam contributed positively to reduce the extent of

cracking. However, in an examination of data from the Hoover dam by Abrams [3], 12 years after the construction, it was concluded that: "*The low-heat-cement-embedded-pipe-system was ineffective (...) and accomplished neither what it was designed for nor what has since been claimed*". We do not pursue that discussion here, but merely note that the curing technology was maybe not mature from the beginning; which then perhaps should not be a surprise for a virgin technology applied in an enormous building project.

The main concern in those days was the temperature differences (i.e. internal restraint) occurring in massive concrete structures and the cracking resulting from it [3][5][6][7], but awareness of external restraint and the complex nature of the cracking problem was growing. Common countermeasures were use of low-heat cements and contraction joints. Estimations of temperature development were possible with the use of analytical or graphic solutions of the fundamental differential equations of heat transfer [7][8].

2.2 External restraint and stress-measurements

The fact that hardening concrete structures are subjected to external restraint -from the base or from adjoining structures- was also recognized in the 1930ies [5][9][10][11]. For both massive structures and medium massive structures there was a growing understanding that this type of restraint could produce "through-cracks". Similarly, drying shrinkage was considered less important for such cracking, since it is a surface effect. Simplified restraint stress calculations assuming full (100%) restraint was performed. And, there was a belief that reinforcement could be used for crack-width control, but not to influence the probability of cracks.

Laboratory tests on 100% restraint specimens subjected to site-realistic temperature histories were reportedly performed in the US as early as in 1937 by Davis et al. [10]. From the results achieved by Davis et al. in Figure 3, and parallel tests, it was concluded that the stress on heating was around half (50%) of what could be expected from the concrete's E-modulus and that this was due to creep (or "plastic flow" as denoted by the authors). On cooling the creep effect was found to be around 30%. These are numbers that are quite in line with figures of today. As we see from Figure 3, the specimen failed in tension during cooling. Unfortunately, the authors did not provide a sketch of the experimental set-up. However, already the year after, Blanks et al. (1938) [2] reported results from similar tests where they also showed the equipment. Cast concrete cylinders equipped with an embedded strain meter were put in a frame, as shown in Figure 4, and the set-up was placed in a temperature-controlled room following a temperature cycle relevant for dams. The length change of the cylinder was balanced manually by applying a gradually load. One frame was used for the compression period and another for the later tension period. The test cylinder was moved from the first to the second frame during the test.

The same year (1938) Carlson [5] stated that: "*The computation of stresses due to complete restraint is merely an economical method of extending test results. It would be better to measure in the laboratory the actual stress required to maintain a specimen at constant length while it is subjected to the temperature changes in question*". In those days it was acknowledged that structures are in fact subjected to less than 100% restraint, but they were not able to quantify the restraint.

The early stress-measurements from the 1930ties discussed above must then be considered to be the forerunner of the much later and more well-known developments in München, Germany, on restraint concrete beams subjected to site-realistic temperature histories: The "Cracking Frame" (high, but unknown restraint, insulated specimen) made in 1971 by Springenschmid et al. [12][13] (see Figure 5), and the improved "Temperature-Stress Testing Machine (TSTM)" by Springenschmid et al. in 1984 [16][17] which was temperature- and deformation-controlled giving 100% restraint conditions (see Figure 7). In the following years, until the present, dozens of TSTMs have been made worldwide. It is notable that deformation-controlled restraint stress set-ups were developed already in the 1970ies by both Orr et al. in 1971 [14] and by Paillére et al. in 1976

[15] (see Figure 6), but these rigs were primarily designed to study the effect of drying shrinkage on cement paste and mortar specimens, and not to study the effects of temperature. For more on stress-measurements in hardening concrete, see review by Mangold (1994) [18].

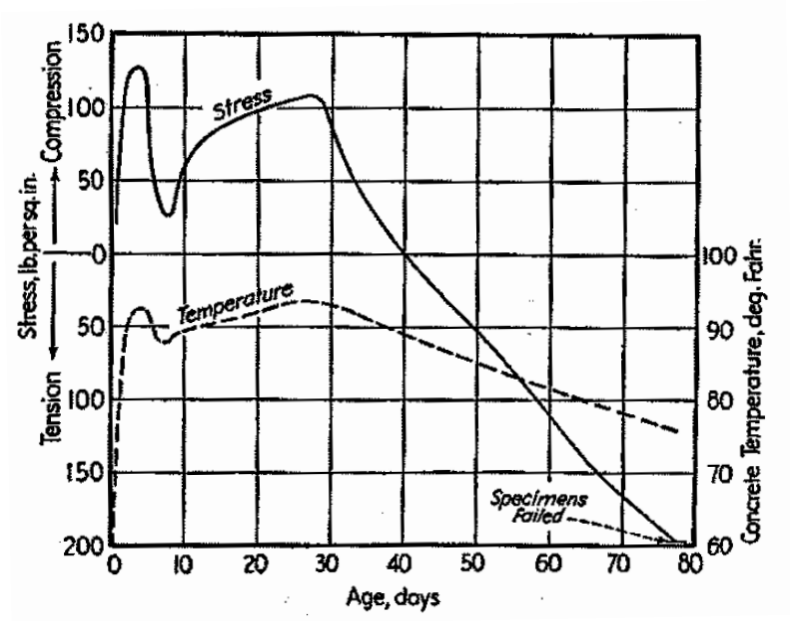

Figure 3 Stress required maintaining a constant length – mass cured concrete. Davis et al. 1937[10]

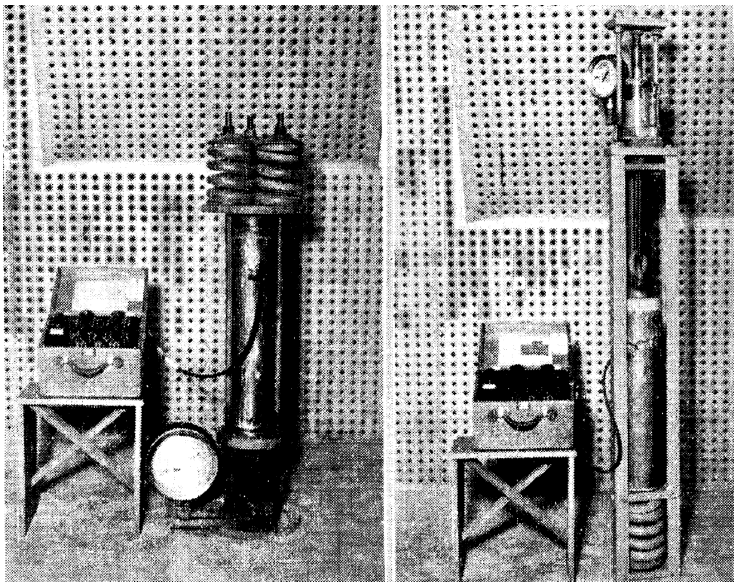

Figure 4 Equipment designed to measure restraint stress in dam-concretes. Left: compressive rig for the first (heating) period with compressive stresses. Right: tension rig for the later (cooling) period with tensile stresses. Blanks et al. [2], 1938.

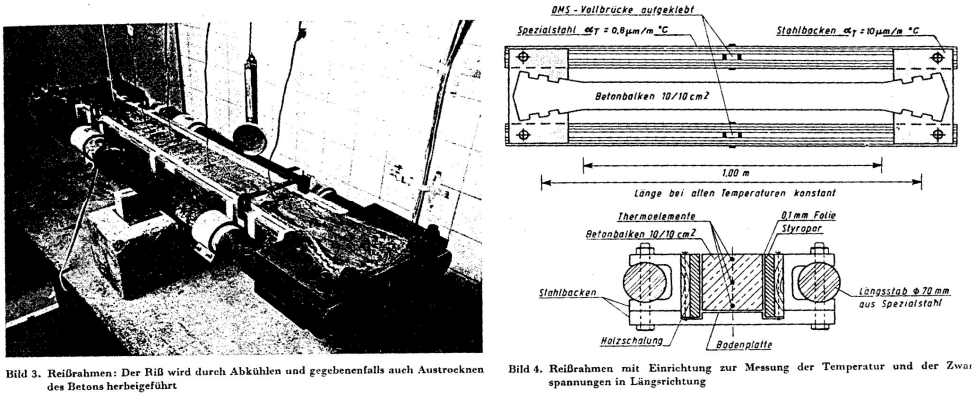

Bild 3. Reißrahmen: Der Riß wird durch Abkühlen und gegebenenfalls auch Austrocknen des Betons herbeigeführt

Bild 4. Reißrahmen mit Einrichtung zur Messung der Temperatur und der Zwangspannungen in Längsrichtung

Figure 5 "The Cracking frame", 1969: Concrete beam restraint from a stiff frame, to study thermal cracking. Around 80% restraint. Springenschmid [12][13]

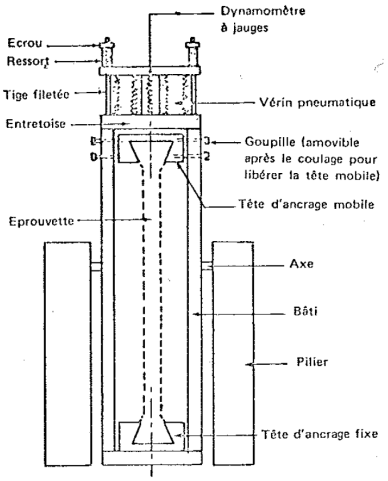

Figure 6 "Linear test bench", 1976: Cement paste and mortar beam, to study drying shrinkage cracking. 100% restraint, air-pressure controlled moveable cross-head, Paillére et al. [15]

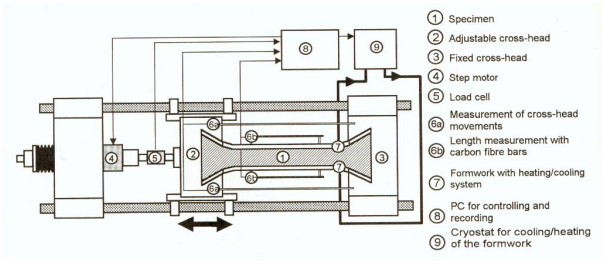

Figure 7 "The Temperature-Stress Testing Machine" (TSTM), 1984: Temperature-controlled concrete beam, to study thermal cracking. 100% restraint, electrical step motor-controlled moveable cross-head. Springenschmid et al. [16][17]

2.3 Structural behaviour

In 1944 Nylander [19] did some elegant optical experiments with 10 mm thick "isolon"-sheets, see Figure 8. A small rectangular isolon sheet (illustrating a wall) was fixed on top of a larger (and restrained) isolon sheet (illustrating a stiff base). By a heating-cooling treatment longitudinal thermal stresses was visualised as buckling of the sheets. From these tests Reinius [20] did in 1945 assumptions on the distribution of stresses for wall-structures subjected to one-sided restraint, and also on how stresses in a wall are affected by its length/height (L/H) ratio as well as by the stiffness of the base. Reinius also discussed the influence of the placing of dilation joints and the existence of cracks in horizontal joints (slip failure) due to bending forces.

During the following decades, into the 1970 ties, there was continuous progress in the research and understanding of the influence of the early mechanical and visco-elastic behaviour of concrete, as well as the structural response during external restraint conditions [13][19][20][21][22][23] [24][25].

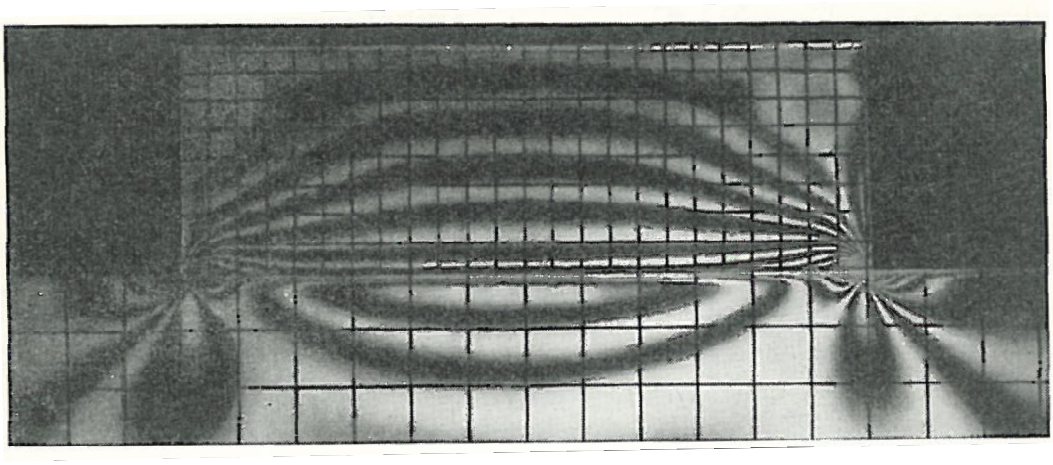

Figure 8 Optical experiment. Buckling of 10 mm isolon sheets due to thermal contraction of the small upper sheet relative to the larger bottom sheet. Nylander 1944 [19]

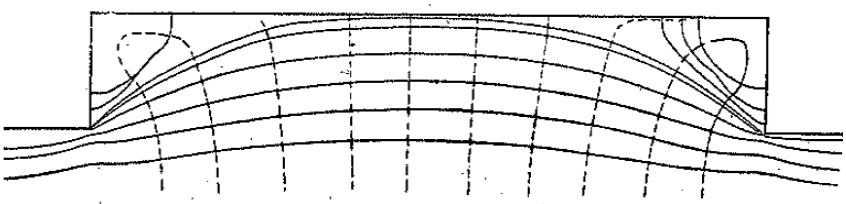

Figure 9 Deduced principal stress lines for a rectangular sheet (with length/height-ratio=6) fixed to an elastic base. Reinius 1945 [20]

2.4 Computer-based curing technology

Curing technology is today based on a "state parameter", and the use of the maturity concept is common in this regard. In 1951 Saul [26] introduced the expression "maturity" and defined it as: "*Concrete having a given composition will at a given maturity have the same strength independent of the time-temperature history that results in that maturity*". Long before this the temperature effects on strength had been known, and various attempts to develop general models for the temperature effect on strength had been made. In this development the work of Saul was a step on the way. Until the 1980ies the approaches to handle restraint conditions and cracking issues, including the visco-elastic behaviour of concrete, was primarily based on measured temperatures or estimations of temperature/temperature differences. Graphic solutions and hand-calulations were predominant.

When it comes to computerized curing technology significant contributions were made by Freiesleben Hansen (Bkf-centralen, Denmark). By 1975 he had systematized the knowledge of the time and developed a computer-based software system denoted the "Maturity Computer". The software treated one-dimensional (1D) heat flow problems, including a refined maturity concept that was based on basic theory of thermal activated processes (Arrhenius), and rough estimations on crack sensitivity were done by comparing the temperature differences/strains over the cross-section with the tensile strain capacity of concrete [27][28][29][30][31][32]. The computer-based system was portable and could be used at e.g. building sites for curing control (i.e. estimation of temperature, maturity and mechanical property development). It was claimed that this system "*brought the concrete technology to an international level on its field*" [33]. The Maturity Computer was the pioneer version of the following release of the commercially available (1D) curing technology program CIMS. Later it was upgraded (1992) to handle 2D in CIMS2D; also

including a stress (and strain) calculation module (i.e. a stress-based curing technology program), then renamed, to the present name, 4C-Temp&Stress (Danish Technological Institute).

During the winter 1978-79 the Danish Building Research Institute did some practical in-situ tests on walls to observe what temperature differences are critical for cracking after form removal (i.e. internal restraint), see Figure 10. The conclusion from these particular tests was that temperature differences over the cross section higher than around 20 ^{o}C were critical with regard to surface cracking. It is notable that the results were picked up by, among others, the Norwegian Public Roads Administration and, thus, forms the basis for requirements that are valid even today.

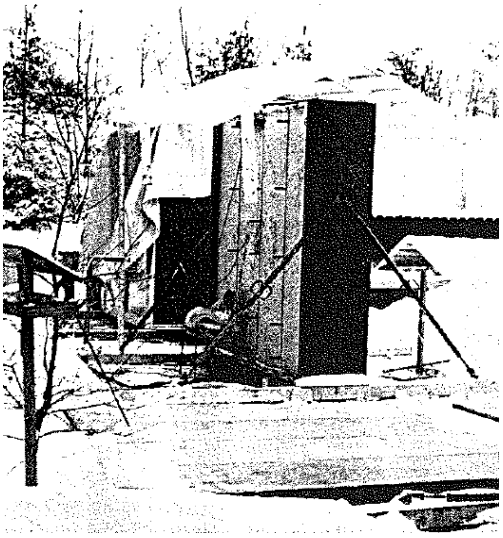

Væggene umiddelbart efter afformning, hvor afkølingen af betonoverfladen er årsag til temperaturbelastningen over tværsnittet. I afkølingsperioden kunne fremkomst og udvikling af revner iagttages. Bemærkelsesværdigt var især, at de konstaterede revner ikke kunne ses på overfladen, når der var opnået temperaturligevægt i tværsnittet.

Figure 10 Tests on critical temperature differences over the cross-section of walls (internal restraint) after form removal at winter conditions. Freiesleben Hansen and Pedersen (1982) [31]

When it comes to programming, parallel developments were achieved in Sweden from late 1970ies when the computer-based curing technology program HETT was released from CBI [34][35]. The program was made by Jonasson, under the leadership of Bergström. Increased understanding of materials behaviour internationally (especially by Bazant on creep), and further developments by Jonasson, Bernander and Emborg at Luleå Univ. of Tech. on materials testing/modelling and computer programs through the 1980ies resulted among others in the dr.thesis by Emborg [36] in 1989 which applied stepwise finite-element stress analyses by sub-dividing hardening concrete structures into discrete laminar element layers involving an integral-type creep law. Later, around 1995, the stress-based curing technology program ConTeSt was released by Jonasson. The program has been upgraded several times up till today. Note that the "Norwegian" program CrackTeSt-COIN, which will be introduced in 2012, is an adjusted version of ConTeSt.

It is no doubt that the achievements discussed above on computer-based hardening phase simulations in the 1970-80ies were pioneering work on the international scene. However, to limit the volume of this literature review the developments in the same period elsewhere are not dealt with, for instance the developments elsewhere in Europe (especially Germany), USA and Asia. Through the 1990ies several computer programs saw the light of day internationally, and numerous stress-based 2D (and some 3D) curing technology programs exist on the market today, some of them are dealt with in Ch.9.

Provided that we have relevant materials data for the concrete in question, the uncertainty of stress calculations and crack risk assessments is probably today mainly a result of the fact that building sites, ready-mixed concrete and the cracking tendency itself have "stochastic nature" which inherently leads to some uncertainty. Hence, the limitation of crack risk assessments is probably

not the computer programs and their given materials models, but merely our ability to measure and implement the relevant concrete materials data, as well as to implement relevant on-site conditions. See Ch.12 for more on this topic.

2.5 Thermal dilation and autogenous shrinkage

Among the relevant materials data are indeed the driving forces to hardening phase cracking: Thermal dilation and autogenous shrinkage. The two types of "deformations" work together, giving the total volume instability of hardening concrete. Since thermal effects are obviously important, hydration heat and the coefficient of thermal expansion of cement paste and concrete has "always" been subjects of interest, see literature review for instance in [93], and Section 7.3 in this report.

Autogenous shrinkage may be denoted as a "joker" in this regard; it is less important than thermal effects in most cases/concretes, but can be very significant in others, and its interdependence with thermal effects is complex. The fact that (isothermal) cement hydration is associated with a volume loss was shown as early as in 1900 by Le Chatelier [37]. Since then this volume loss has been denoted Le Chatelier shrinkage or chemical shrinkage, and it is easily measured as the water suction from cement paste cast in a graduated flask with water on top. As hydration proceeds the water that is sucked into the cement paste can be monitored, see Figure 11.

This (internal) chemical shrinkage is believed to be the main contributor to (self-desiccation and) autogenous shrinkage in concrete (see Ch.7.2). Autogenous shrinkage is sometimes denoted "external" or "bulk" chemical shrinkage", or "self-desiccation shrinkage" to link it directly to the mechanism assumed to be the predominant. The existence of autogenous shrinkage, which then is the external (dimensional/bulk) component of chemical shrinkage, was discovered at least as early as in 1934 when Lynham [39] stated: "*In a conservative system, in which water neither entered nor left a mass of concrete, and neglecting thermal effects, the concrete would shrink continuously till all the cement was hydrated, all the water was used up, or all movement of water rendered impossible.(...)It is convenient to refer to this type of shrinkage as 'autogenous shrinkage' to distinguish it from others which are due to thermal causes or to loss of moisture to the air*". Based on the status at that time he stated further that there was: "*(..)a lack of differentiation between autogenous shrinkage, thermal effects, and induced movements due to alterations in moisture*". Davis [40] goes in 1940 deep into the mechanisms governing autogenous shrinkage and its practical consequences, see example of test result in Figure 12. He also discussed expansive mechanisms that are: "*autogenous in character*". Hence, "autogenous strains" are commonly shrinkage, but can sometimes occur as a swelling. The swelling mechanism(s) is not entirely understood, even today (but for instance early etringite formation has been proposed as one possible mechanism). In 1942 Swayze [41] gave an insightful discussion on similar matters.

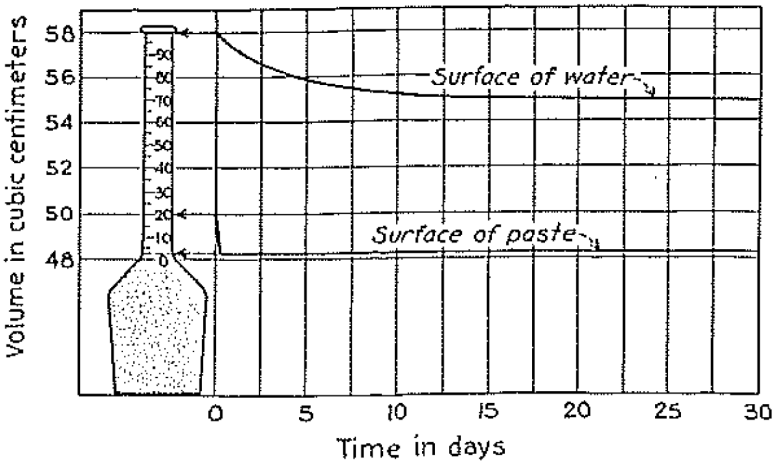

Figure 11 Behaviour of neat cement paste while hardening under water. Powers 1935 [38]

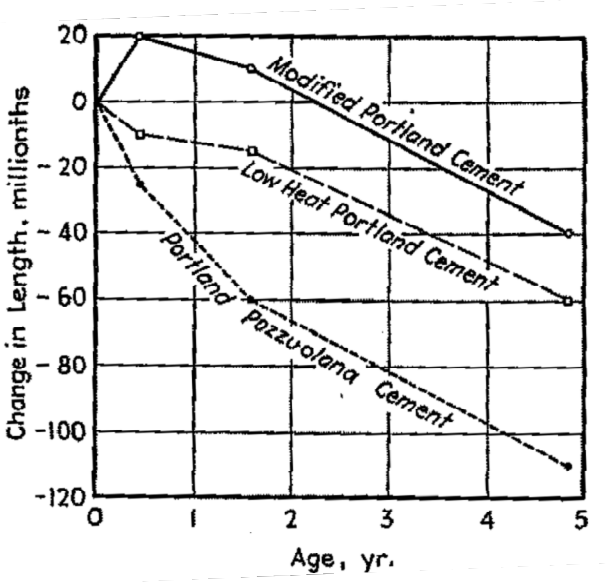

Figure 12 Long-term autogenous shrinkage of 10x10x100 mm sealed concrete bars. Negative strain is shrinkage. Davis 1940 [40]

In connection with the design of the Dworshak Dam, Ohio, USA, the presence of autogenous shrinkage was taken very seriously. Autogenous shrinkage was tested on various concretes, and the effect of pozzolan addition, cement content, cement fineness and temperature were reported by Houk et al. in 1969 [42]. The authors stated that: "*(..) Therefore, the development of concrete mixtures having satisfactory strength, autogenous shrinkage, and low temperature rise properties was an important design consideration for a structure such as the Dworshak Dam*".

When it comes to the existence of autogenous shrinkage and its contribution in creating restraint stresses and cracking of hardening concrete structures, it is clear that the developments discussed above from the US were in the forefront. In Europe autogenous shrinkage seems to be either unknown or ignored for many decades, and it appears to be not before around 1980 that European researchers made serious notice to the phenomenon, see Paris conference in 1982 [43]. However, after this, and especially from around 1990, the interest in autogenous shrinkage, and the whole topic of stress-based curing technology as such, has been extensive worldwide.

2.6 Conferences and research projects

During the last decades, the increased use of high strength concrete structures led to increased interest worldwide on early age cracking problems. High strength concrete normally contains more binder producing more heat during hydration, and the low w/b-ratios imply finer pore structure resulting in strong self-desiccation/high autogenous shrinkage. Both factors lead to increased volume instability relative to normal strength concrete – and also increased vulnerability to early age cracking.

The widespread interest in early cracking has resulted in much research, and many conferences devoted exclusively to aspects of the topic since the RILEM conference in München 1994 [44], seminars/workshops in: Trondheim 1996 [45], Hiroshima 1998 [46], Lund 1997, 1999, 2002 and 2005 [47][48][49][50], Paris 2000 [51], Sendai 2000 [52], Haifa 2001 [53], Trondheim 2005 [56] and Quebec 2006 [57][58]. Conferences with special sessions on the topic have also been the trend, for instance Phoenix 2002 [59], Colorado 2003 [60] and Evanston 2004 [61]. RILEM has had several committees on the topic; TC 119-TCE München [44], TC 181-EAS [53], TC 195-DTD [54] and TC 196-ICC [55].

Several research projects have been carried out with Norwegian participation. Participants have been NTNU/SINTEF, contractors, materials suppliers and public authorities, and the Research Council of Norway has contributed financially. Genuine Norwegian projects were NORCON (1993-1996, project leader NTNU), NOR-IPACS (1996-2000, project leader Skanska), NOR-CRACK (2001-2005, project leader NTNU [62], see APPENDIX 4) and the on-going COIN (2007-2014, project leader Sintef Byggforsk) where hardening phase cracking issues is a sub-activity in one of the many sub-activities. The large European Brite-EuRam project IPACS (1997-2001, project leader Scancem AB) had also several Norwegian participants (a complete survey of all IPACS-reports is given in APPENDIX 5).

2.7 Norwegian developments

The practical approaches to curing technology internationally from the 1970ties did not go unheeded in Norway. During the period 1981-1985 Freiesleben Hansen (Bkf-centralen) was invited several times to Norway, both by Ing.F.Selmer (today Skanska) and NTNU, to hold courses in curing technology. In 1982 Ing.F.Selmer and NTNU bought the simulation program CIMS from Bkf-centralen, which then was run on a big main-frame computer [63]. The same year Helland [66][67] implemented own data (strength, activation energy, heat) in a self-made program written in "Basic" for PC use; based on the maturity concept and the decrement-method developed at Bkf-centralen in Denmark. The tool was adapted in building projects to help workers at Ing.F.Selmer to solve practical problems on-site (first time used for the Solbergfossen power plant project). Furthermore, the semi-adiabatic calorimeter was also developed to measure hydration heat, and a special program (also programmed in Basic) was made to handle the data. In 1988 Smeplass (FCB) [68] made another program version for evaluation of semi-adiabatic calorimeter data. This is notable since updated versions of this program (in Excel-format) are widely used in Norway even today. The program transforms measured temperatures from calorimeter tests to adiabatic temperature and isothermal heat evolution; the latter being the basis for temperature calculations of structures. The procedures that now had been developed to determine the heat- and activation energy parameters was later adapted into the Norwegian standards NS 3656:1993 Rate of reaction, NS 3657:1993 Heat development, and NS 3099:1991 Reference concrete. All these standards are valid Norwegian standards even today.

In the dr.thesis of Sandvik from 1984 [64] the temperature sensitivity (activation energy) of the strength development in various concretes was studied, and the various maturity concept models available at that time were reviewed. Illustrative for the time of entry of computers was the NTNU-course "Curing technology of concrete" (Betongens herdeteknolgi) in 1988 [65] which informed that: "*The use of so-called PCs have increased during the last years*". In addition, it was stated that the program system HERD, developed at NTNU, had been available in Norway from 1986. Computer programming for curing technology apparently was popular in this time period since other programs were also made. When it comes to practical use of computer-based curing technology especially Skanska has been an active user, and over the years also applied the various versions of the Danish curing technology programs mentioned earlier, as well as the Swedish program ConTeSt.

In 1988 the Norwegian Public Roads Administration (NPRA) introduced new requirements for their concretes. The maximum allowable water-to-binder ratio was lowered from 0.45 to 0.40, and silica fume addition was required. In following projects there was a tendency of more pronounced problems with cracking on-site, especially on large bridge decks, presumably due to plastic shrinkage. Site-observations with the problem was reported some years after by Kompen in [69][70][71]. NPRA then initiated and sponsored a project at the Norwegian University of Science and Technology (NTNU) named "Cracking of high strength concrete at early ages" (1992-1994), under the leadership of Sellevold. Enhancement of the knowledge of the plastic phase was naturally a central part to resolve the mechanisms behind the observed problems, but also the hardening phase was addressed. On a fundamental level the plastic phase was studied with regard to cement

chemistry, chemical shrinkage, bulk chemical shrinkage ("the condom method"), pore water under-pressure, RH-development, and early strength development (by ultra-sonic pulse) [72][73][74][75]. On more macro (materials response) level plastic shrinkage cracking was measured [76][77], using a wind tunnel system developed by Johansen (FCB) in 1980 [78]. In addition, attempts were made to measure both the early age strain capacity and to measure restraint stresses in simple rigs, but those tests failed due to lack of adequate equipment. When it comes to the very early strain capacity of concrete, and many of the aspects of plastic shrinkage cracking mentioned above, the work was continued later, especially by Hammer (Sintef) who used among others an advanced "tension rig" for plastic concrete, see dr.thesis from 2007 [79].

In 1992 Sellevold (NTNU) went on a trip to Paris (LCPC) and München (Tech. Univ.) to study restraint stress measuring systems [80]. Even though the main motive of the trip was to look at very early age (plastic phase) concrete measuring systems, this trip may be regarded as a milestone with regard to the stress-based curing technology in Norway as it gave inspiration to build a TSTM-rig, and led to Norwegian participation in the early mentioned BriteEuram project IPACS. The TSTM was built at NTNU in 1995 as a part of the NORCON project sponsored by the Research Council of Norway and industrial partners, see Figure 13. The year before that, in 1994, Kanstad (NTNU) had spent 6 months at TNO in Delft, The Netherlands, to immerse himself into the achievements internationally on calculation solution methods for restraint stresses in hardening concrete [81]. In the following years, and until today, several projects and Ph.D.-studies [82][83][84][85] have been carried through within the succeeding national and international projects described in the previous section. It is notable that within the COIN-project the TSTM-rig was reconstructed in 2009-2010 to open for more extensive materials output and with selectable degree of restraint during the test. Regarding input data for hardening phase stress simulations, the NTNU/SINTEF-laboratory in Trondheim have been, and is today, the only place in Norway were all relevant concrete properties can be measured.

In a way the Norwegian knowledge on hardening phase cracking of concrete culminated with the submerged tunnel project in Bjørvika in Oslo (construction period 2006-2010). For the first time in Norway direct requirements were set with regard to stress-based curing technology. In order to make probable that crack-free structures were obtained, the involved contractors had to carry out experiments on the early age concrete properties and to perform pre-calculations of the restraint stress development of the various structural members to show that the crack index was not above 0.75. Experience regarding crack-control in this project was reported in 2010 [86], and a seminar was arranged the same year with all the involved parties [87]. In the various sub-projects of the Bjørvika tunnel project high volume fly-ash concretes were used to reduce hydration heat and crack sensitivity. The laboratory equipment and competence at NTNU/SINTEF was highly involved both in the pre-documentation tests by the Norwegian Public Roads Administration (NPRA) and in the project-specific documentation performed by the contractors. In 2011 the client (NPRA) and the entrepreneurs of the Bjørvika submerged tunnel projects (AF Gruppen Norge AS: Sørenga, Skanska Norge AS/Volker Stevin BV/BAM Civiel BV: Senketunnelen, and NCC AS: Havnelageret) received the concrete price of the year (Betongtavlen) from the Norwegian Concrete Association. The price was given for the developments in concrete technology in terms of low-heat fly-ash concretes with reduced carbon footprint, as well as for crack control by the use of hardening phase stress simulations and crack-risk reducing measures on-site.

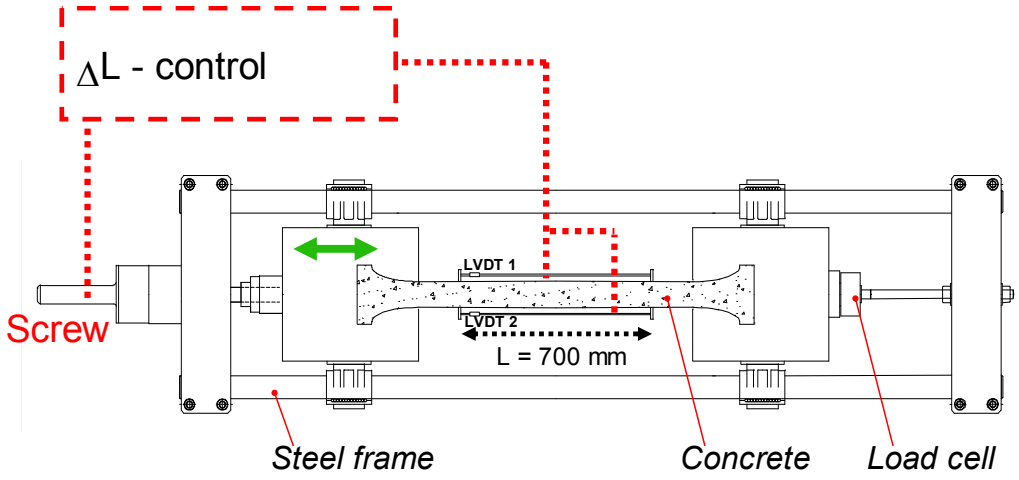

Figure 13 Above: From introductory tests in the newly build Temperature-Stress Testing Machine (TSTM) at NTNU in 1995. Participants in the Norwegian NORCON project (from right to left): Erik J. Sellevold (NTNU), Tor Arne Hammer (Sintef), Per Fidjestøl (Elkem Materials), Reidar Kompen (NPRA), Steinar Helland (Skanska) and Øyvind Bjøntegaard (NTNU, Ph.D.-student). Below: Sketch of the TSTM-rig.

At present, however, the competence on stress calculations of hardening concrete structures is on rather few hands in Norway. It is a pity since it can be such a useful tool for rational planning and production of concrete structures; a tool to plan the progress on-site and to obtain aesthetical and water-tight structures in the long term. The reason for little interest on the subject in Norway in the past is likely that the focus has been on temperature criteria, which is “a step on the way”, but clearly insufficient from a technical point of view. We can hope that this will change to the better in the future as an activity within COIN, in cooperation with the Norwegian Concrete Association, is to arrange practical courses on the use of the simulation program CrackTeSt-COIN.

Side-remark: A result of this literature study is that it appears that a Cracking Frame rig existed at FCB (today SINTEF) in 1980. The rig was built in connection with a specific assignment for Norwegian Contractors, see Figure 14. The fact that it was a confidential assignment, and with other people involved, may explain that possible useful experiences from it was not known a decade later during the very onset of "un-confidential" research on the topic.

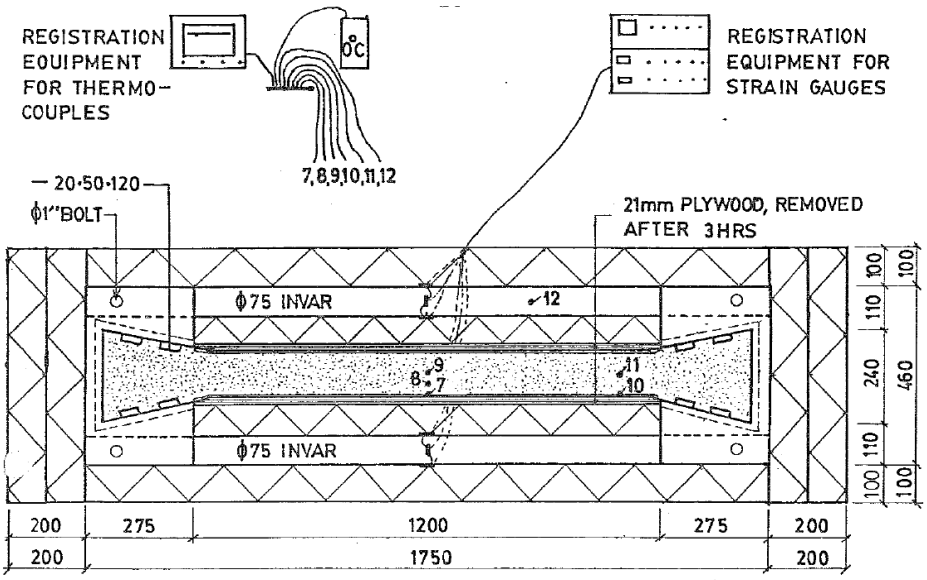

Figure 14 Cracking frame test set-up at FCB in Trondheim, 1980. Hoff [88]

3 The hardening phase and definition of t_0

An illustration of the different phases of the concrete "life" is indicated in Figure 15. The *fresh phase* involves mixing, transport, casting and the onset of hardening in the formwork. The initial hydration reactions develop slowly during this period. The cast concrete gradually loses all workability due to weak physical bonds between particles and initial chemical bonding between the cement particles (semi-plastic phase). t_0 is the point in time at which the hydration has developed sufficiently for the concrete to develop measurable mechanical properties. t_0 is related to the so-called 'final setting' and can be seen as the on-set of the property development of the concrete. t_0 varies with concrete temperature, binder type, and type and dosage of admixtures. t_0 may typically be from 6 to 14 hours after mixing.

The concrete develops much of its mechanical and durability properties during the *hardening phase (thermal phase)*. This occurs together with significant heat generation (exothermic chemical reactions). For massive structures (thickness 1.0 m ± ca. 0.5 m) the maximum temperature will generally occur after around 1-3 days. Heat generation becomes more moderate thereafter and the heat loss to the surroundings will then dominate and the concrete will start to cool. The cooling period takes place until the structure reaches thermal equilibrium with the surroundings, which usually occurs after some weeks. For very massive cross-sections, e.g. in dam constructions, it may take years before the concrete is completely cooled.

In *the service phase* the concrete (the structure) is close to thermal equilibrium with the surrounding air at all times and it is exposed to service loads and the surrounding climate.

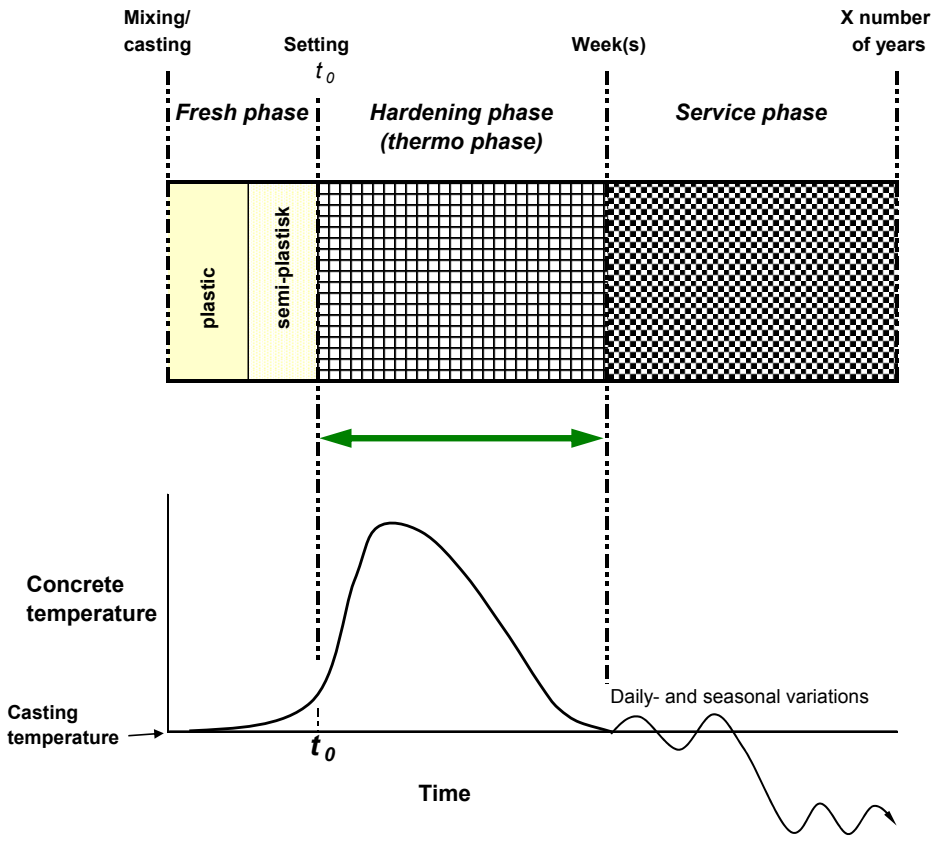

Figure 15 Different phases of concrete – schematic diagram.

A simple principle sketch of cement hydration is given in Figure 16, where (a) represents the fresh phase (dormant period), (b) can illustrate the time t_0 where hydration products bridge between cement particles - producing a stiff skeleton, (c) further hydration in the hardening phase, and (d) long-term complete hydration.

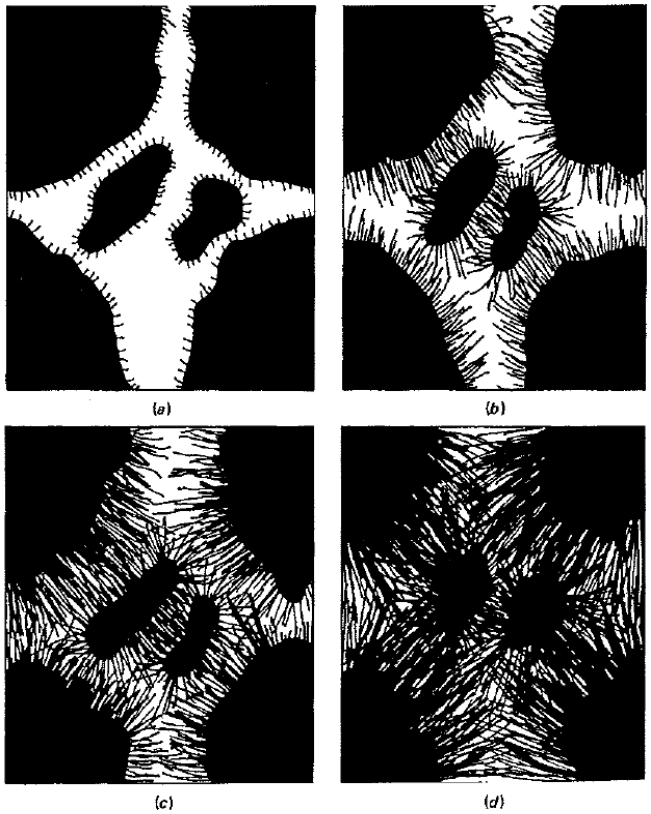

Figure 16 Different phases of cement hydration – principal sketch. (a) Fresh phase, (b) around t_0, (c) hardening phase and (d) well-hydrated (service phase)

4 Internal and external restraint

Stresses in concrete develop when its volume changes are restrained internally and/or externally.

Temperature gradients over the concrete cross-section give differential thermal strain and **internal restraint**. When the formwork is removed from a hot structural element, there is rapid cooling (contraction) of the surface, see Figure 17. This contraction is restrained by the core and results in tensile stresses that can result in surface cracks. Tensile stresses and surface cracks may also occur during the heating phase (even with formwork) if the surface temperature lags behind the core temperature due to heat loss through the formwork. Typical damage due to internal restraint is indicated at the top of the wall in Figure 18 (see 'Expansion phase'). However, surface cracks of this type have a tendency to close later in the cooling phase when the core also cools, but they can nonetheless be unfortunate 'initial' damage serving as weak points during later climate exposure. Figure 18 also indicates that the expansion of the wall during the expansion (heating) phase may produce cracks in the base, but in practice this is not experienced to be a problem.

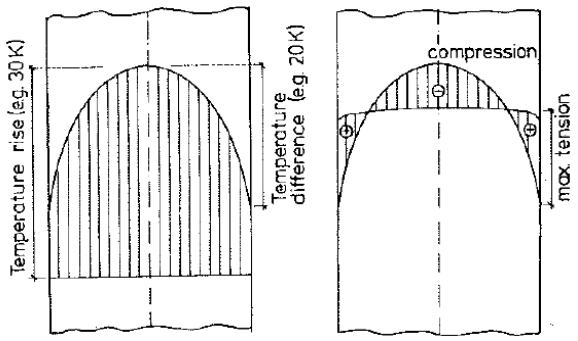

Figure 17 Illustration of internal restraint

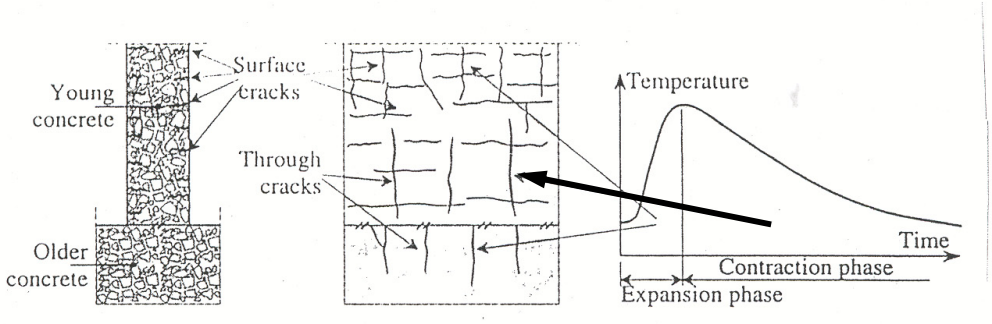

Figure 18 Example of cracking in a concrete wall due to internal and external restraint. [105]

External restraint is associated with casting joints, i.e. the hardening structure is restraint by stiff and mature adjoining structural members. The classic example is a wall that is cast on a stiff foundation/slab. During the cooling phase (see thick arrow in Figure 18) the wall contracts, but it is restraint by the stiff foundation. The stresses that arise in this situation are mainly longitudinal. The critical time with regard to cracking (or not) will vary according to structural thickness, type of concrete, etc, but it can typically be from around 5 days to a few weeks after casting. Such cracks are generally "through-cracks", i.e. the cracks span through the entire thickness of the wall. The cracks often go from close to the joint and (for a wall) vertically several meters up. The crack widths may vary from very thin ones (0.05 mm) to 0.3 mm and even wider. An illustration of external restraint of a wall-structure is shown in Figure 19, and various situations with external restraint are shown in Figure 20.

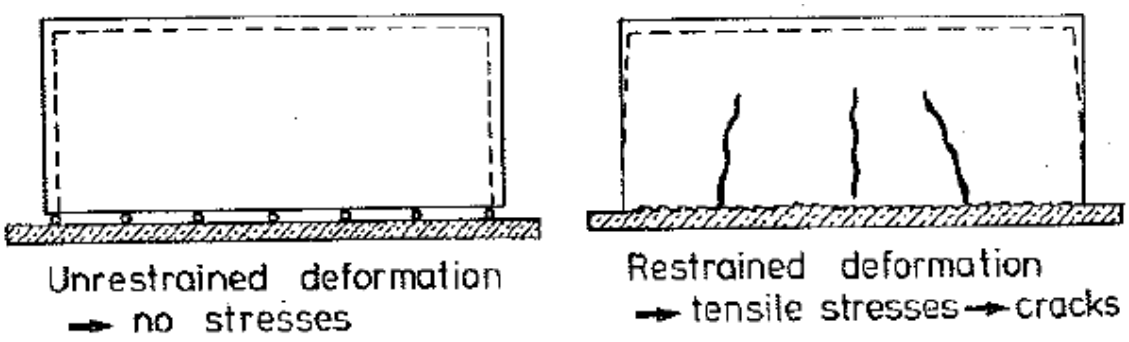

Figure 19 Illustration of a wall with (artificial) no restraint (left) and external restraint (right)

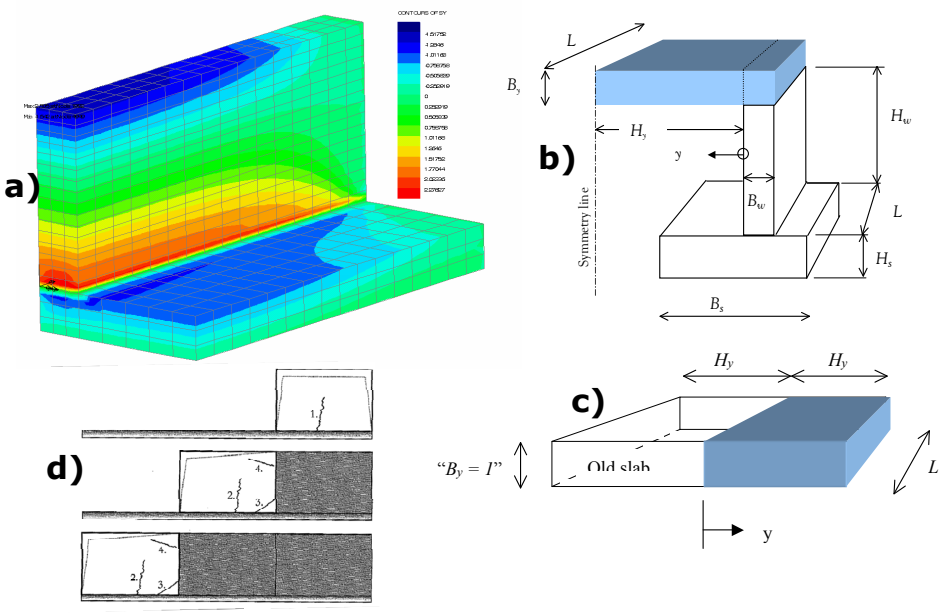

Figure 20 Examples of different conditions of external restraint: Wall on slab (a), slab on wall (b), slab against slab (c) and successive casing of wall sections (d). [116]

The degree of restraint over the length of two wall-on-slab structures is shown in Figure 21. The lower parts of the walls are most restrained. During the cooling phase the cracks are likely to be initiated in the lower part (around one wall-thickness up from the casting joint) of the wall since the lower part often has the most unfortunate combination of high curing temperature and high restraint. The crack will then develop vertically in both directions during further cooling. Close to the joint the temperature increase will be less due to transmission of heat to the slab. If cracking occur in the wall, the final result may be many vertical cracks, often several meters high. Figure 21 shows that for a long wall (high L/H-ratio) the restraint is generally high for the whole structure, while for the shorter wall (low L/H) we find high restraint only around the lower mid part. Hence, a long wall generally will develop more cracks and longer cracks than a short wall.

Plots from a FEM-analysis show how a wall may deform during heating, see Figure 22-a, and after end of cooling, see Figure 22-b. The given wall is relatively short (low L/H-ratio) and is able to rotate. Note that the slab is also rotated by the wall. In the cooling phase the wall and the slab are lifted upwards at each end. This freedom a rotation means that the longitudinal tensile stresses will vary over the length of the wall and the longitudinal stresses will be highest towards the centre of the wall, as discussed above.

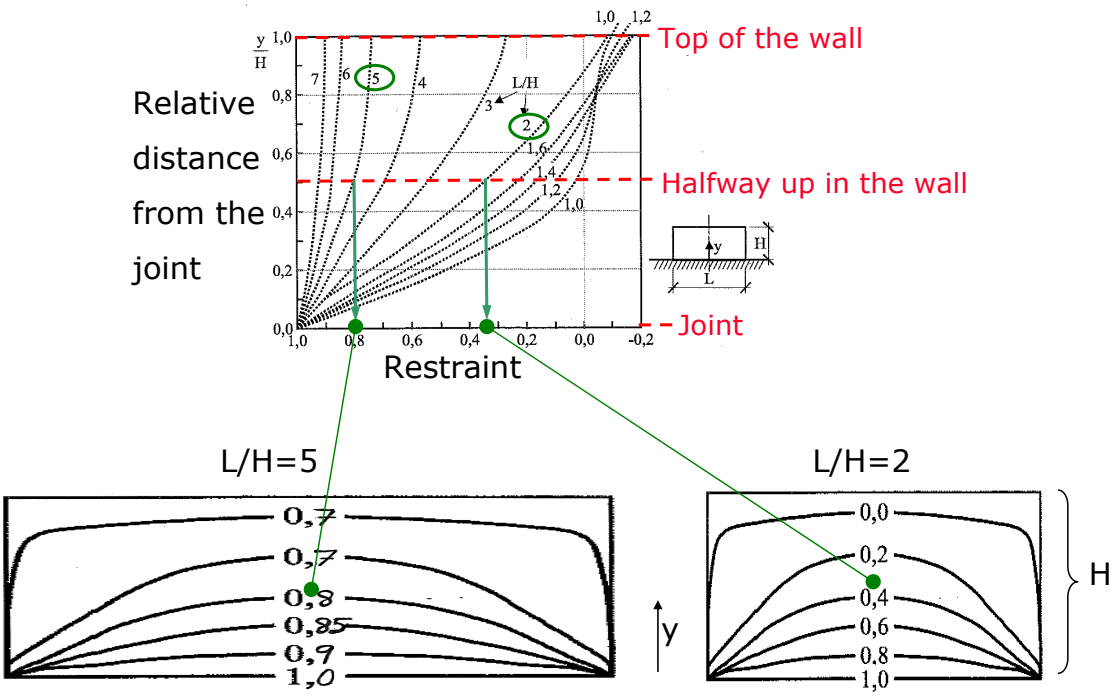

Figure 21 Example: Effect of the length/height (L/H)-ratio on the degree of restraint over the length of wall structures with L/H = 5 (left) and L/H = 2 (right).

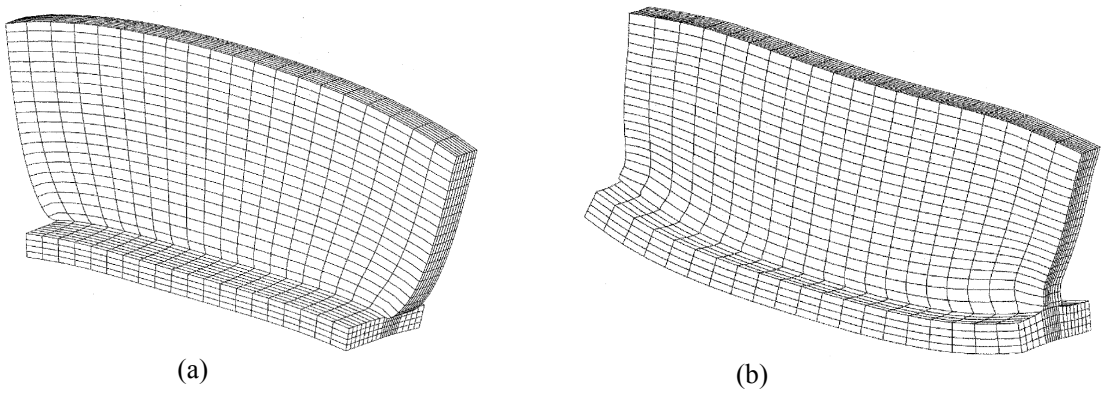

Figure 22 Example: FEM-analysis, wall on slab. (a) Deformation at maximum wall temperature, and (b) deformation after the end of the cooling phase. The deformations are exaggerated [104]

An example of stress distribution in a wall during the cooling phase is shown in Figure 23. The figure shows half the structure, with the wall centre (axis of symmetry) to the left. The main tensile stresses in the wall (σ_x) develop from the end and increases towards the centre of the wall (see $\sigma_{x,max}$ in Figure 23-a). Note that maximum σ_x occurs a distance up from the bottom of the wall, as mentioned earlier. These main/principal stresses are the cause of through-cracks.

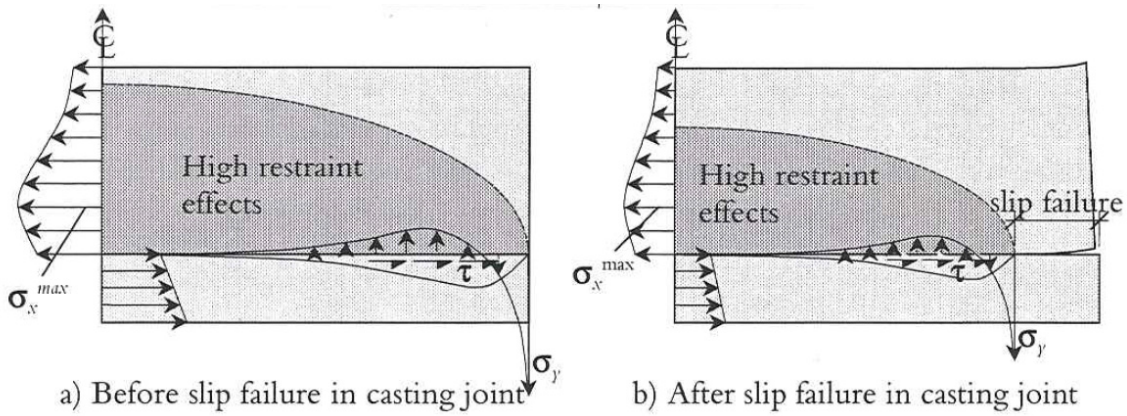

Figure 23 Tensile stress distribution in a wall on slab in the cooling phase: Before (a) and after (b) slip failure at casting joint end. Both figures show half the structure, i.e. axis of symmetry to the left. [105]

Due to the unsymmetrical restraint by the slab, and subsequent rotation, vertical stresses (σ_y) and shear stresses (τ) also develop. These stresses often cause slip failure (micro-cracks) along the joint at the wall ends, see Figure 23-b. This effect is particularly important for short walls (low L/H-ratio) and the consequence is that the overall degree of restraint in the wall is reduced. Calculation programs are not normally able to simulate slip failure and ignoring this "parameter" (slip failure) contributes to overestimation of stresses in calculations. Stress calculations depend on a large number of parameters; each of them associated with some uncertainty, hence it could be argued that there is sense in not considering the slip failure effect since it constitutes a built-in safety factor. However, the stress-reducing effect of slip failure can be taken into account by using a reduction factor [106] for the degree of restraint. In most practical cases the slip failure effect has a 0-20% reducing effect on the degree of restraint in a wall-on-slab structure [105][106].

Examples of crack observations from full-scale laboratory tests of walls are shown in Figure 24, upper figure: high L/H ratio, bottom figure: low L/H-ratio. The cracks in the mid part of the wall are usually vertically oriented while there is a tendency to more inclined cracks towards the ends because the stress condition is more complex ($\sigma_x + \sigma_y$). Note that slip failure was observed in both walls in Figure 24.

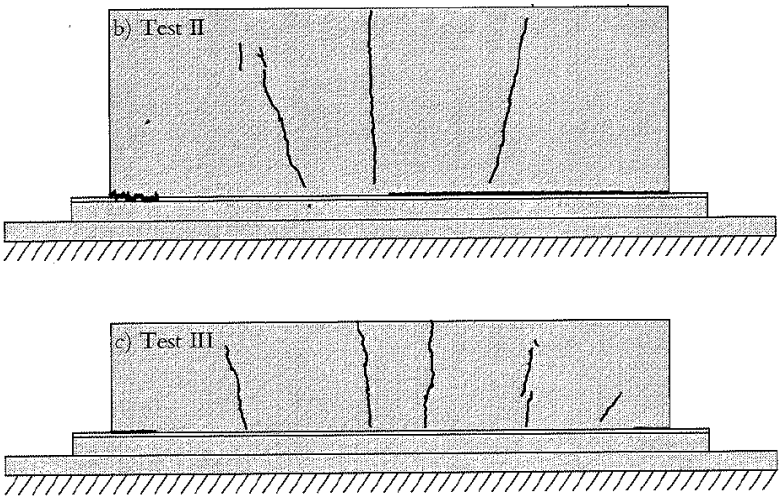

Figure 24 Typical through-cracks due to restraint by the slab, full-scale tests. Upper figure: wall with low L/H ratio (large height H). Bottom figure: wall with high L/H ratio (small H). [105]

The flexibility and stiffness of the ground also influences the deformation of the slab, which again influences the freedom of rotation/degree of restraint in the wall. Inflexible ground (for instance rock) allows no flexibility of the base slab and contributes to high restraint over the whole length of the wall, see Figure 25-a. Soft ground allows the slab to penetrate into the ground so that the wall may rotate more, giving reduced restraint, see Figure 25-c. The mid-section of the wall does not necessary notice these end effects, especially in longer walls. This is due the self-weight of the structure which gives a counter-moment against the rotation (see Figure 25-b). The effect of ground stiffness is difficult to model correctly, but stiffness parameters for various types of ground have been proposed.

Based on a number of 3D-analyses it was stated in [116] that the following restraint factors (R) were typical for the given restraint problems:

Slab to slab:	R=0.05-0.52
Wall on slab:	R=0.37-0.70
Top slab on wall:	R=0.12-0.52

As a summary, the degree of external restraint in a hardening concrete wall depends on the following issues:

1. The geometry of the structure (the L/H-ratio) influences the stress distribution over the height and over the length. High L/H-ratio give larger areas with high degree of restraint and possible cracking may occur over a larger portion of the wall.
2. Stiffness (E-modulus and cross-section area) of the restraining structure has significant influence.
3. Joint-end slip failure decreases the degree of restraint, but is difficult to model and generally not included in analyses. However, some simulation programs may take this effect into account.
4. The flexibility and stiffness of the ground (for wall on slab).

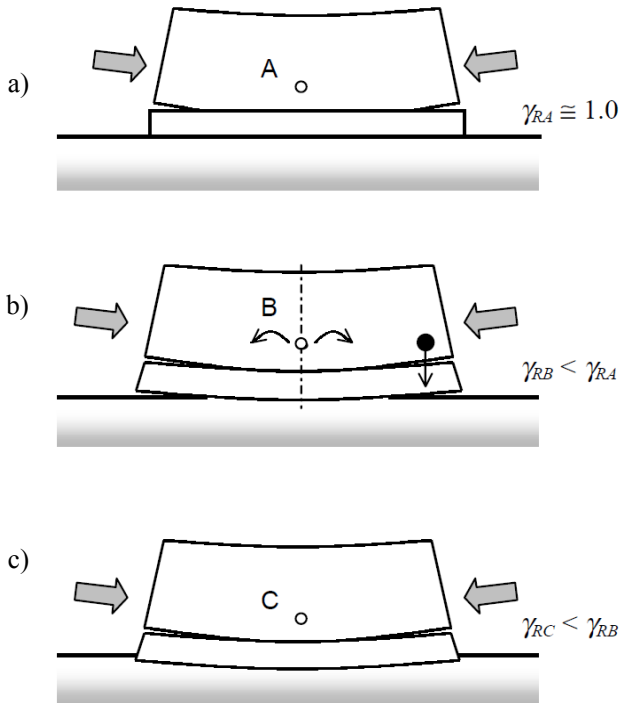

Figure 25 Influence of ground stiffness on freedom of rotation. (a) Stiff ground and little freedom of rotation, (b) semi-stiff ground, and (c) soft ground (γ_R=restraint in point A,B,C)[124].

5 Stress development and "crack index"

Crack risk is assessed by comparing self-induced concrete stresses with the tensile strength during the entire hardening period. In finite-element-method (FEM) simulation programs the temperature and stress development over time at critical positions in the structure are identified, based on concrete properties, structural configuration and environmental conditions. The major factors in early age cracking are illustrated in Figure 26.

Thermal dilation and autogenous shrinkage are the driving forces, while the other parameters can in simplified terms be called 'the response'. The net result is concrete stresses.

The risk of cracking is usually expressed as the ratio (over time) between generated concrete tensile stress and tensile strength. This ratio is called "the crack index", C_i, (or relative stress), see Equation 1. The crack index is normally highest well into the cooling phase, as discussed earlier. A calculated crack index of 1.0 (or higher) indicates that cracking will occur; if below 1.0 cracking will in theory not occur. If the crack index is e.g. 0.5 at a given time, this means that 50% of the concrete's tensile stress capacity is being utilized or 'challenged'. In cases where calculations are required as pre-documentation, a crack index clearly below 1.0 is generally required. The use of the crack index as a "crack-risk criterion" is discussed further in Chapter 12.

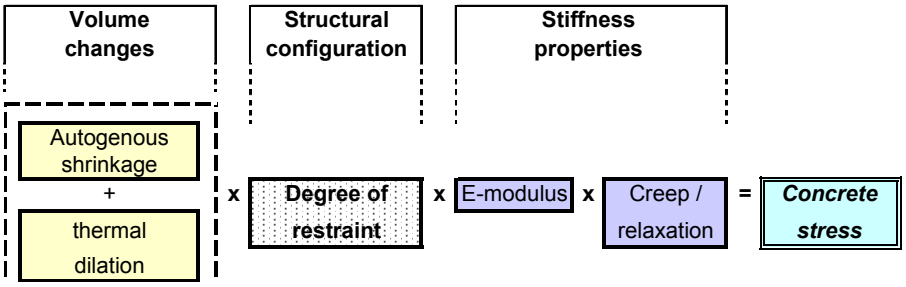

Figure 26 Stress development during the hardening phase – schematic diagram

Equation 1

$$\text{Crack index},(C_i(t)) = \frac{\text{Concrete stress}(t)}{\text{Tensile strength}(t)} = \frac{\sigma(t)}{f_t(t)}$$

and

$$\frac{\sigma(t)}{f_t(t)} < 1.0 \text{ indicates no cracking}$$

$$\frac{\sigma(t)}{f_t(t)} \geq 1.0 \text{ indicates cracking}$$

Examples of measured stress development under external restraint conditions are given in Figure 27. The results are from three laboratory tests where 1 metre long prismatic specimens, all with the same concrete, were 100% restraint during hardening (1-dimensional restraint test). The time scale reflects the time after mixing. The three test samples were subjected to three different temperature histories (Figure 27-a). The temperatures were calculated in advance with a curing technology program and represent the average temperature for this concrete used in walls with thicknesses of 30 cm, 50 cm and 1 m, respectively. The three calculated temperature histories were then used to control the temperature in the laboratory tests.

All tests show the typical stress development for external restraint conditions (Figure 27-b): during the heating period (expansion phase) compressive stress develop, whereas tensile stresses develop during the subsequent cooling phase (contraction phase). The highest temperature (curve 1) resulted in the highest compressive stress in the heating phase and the fastest tensile stress development in the cooling phase.

In the two tests with the highest maximum temperature, (curve 1 and 2), the specimens failed in tension after approximately 2 days; at that time the stress reached the tensile strength, i.e. the crack index is 1.0. Note that heating takes place in a very young and soft concrete (low E modulus), while cooling occurs in a more mature and stiff concrete (high E modulus). This is the main reason why very little cooling is necessary to bring the concrete from maximum compressive stress after approximately 1 day and all the way to tension failure about one day later.

The specimen with the lowest maximum temperature (40°C, curve 3), "survives" the entire hardening phase, and after 168 hours the tensile stress is 3.0 MPa. The tensile strength at that time is 3.4 MPa and the crack index at 168 hours is thus (3.0 MPa/3.4 MPa =) 0.88. The direct implication of Figure 27 is therefore that the tested concrete will crack if the temperature gets slightly above 40°C (valid for: 100% restraint, 20°C fresh concrete temperature and 20°C ambient temperature). In a structure the degree of restraint is generally much lower than 100%, hence the stress development for the given concrete in a structure would therefore be more moderate than shown in Figure 27-b.

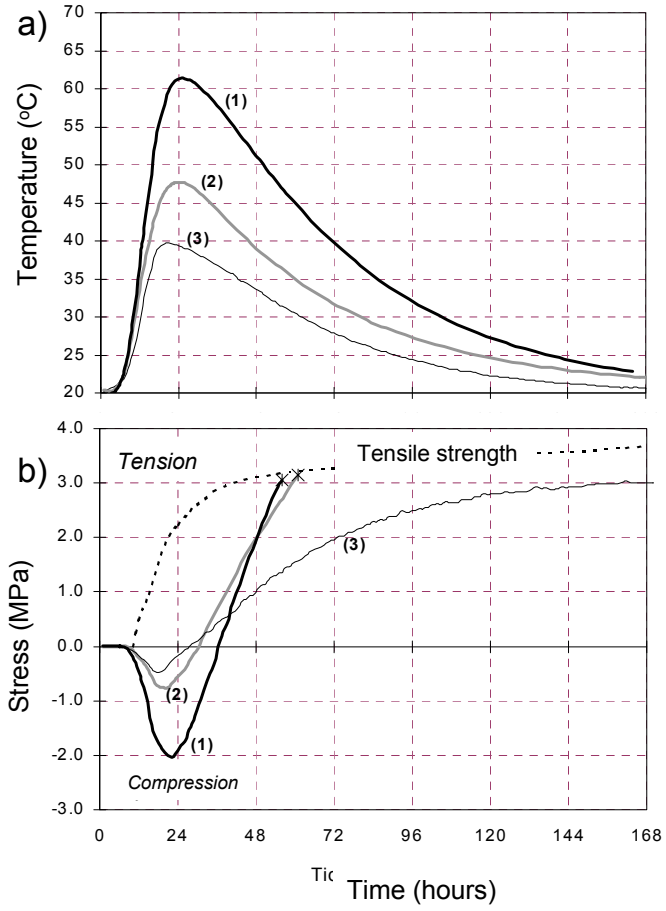

Figure 27 (a) Measured (and imposed) temperature, and (b) stress development in laboratory tests on 100% restrained concrete specimens. The time axis corresponds to the time from mixing. The tensile strength development (dashed line) is also indicated. The same concrete was used in all tests (w/b = 0.40, f_{c28} = 80 MPa). [82]

6 Maturity time – the "state parameter"

In curing technology and early age stress simulations of concrete a "state parameter" is used for defining the state of hardening (i.e. the property development) of the concrete at all times from mixing and through the entire hardening phase. In the Nordic countries (and also other countries) "maturity time" is generally used as the state parameter. "Maturity time" is often denoted "equivalent time" and the two terms means the same.

The maturity concept takes into account that the hardening process is a thermally activated process. The rate of hydration of concrete (i.e. the cement/binder) increases with increasing temperature, and as the hydration process produces heat the temperature increases and the reaction process becomes self-accelerating. The property development (strength, E-modulus, etc.) of concrete is closely linked to the progress of cement/binder hydration which leads to the proposition that the progress of the property development can be expressed as a function of a time-temperature combination – i.e. maturity time.

The reference temperature is generally set to be 20 °C, and the rate of hydration (H) at this temperature is thus defined to be 1.0. Temperatures above 20 °C gives H>1.0, and below 20 °C then H<1.0. At around -10 °C hydration more or less stops and H=0.

According to the Arrhenius principle, the rate of hydration (H) can be expressed as shown in Equation 2. The temperature development of a concrete is divided into short time increments with an average temperature in each interval T_i. For each T_i the H-function value is calculated as:

Equation 2

$$H(T_i) = e^{\frac{E(T_i)}{R}\cdot\left(\frac{1}{293}-\frac{1}{273+T_i}\right)}$$

Where H is the rate function, E_T is the activation energy, and $E_T = A + B(20 - T_i)$. For T>20 °C then B=0, and for T < 20°C then B has a given value. A has a given value for all temperatures. R is the gas constant (8.314 J/(mole · K))

The maturity "growth" within a time increment is then $H(T_i)\cdot\Delta t_i$. The maturity time at a certain concrete age (after n time intervals) is then the sum of all maturity growth increments as shown in Equation 3.

Equation 3

$$M = \sum_{i=1}^{i=n} H(T_i)\cdot\Delta t_i$$

Where M=maturity time (which equals t_e=equivalent time), n is the amount of time intervals, H is the rate function, T_i=the average temperature in each time interval Δt_i.

As mentioned, 20 °C is commonly used as the reference temperature (note 20°C equals 293 K in Equation 2). The actual H-value at a given temperature depends on the temperature sensitivity (the activation energy) E_T. For instance, at 35 °C the cement reaction may be around twice as fast (H=2) compared to that of 20 °C. Hence, the property (for instance strength) obtained after 24 hours at 35°C temperature equals to 48 hours curing at 20 °C, i.e. the maturity time is for both cases 48 hours in this example. This kind of time-shift may then transform property developments from any arbitrary temperature history to maturity time (i.e. the equivalent hydration time at 20 °C). A given concrete subjected to various temperature histories within a structure means that there is individual maturity time developments for each point in the structure. The maturity development can then be

inserted in maturity based models (see further chapters) and the property development at each point in the structure can be found. Examples of activation energy and resulting rate function are given in Figure 28.

A limitation of the maturity concept is that it assumes that the final property is independent of the temperature history, i.e. the temperature history only affects the rate of property development towards the final value. This is, however, not the case always in practice, since for instance high temperatures increases strongly the rate of early property development, but it produces weaker bonds between particles on the long run which alter the final potential after longer times. And, low temperatures mean slow early development, but higher final properties. This is illustrated in Figure 29 (top+left), which shows curing temperatures and examples of measured strength vs. (real) time at three different constant temperatures and one realistic (semi-adiabatic) temperature. In Figure 29 (right) it can be seen that the same results can be fitted well in a maturity time plot up to a certain maturity level, but after longer times the tendency of reduced strength at high temperatures can also been seen. The high and artificial 50 ^{o}C constant curing temperature gives the most pronounced strength reduction after longer times, whereas this tendency is generally much less for realistic (semi-adiabatic) temperatures.

The different materials models uses maturity as time parameter and the maturity concept has shown to be a very applicable engineering tool for predicting the property development of concrete during the period with most dramatic changes of the various properties, i.e. from setting and through the hardening phase.

Another state parameter that is used in some countries is the "degree of hydration" α. Since α is very difficult to determine experimentally it is often defined as the heat release at a given maturity time divided by the final heat release after infinite time, i.e. α develops from 0 at setting to 1 at infinite time. This definition considers also the temperature-maturity time relation and, thus, the concept of using α then pretty much equals the maturity concept, but the materials models using α requires different mathematic formulations.

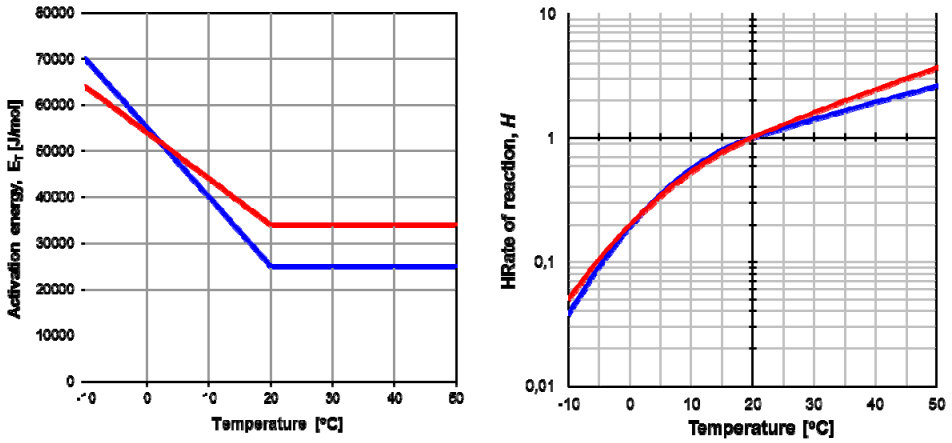

Figure 28 Activation energy (left) and rate function (right). Red curves: A=34000 and B=1000, blue curve: A=25000 J/mole and B=1500 J/(mole·K)

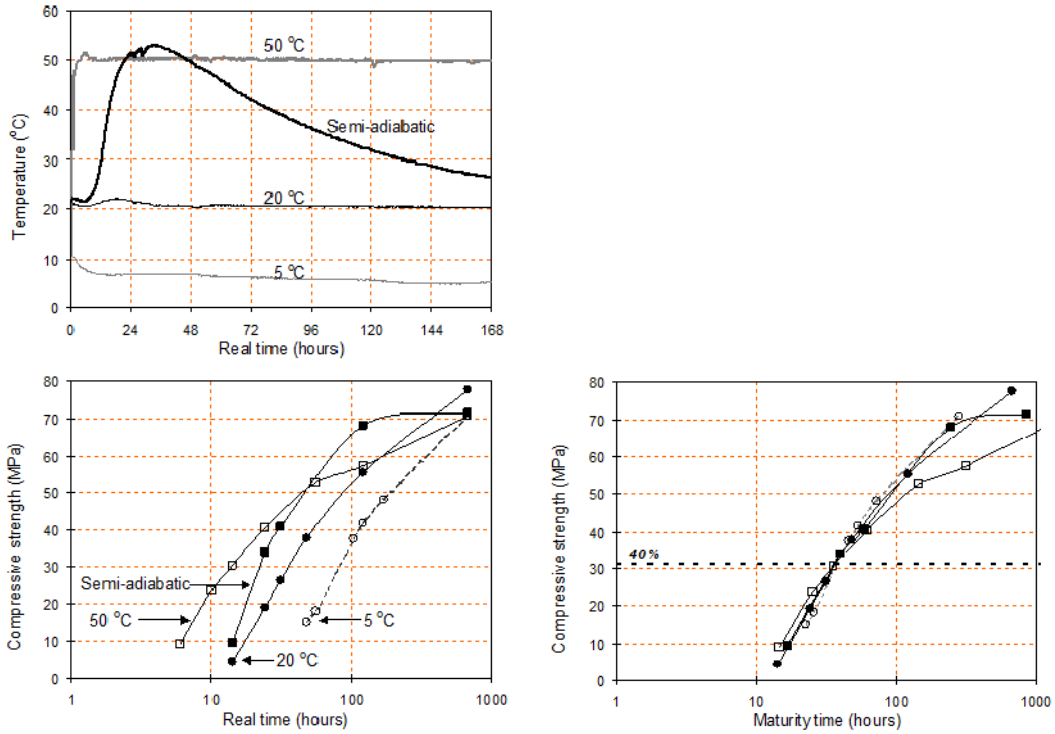

Figure 29 Curing temperatures (top), and measured strength results plotted against real time (left) and maturity time (right). The strength level of 40% of 28-days strength measured at 20°C is indicated in the right figure as it is the level proposed for the determination of activation energy in NS 3656

7 The driving forces to stress generation

7.1 General

Heat is generated when cement (+silica fume, fly-ash, slag) reacts with water. The reaction forms solid hydration products with fine pores that are partly filled with water. The heat causes thermal strains (thermal dilation), while formation of partly water-filled pores (self-desiccation) results in autogenous shrinkage. These are the two driving forces behind cracking in hardening concrete. If the temperature of the concrete is constant (isothermal conditions), autogenous shrinkage operates alone, while under normal conditions where the temperature varies, thermal dilation and autogenous shrinkage operate simultaneously to produce stresses, hence:

Equation 4

$$\varepsilon_{tot} = \varepsilon_T + \varepsilon_{as}$$

Where:
ε_{tot} = total deformation, ε_T = thermal dilation, ε_{as} = autogenous shrinkage

7.2 Autogenous shrinkage

The term "autogenous" means something like 'automatic process' or 'self-produced' and means that the shrinkage develops independent of external influence. The reason for this is that the cement-water reaction is associated with a loss in volume; the reacted solid product fills a lesser volume than the reactants (cement + water). The phenomenon is called chemical shrinkage and is a fundamental property of cement hydration. Chemical shrinkage starts when water meets cement in the mixing process and continues as long as the hydration process goes on in the concrete. Chemical shrinkage is approximately 0.06 cm^3 per gram of reacted cement, which for a cement paste with a w/b-ratio of 0.40 results in a volume of air-filled pores of around 8% (assuming complete hydration and a constant external paste volume).

The pore structure that is formed during hydration will thus gradually undergo a reduction in the degree of water saturation since water is consumed as the cement hydration proceeds - this is called self-desiccation. As a consequence, the relative humidity (RH) of the pore system drops. This applies especially to high performance concretes with w/b<0.45, and the RH for such concretes may drop from around 100% in the fresh phase to 80-90% after a few weeks. For very low w/b concretes, the RH may drop even more (down to around 70%). Self-desiccation creates capillary forces and negative pore water pressure which is transferred to the solid phase and results in an external (bulk) contraction of the concrete which is called autogenous shrinkage.

Note that these arguments assume that no extra water is supplied during hydration (as is the case for massive structures in nearly all practical applications). If the element is very small and water is available on the surface it will be sucked in and the element remains saturated and no autogenous shrinkage will develop.

Self-desiccation and negative capillary pressure are assumed to be the main mechanisms behind autogenous shrinkage in concrete. There are also other possible mechanisms, probably of minor importance, but these are not addressed here. Still, due to the complex nature of autogenous shrinkage it is sometimes denoted 'autogenous deformation' to incorporate the fact that it can sometimes occur as an autogenous swelling.

A fundamental relationship between (internal) chemical shrinkage and (external) autogenous deformation (shrinkage) is shown in Figure 30. Chemical shrinkage occurs from the moment the cement comes in contact with water. During the plastic phase (initial period), autogenous shrinkage

is equal to chemical shrinkage because the chemical shrinkage leads simply to a vertical collapse. Autogenous shrinkage thus contributes to concrete settlement during the plastic phase. Around t_0, the cement paste develops strength and becomes 'self-supporting' so that pores can form and gradually a negative capillary pressure can build up. The autogenous shrinkage now goes from being a vertical deformation to a uniform volume reduction, i.e. the deformation is equal in all directions. This means that from t_0 the autogenous shrinkage can be measured in horizontally oriented test set-ups, and it will create stresses if the concrete is restraint.

The difference between the curves in Figure 30 expresses the empty pore volume in the binder phase that is formed by chemical shrinkage. The autogenous shrinkage after t_0 may seem insignificant in the figure, but it is often significant in terms of creating concrete stresses, especially in high quality concretes. Autogenous shrinkage has been the object of much attention in Norway and internationally during the last couple of decades in step with the more widespread use of high performance concrete. Figure 30 is a schematic diagram which is based on laboratory tests, see for instance [89][90][91][92].

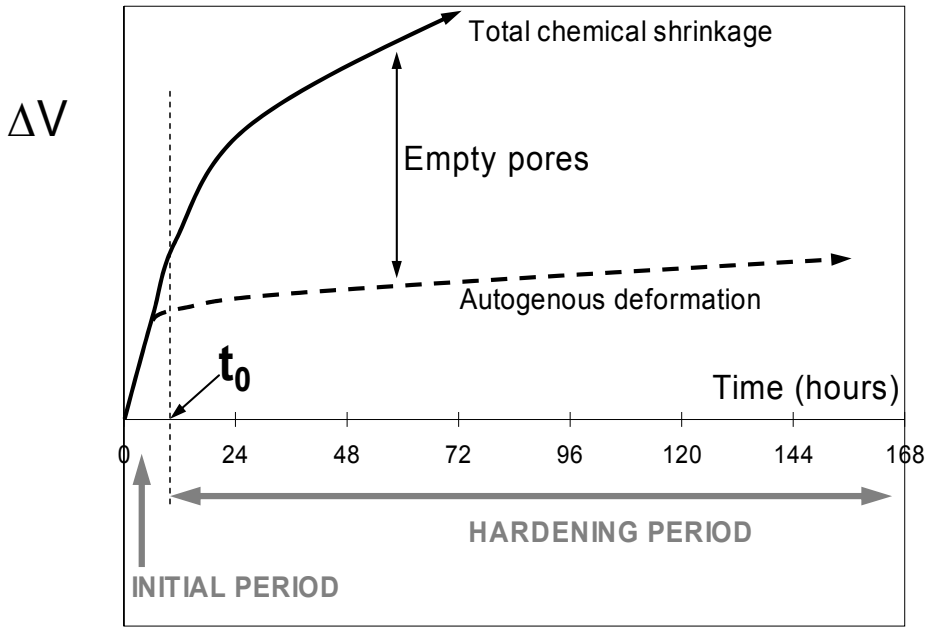

Figure 30 Total chemical shrinkage and external volumetric autogenous deformation (shrinkage) in cement paste. 20°C isothermal conditions. Schematic diagram.

An example of the effect of autogenous shrinkage on restraint stresses in a concrete (w/b = 0.40) is shown in Figure 31. The figure shows parallel measurements on an unrestrained specimen (free dilation tests) and a 100% restraint specimen, both at a constant temperature of 20°C (i.e. no thermal dilation). Note that autogenous shrinkage is also recorded in the fresh phase, but does not create measurable stresses in the restrained sample until after t_0. This early shrinkage is not discussed in more detail here, but it occurs in a plastic and semi-plastic concrete. It should be noted that autogenous shrinkage before t_0 (initial period) will contribute both to settlement (as previously mentioned) and to 'plastic shrinkage'. Plastic shrinkage is usually explained by the concrete losing water to the surroundings.

The fact that autogenous shrinkage in Figure 31 shows expansion for a short period around t_0 (creates a slight compressive stress) clearly illustrates that the phenomenon is complex and that self-desiccation is not the only mechanism.

The figure shows that this concrete developed an autogenous shrinkage of approximately $80 \cdot 10^{-6}$ between t_0 and 168 hours (the first week), and this shrinkage produced a tensile stress in the restraint specimen of just below 1 MPa. After 1 month it is notable that this particular concrete failed at a tensile stress of 3 MPa due to autogenous shrinkage alone! Autogenous shrinkage was at that time $200 \cdot 10^{-6}$.

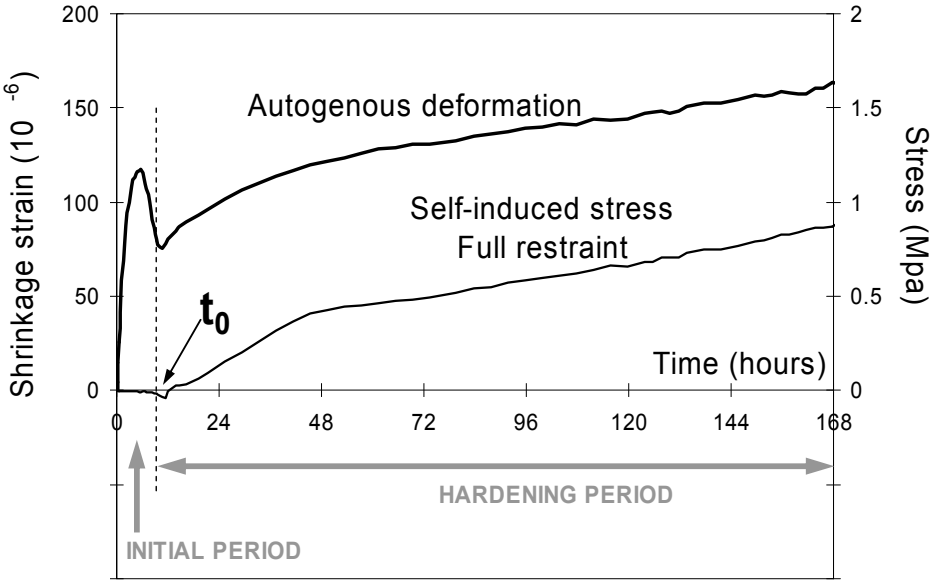

Figure 31 Parallel measurements of autogenous shrinkage (horizontal dilation test) and stress development at 100% restraint. 20°C isothermal tests (w/b = 0.40, f_{c28} = 80 MPa). [82]

7.3 Hydration heat and thermal dilation

The heat produced by the hydration reactions results in an increase in the concrete temperature. For adiabatic conditions (no heat loss to the surroundings) the relationship between heat and temperature is:

Equation 5

$$\Delta T_{ad} = \frac{Q_c \cdot C}{\rho_c \cdot c_p}$$

where
ΔT_{ad} = adiabatic temperature increase [°C], Q_c = heat generation per kg cement (or per kg binder) [kJ/kg], C = the binder content per m^3 concrete [kg/m^3], ρ_c = concrete density [kg/m^3], c_p = concrete heat capacity [kJ/(kg • °C)].

In all practical cases there is heat transfer between the structure and the surroundings. The heat transfer to (or from) the surroundings can be expressed in terms of a temperature difference and a heat transfer coefficient k, and the heat exchange/heat flow Q_{loss} is:

Equation 6

$$Q_{loss} = k \cdot (T_{cs} - T_{ext})$$

where T_{ext} is the external temperature and T_{cs} is the concrete surface temperature.

The overall heat transfer coefficient k is a product of the formwork, insulation (if used) and wind velocity [30], and is determined as:

Equation 7

$$k = \left[\frac{1}{\alpha_C} + \left(\frac{e}{\lambda} \right)_{ins} + \left(\frac{e}{\lambda} \right)_{form} \right]^{-1}$$

where

k	=	overall transmission coefficient
α_C	=	convective surface transmission coefficient
e	=	thickness of insulation and of form work, respectively
λ	=	thermal conductivity

and α_c is the value that depends on wind (forced convection)

The degree of heat accumulation (temperature rise) in the concrete structure, and its temperature distribution is dependent on the thermal diffusivity of the concrete, the thickness of the structure and its surface temperature (T_{ext}). For normal density concrete the thermal diffusivity does not vary very much from concrete to concrete, hence the heat accumulation in the structure is most dependent on the concrete thickness. More heat is accumulated in massive structures than in slender structures.

The heat balance, giving the concrete temperature T_c for time $t>0$, can in principle be calculated from [31]:

Equation 8

$$T_c = T_{ci} + \int_{Q_c} dT + \int_{k} dT$$

where

T_{ci} is the initial concrete temperature, $\int_{Q_c} dT$ is the temperature increase caused by the hydration heat, and $\int_{k} dT$ is the temperature decrease caused by the loss of heat to the surroundings.

In simulation programs the heat balance, i.e. the analyses of a temperature field in hardening concrete, is solved numerically in time steps; based on solving a Fourier differential equation. Hand solution methods for temperature calculations have existed for quite a long time, but today simulations are computer-based.

Figure 32 and Figure 33 below illustrate the effect of degree of insulation and the thickness of a concrete wall structure, respectively. In Figure 32 the thickness is the same in all sub-figures, whereas the degree of insulation decreases as we go in right direction. In Figure 33 the degree of insulation is the same in all cases, whereas the thickness varies. The adiabatic case in Figure 32-a may represent an (artificial) infinite thick structure were all hydration heat is accumulated in the structure, meaning that the heat exchange with the surroundings is negligible during the hardening phase and the term "$\int_{k} dT$" in Equation 8 is zero.

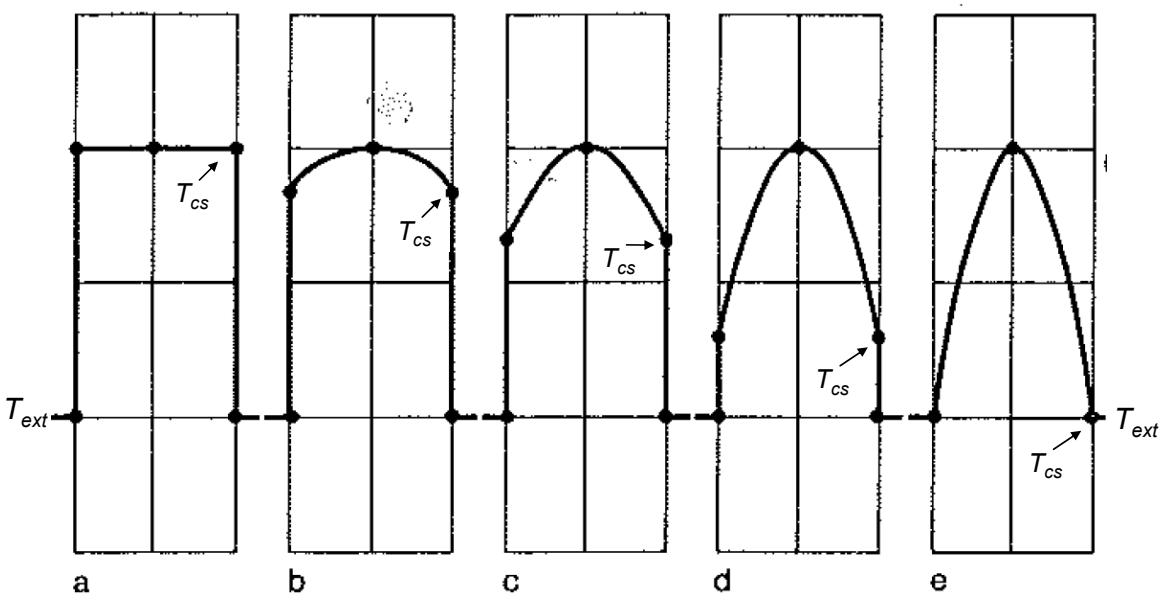

Figure 32 Degree of insulation and the effect on the shape of the temperature distribution over a given concrete wall section during cooling. (a) Adiabatic conditions/infinite insulation, (e) Isothermal conditions/no insulation. (b-d) Practically relevant intermediate insulation conditions [31]. T_{ext} **= external temperature,** T_{cs} **= concrete surface temperature**

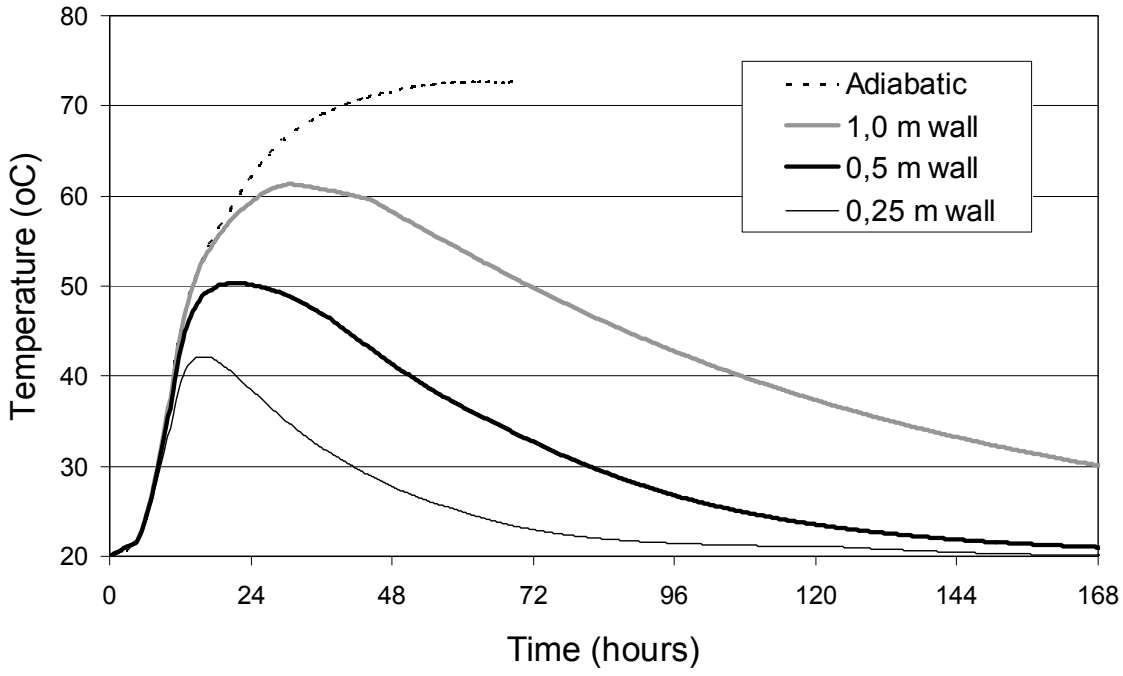

Figure 33 Examples of core temperature development for a given concrete used in walls of varying thickness (all walls has the same degree of insulation). The adiabatic temperature increase is also given.

The temperature variations in the hardening concrete create thermal dilation (thermal strain). The relationship between the change in temperature (ΔT) and thermal dilation (ε_T) is given by the thermal expansion coefficient (α_T) according to:

Equation 9

$$\varepsilon_T = \alpha_T \cdot \Delta T$$

If α_T is unknown the value $10 \cdot 10^{-6}$/°C (0.01‰ /°C) is often used as a "default" value for concrete. This means that a ΔT of, for example, 40°C cooling will cause a thermal contraction, ε_T, of $10 \cdot 10^{-6}$/°C × 40°C = $400 \cdot 10^{-6}$ (0.4‰). For a concrete structure 10 m long, this results in a contraction of ($400 \cdot 10^{-6}$ x 10000 mm =) 4 mm. If the restraint is sufficiently high, the result might be vertical through-cracks.

In reality, the thermal expansion coefficient α_T of concrete depends on the type of aggregate and the moisture condition of the cement paste, and the actual α_T will often deviate significantly from the 'standard value' of $10 \cdot 10^{-6}$/°C. Table 1 shows α_T data for some minerals and rock types and, as can be seen, large variations exists. Generally quartz has a high α_T value while calcite has a low value. The variations in α_T for aggregates are reflected in concrete, which is not surprising since aggregate makes up 65-70% by volume of concrete. The literature indicates a variation range of 5.6-13$\cdot 10^{-6}$/°C for α_T in concrete (ASTM 169B). Using the standard value $\alpha_T = 10 \cdot 10^{-6}$/°C to calculate thermal dilation will therefore often introduce inaccuracies in the calculated thermal dilation and, consequently, also inaccuracies in stress calculations.

The moisture condition of the cement/binder phase also influences α_T. A semi-dry cement paste (relative humidity RH = 60-80%) has a significantly higher α_T (around $20 \cdot 10^{-6}$/°C) than a water-saturated one (around $10 \cdot 10^{-6}$/°C) [108]. This moisture effect is related to the fact that the α_T for a semi-dry cement paste is made up of two dilation components:

(1) a fundamental thermal dilation component; similar to most materials.
(2) for intermediate RH-levels a thermal dilation component which is related to thermally induced RH-change (caused by redistribution of moisture) within the pores of the concrete. During heating the internal RH will increase, producing an expansion in addition to the fundamental expansion, and vice versa. For water-saturated or completely dry cement paste there is no component (2). [93].

The influence of cement paste RH and -volume on α_T in concrete is clearly shown in Figure 34. The concrete (around 65-70% aggregate) and pure cement paste (0% aggregate) measurements were done on 6 months old samples. All specimens were subjected to temperature changes between 20 and 40 °C. The letters Q and QK means quarts-rich sand (Q) and a 1:1 combination of quarts-rich sand and limestone (QK).

As mentioned earlier, hardening concrete will self-desiccate and the relative humidity (RH) in the pore system will decrease over time. This means that the cement paste dilation component (2) ('thermally induced RH-change') increases and thus contributes to increasing α_T over time for concrete. Measurements of a hardening w/b=0.40 cement paste and corresponding concrete are shown in Figure 35. At the end of each test the specimens were water-cured (water cured and water-pressurized, respectively) with immediate reduction of α_T as a result (i.e. elimination of component (2)). In the fresh phase (before t_0) α_T is high due to the dominance of free water, which has a very high α_T.

α_T for different hardening concretes (after t_0) is shown in Figure 36. α_T is generally low around setting (from around t_0) and increases gradually after that. Over time the trend is more α_T-increase for low w/b-ratios, because of the most pronounced self-desiccation. Note that the concrete with the

extremely low w/c ratio of 0.23 (high and fast self-desiccation) attains a very high α_T at an early stage, while the concrete with the highest w/b-ratio of 0.6 has the most moderate increase over time (slow/moderate self-desiccation). The four concretes with w/b=0.40-0.50 uses very different aggregate types. The measurements were carried out in the laboratory by varying the temperature of the samples between 23 and 17°C, measuring the thermal dilation during each temperature change and then calculating α_T according to Equation 9.

It should be mentioned that variable results for the time-dependence of α_T is reported in international literature. Constant α_T over time, increasing α_T over time and even decreasing α_T over time has been reported. The reasons for this evident discrepancy are not clear, but the type of binder and water-to-binder ratio will naturally have an influence. In view of the discussion above it appears that a reason may also be lack of moisture control.

Table 1 **Coefficient of thermal expansion for some minerals and rock types. [110]**

Mineral	**Rock**	α_T **[10^{-6} / °C]**
Calcite (pure calcium carbonate)		4 - 6.5
Plagioclase		3.8 - 5.8
Quartz		10.6 – 15
	Limestone	5
	Marble	6.3
	Trondheimite	7.2
	Gneiss	7.3
	Basalt	8.5
	Sandstone	11
	Quartzite	12.1

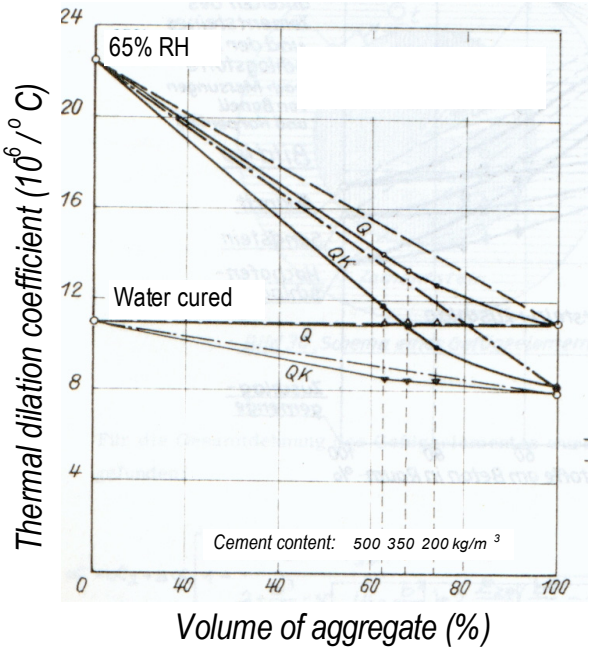

Figure 34 Coefficient of thermal expansion, effect of aggregate content and RH (relevant for concrete: 65-70 vol% aggregate). [94]

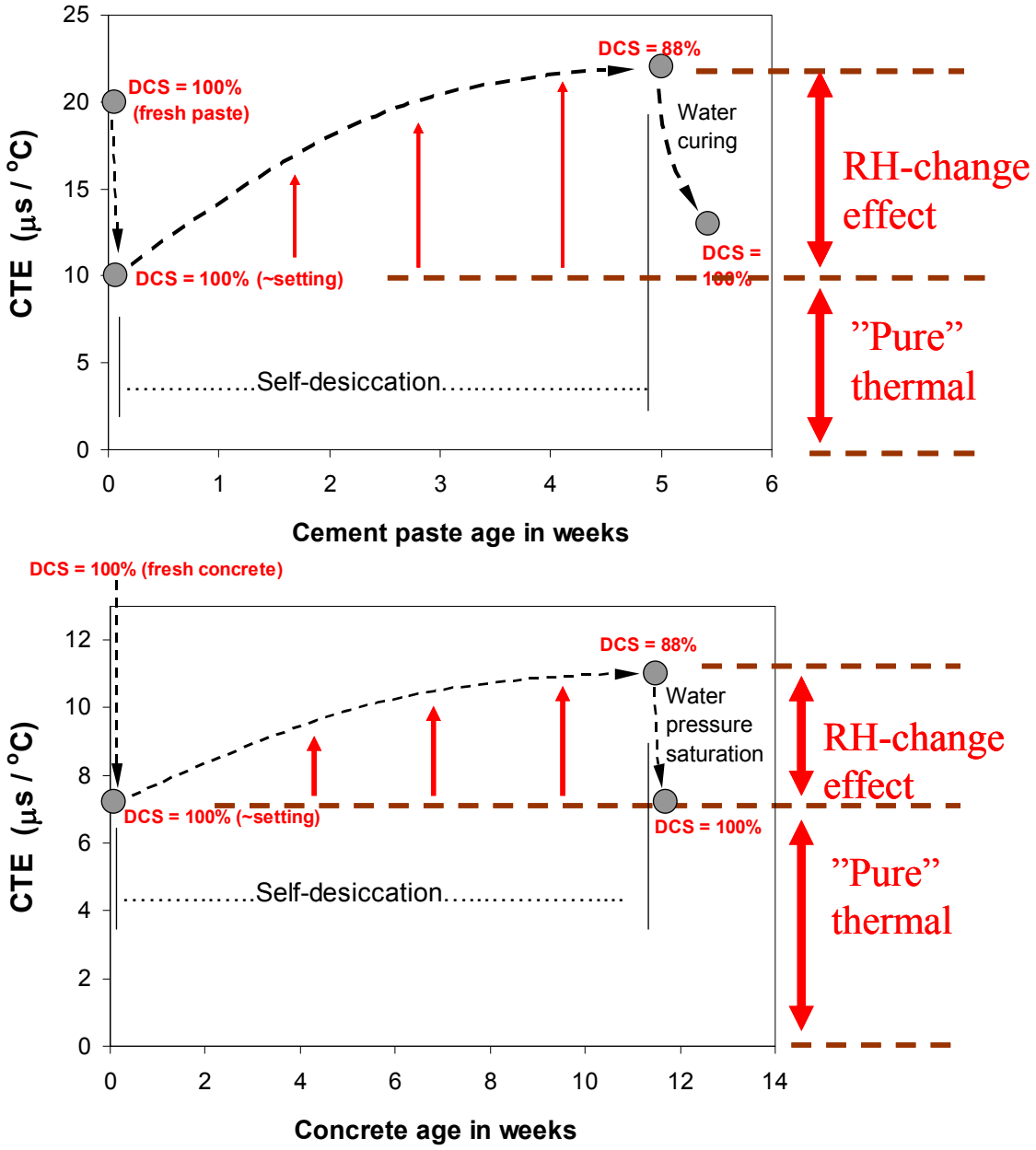

Figure 35 Measured coefficient of thermal expansion (CTE) as a function of time (self-desiccation): (a) cement paste sample (w/b=0.40) and (b) a concrete sample made with the same cement paste. Based on temperature variations between 23 °C and 17 °C. DCS=degree of capillary saturation [82]

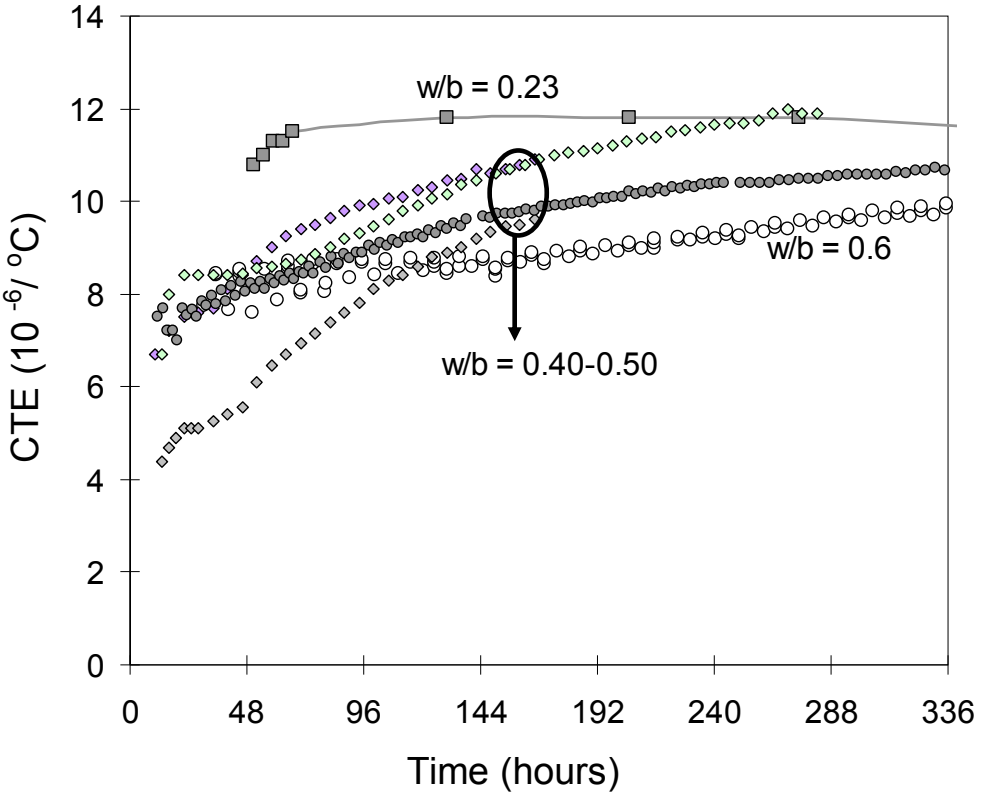

Figure 36 Laboratory measurements of the coefficient of thermal expansion (α_T = CTE) over time for different concretes with variable water-to-binder (w/b) ratio. [82]

7.4 Thermal dilation and autogenous shrinkage in structures

The hydration heat always creates thermal changes in hardening structures, as already discussed. Thermal dilation and autogenous shrinkage therefore take place simultaneously. Thermal dilation is dominant in most cases, but autogenous shrinkage can also play a significant role in many cases, particularly in low water-to-binder (high strength) concretes.

In hardening phase stress calculations, the effect of the two driving forces must be implemented by means of separate formulations/models. In tests it is simple to measure the total deformation; this is done simply by applying a realistic temperature history (ΔT) to a specimen and then measuring the total deformation (ε_{tot}) directly during the test, but what is the thermal- and what is the autogenous effect is not obvious. One way to separate the two effects is to conduct tests with rapid temperature changes to determine the thermal expansion coefficient (α_T), and then calculate the thermal dilation ($\alpha_T \bullet \Delta T$). The autogenous shrinkage (ε_{as}) is then determined as the difference:

Equation 10

$$\varepsilon_{as} = \varepsilon_{tot} - \alpha_T \bullet \Delta T$$

Examples from a dilation test program on a w/b=0.40 concrete is shown in Figure 37, where the maximum temperature during each test is indicated. The temperatures were imposed to the specimens by a temperature control system and also measured in the concrete during each test. The different specimen temperature developments (either smooth or step curves) produce mirror images as measured total deformation curves. As can be seen, the companion "smooth" and "saw-toothed" realistic temperature gives overall the same total deformation, but only the imposed saw-toothed

temperatures allow a separation between thermal dilation and autogenous shrinkage. At each temperature step α_T can be calculated and during each period with constant temperature the measured deformation reflects autogenous shrinkage (and swelling (!)) directly.

Calculated α_T-values from the saw-toothed test "50" are shown in Figure 38. α_T drops from a high value initially, but increases with time after t_0, as shown earlier. A variable function is fitted to the α_T-results and such function could in principle be used in stress simulations. The tradition is, however, to use a constant (average) α_T in simulations for simplicity. When a simplified and constant α_T is used to calculate the thermal component from a dilation test the remaining deformation is then a somewhat incorrect determination of autogenous shrinkage, see Equation 10. However, when the two deformations (thermal+autogenous) are summarized in a simulation the sum will be quite correct as long as the overall temperature in the structure is rather similar to the one from the test. Therefore, it is proposed to consider what temperatures will occur in the given structure before performing a dilation test (see also Ch.15). From a "smooth" temperature dilation test the thermal (α_T) and autogenous part cannot be separated, and α_T must be "guessed". The deduction of the individual development of the two deformations therefore gets more uncertain. Still, as mentioned above, the calculated total deformation in simulations will be quite precise when test- and structure temperature are rather similar.

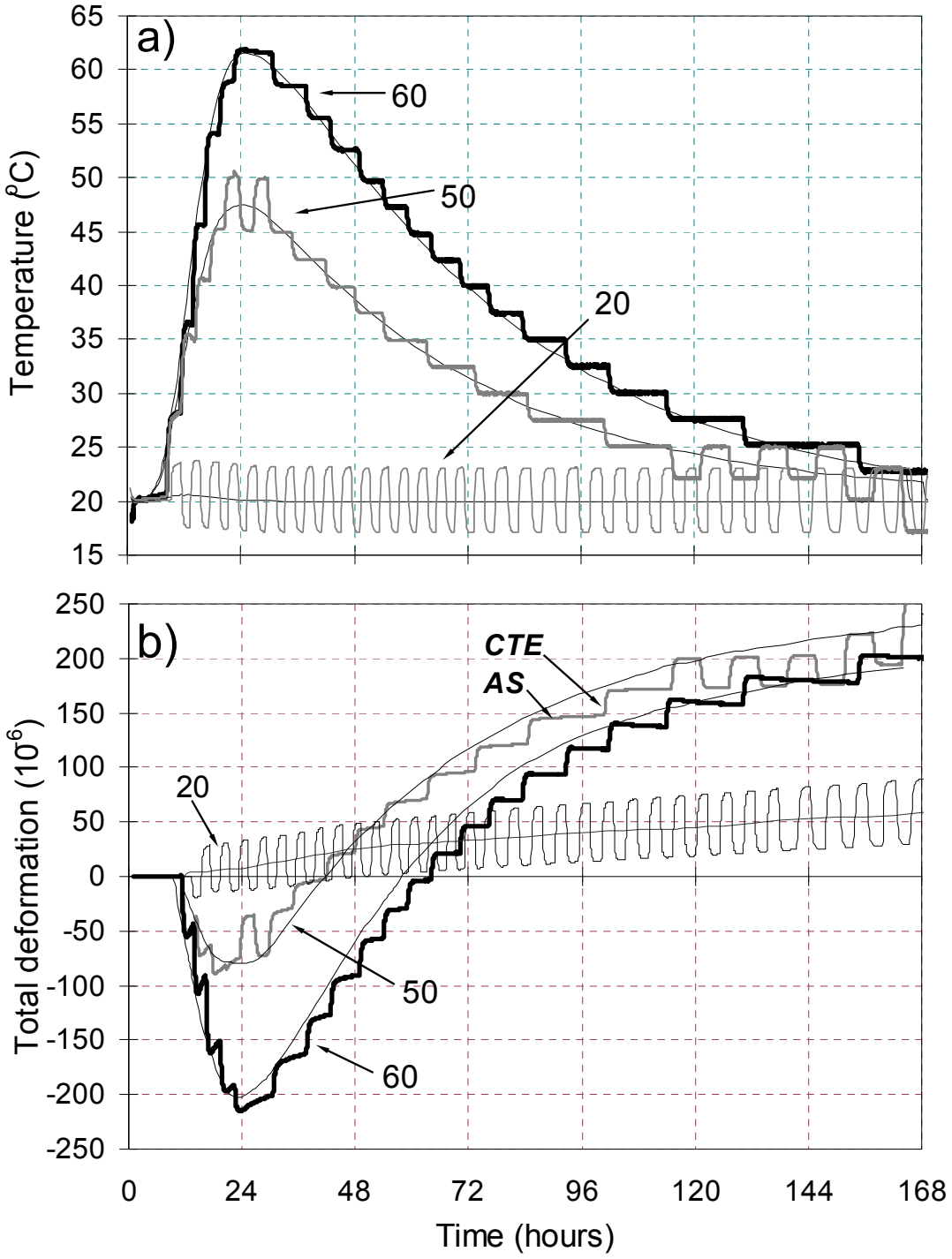

Figure 37 Dilation tests: (a) Measured (and imposed) smooth- and "saw-toothed" temperature histories, and (b) measured total deformation.[82]

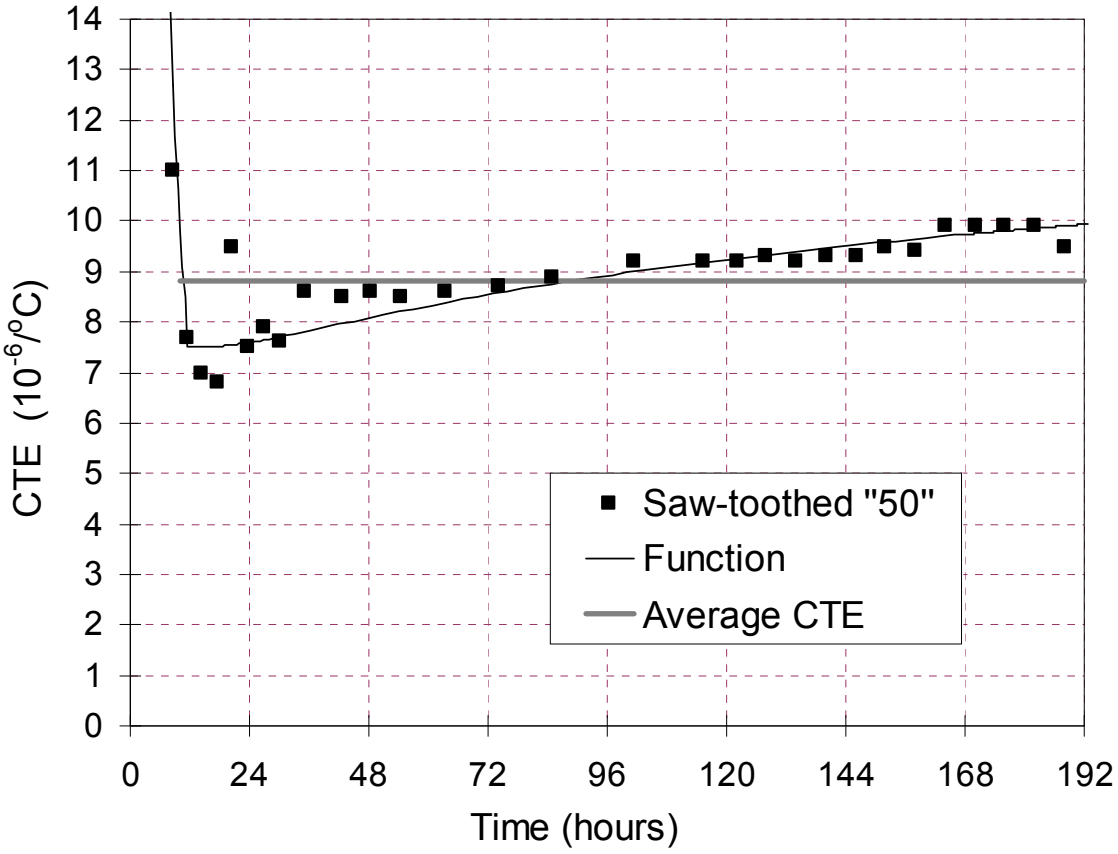

Figure 38 Calculated coefficients of thermal expansion (CTE) from the saw-toothed test "50" (as shown in Figure 37)

The relative importance of thermal dilation and autogenous shrinkage in generating stresses is illustrated in the following. The example in Figure 39 shows a concrete specimen that was subjected to a realistic temperature history with T_{max} = 48°C (Figure 39-a). The total deformation was measured directly in a (free) dilation test. Thermal dilation and autogenous shrinkage were then deduced by means of the procedure described above (by means of a saw-toothed temperature test). Note that the temperature curve in Figure 39-a was calculated first by a 2D-program, then applied to the test specimen by means of a temperature control system and simultaneously measured in the specimen as control.

In a parallel restraint specimen test (subjected to the same temperature history), the stress was measured at 100% restraint conditions, see curve labelled "measured" in Figure 39-b. The restraint specimen developed failure in tension after approximately 60 hours. However, what is the most important here is the calculated stresses, which are also given in the figure. These are stress calculations based on E-modulus and creep data for the same concrete and use of the calculation principle "linear superposition with aging effects" [82] . Three calculations were carried out to illustrate the relative contribution of thermal dilation and autogenous shrinkage in terms of stress generation in this particular test:

1. One calculation with the total deformation from the dilation test as input (Figure 39-a). It can be seen that the calculation agrees well with the 100% restraint test (before tensile failure), as it should since it is the total deformation that is the driving force to the

development of stresses in the test. Note that in calculations the stresses can go far above the realistic tensile stress capacity of the concrete.

2. One calculation using only thermal dilation as input. It can be seen that when autogenous shrinkage is not included in the calculation, the calculated compressive phase is overestimated and the subsequent tensile phase underestimated.
3. One calculation using only autogenous shrinkage as input. Not surprisingly, the calculated stress now goes directly into tension. It also shows that autogenous shrinkage alone contributes to 1.5 MPa tension in the concrete after 1 week (168 hours) and it clearly plays a significant role for this particular concrete.

In this specific example autogenous shrinkage contributes to 27% of the tensile stresses after 1 week, while thermal dilation is responsible for the remaining 73%. In other words, it is absolutely necessary to include both types of deformation in stress calculations. The relative contribution from autogenous shrinkage may however be different than shown here, depending on the composition of the concrete and the temperature history.

An illustration of the influence of autogenous shrinkage on the total deformation of concretes is shown in Figure 40, where four different concretes (all with w/b=0.40) display very different behaviour despite that the temperature history in the tests was the same. During the cooling phase thermal contraction and autogenous shrinkage work “together”, producing the net contraction of the concrete. The different behaviour is caused by very different autogenous shrinkage since the coefficient of thermal expansion (α_T) for the concretes varied very little [82], i.e. the concrete composition plays a major role for autogenous shrinkage, but less for α_T (of course assuming similar aggregate properties). Larger contraction due to autogenous shrinkage is unfavourable with regard to the probability of cracking.

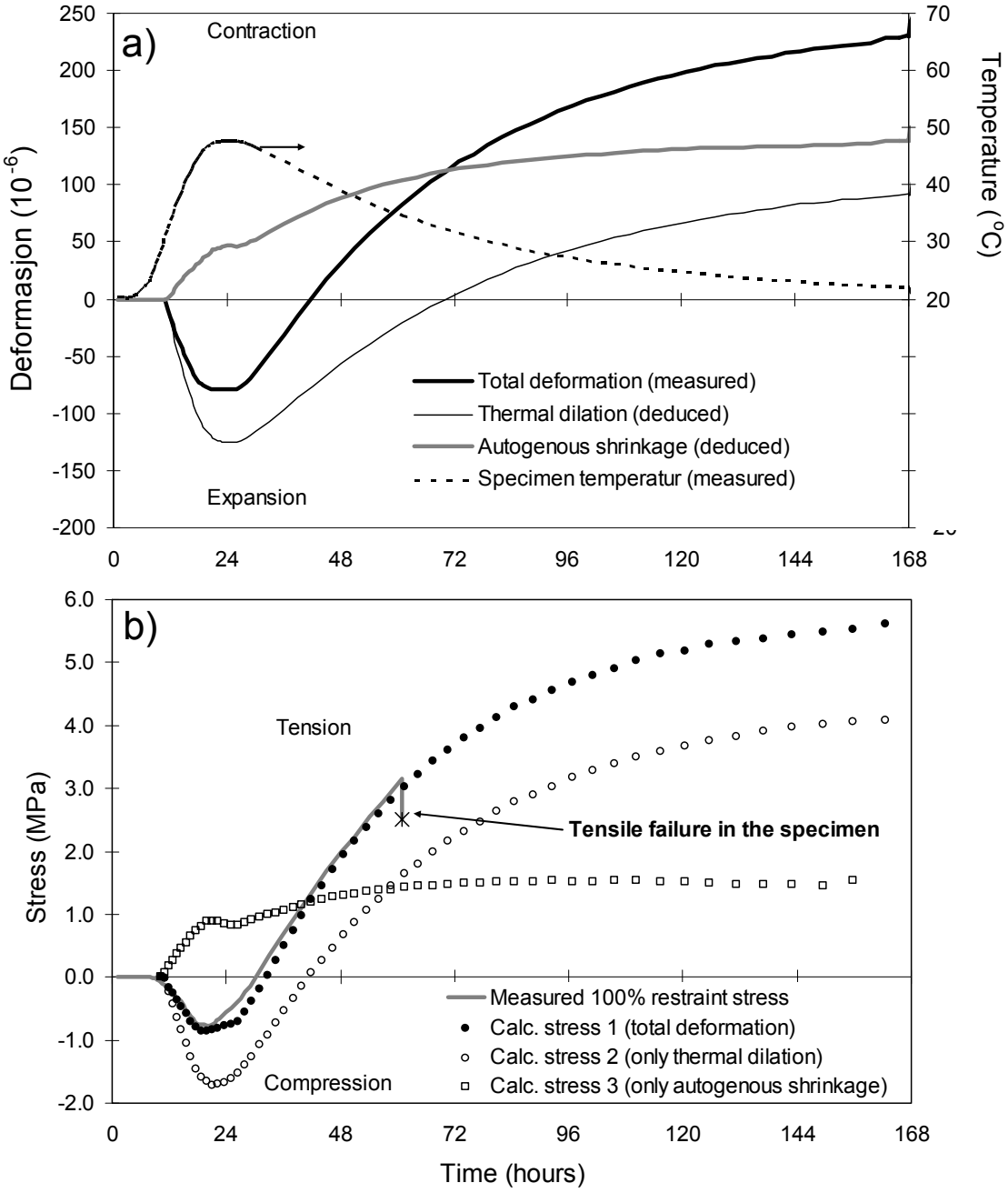

Figure 39 a) Free dilation test (from t_0), and b) 100% restrained stress for a concrete with w/b=0.40 subjected to a realistic temperature history. In a) the temperature and total deformation are measured directly in the test, while individual contributions from thermal dilation and autogenous shrinkage are deduced by means of a supplementary test. In b) one curve is the measured 100% restraint stress and three curves are based on calculations (see text). [82]

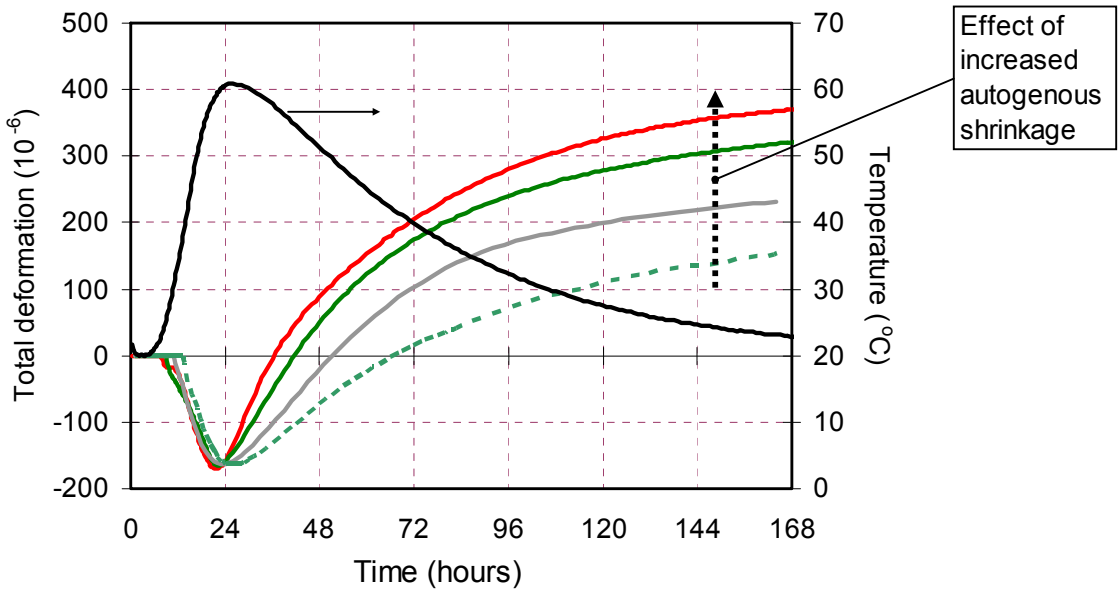

Figure 40 Total (free) deformation from dilation tests (plotted from t_0): Four different concretes (all with w/b=0.40) were subjected to the same temperature history, as indicated. The different total deformation behaviour is due to very different autogenous shrinkage among the concretes. [82]

To make general models for autogenous shrinkage has proven to be difficult because the behaviour of autogenous shrinkage may totally change its character during realistic (i.e. variable) temperature histories. This is especially the case at high maximum temperature histories, which may produce thermally induced autogenous swelling. The term autogenous shrinkage is used in this report despite the fact that autogenous strains may be both shrinkage and swelling. Thus, a better and more neutral term of the phenomenon is probably autogenous deformation. The temperature effect on autogenous shrinkage is discusses in for instance [82][93][95][96] and [108][109].

The dilation test example in Figure 41 shows clearly the unsystematic effect of realistic temperatures on autogenous shrinkage/swelling, where all tests are for the same concrete [82]. Figure 41-a gives the maximum temperature (around 24 hours) in each test as well as measured total deformation. For the isothermal test (20 ^{o}C) the measured result directly reflects autogenous shrinkage since there is no temperature change. The coefficient of thermal expansion (α_T) for this concrete was found in supplementary tests (actually those in Figure 37) and used to deduce autogenous shrinkage for the realistic temperature tests, see Figure 41-b. The trend is that the initial rate of autogenous shrinkage increases with temperature maxima, but it is clear that the overall temperature effect is unsystematic with respect to both the magnitude of autogenous "shrinkage" and to the development with time (thus the behaviour cannot be presented coherently by the maturity concept). For the "60 ^{o}C" case the autogenous deformation even turns to expansion after about 3 days. This phenomenon has been observed in several other cases [82][93][94][95][96] – and it is considered to be real - but today we do not have sufficient knowledge to predict the occurrence of the effect, and far from enough to formulate a general model. For more reading on this topic, see APPENDIX 1 and APPENDIX 2.

(a)

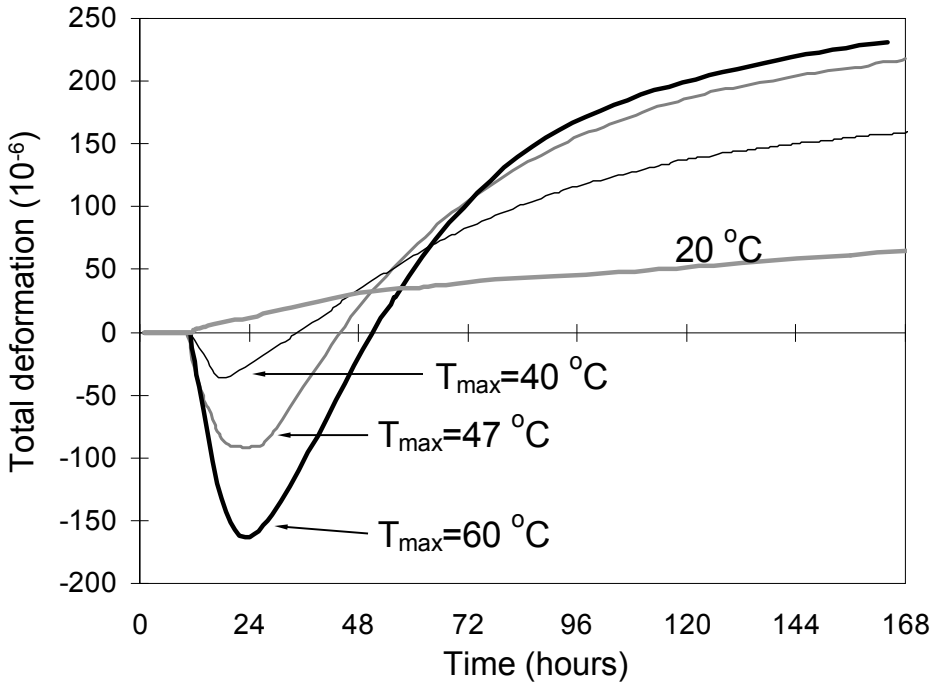

(b)

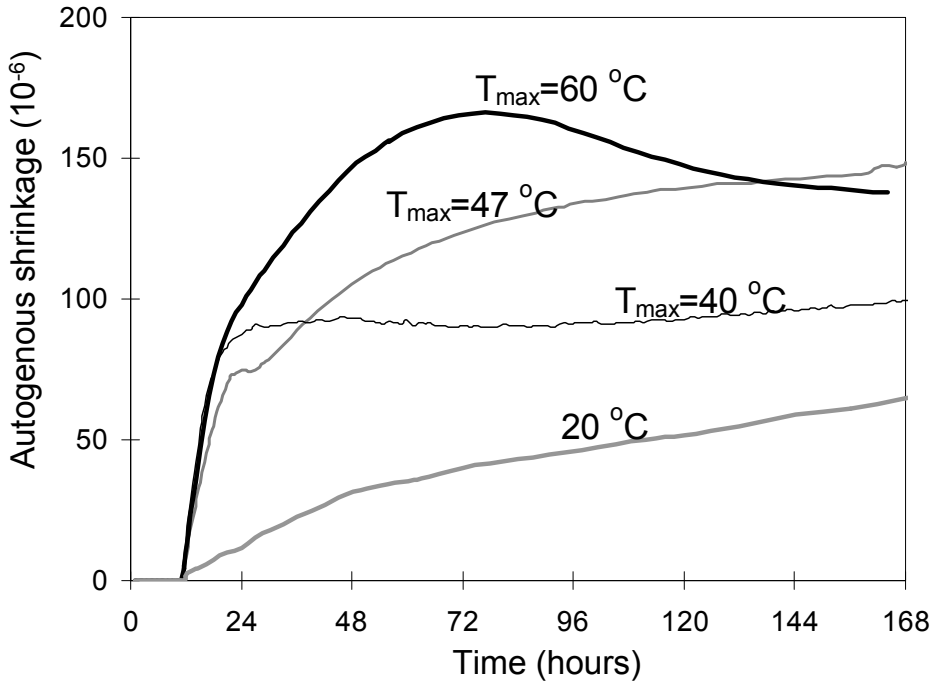

Figure 41 Results from several Dilation rig tests (from t_0) on the same concrete subjected to different realistic temperature histories. (a) Total deformation (thermal dilation + autogenous shrinkage), where the maximum temperature in the test is given. One test had constant (isothermal) temperature (20°C). (b) Autogenous shrinkage as deduced from Fig.(a) according to the procedure described in Section 7.4. [82]

8 Concrete properties input data for simulations

8.1 General

Hardening phase simulation programs needs continuous data for the concrete property development from time=0 (time of mixing) and through the entire hardening phase. For implementation such data is normally formulated as mathematical functions after fitting to experimental data, or discrete data taken directly from experiments; the choice depending on the degree of freedom given by the simulation program. Functions as well as discrete data are normally implemented as a function of maturity time, hence many simulation programs uses maturity as time parameter to calculate the concrete property development for any arbitrary temperature history. This type of input data can be denoted as "empirically based engineering models", hence the term "model" is somewhat pretentious since it is often only a question of curve-fitting of functions to empirical data for a given concrete. Examples of such empirically based "models" (i.e. functions and discrete data) are given in the following.

Some simulation programs uses what could be denoted as "fundamental materials models". Such models go into the chemistry and various hydration reactions of cement paste and concrete on a nano-level and simulate the concrete hardening process through the growth of hydration products and pore structure according to w/b-ratio, cement- and aggregate type etc. This type of models and programs are not dealt with here, since none have been applied successfully to for instance autogenous shrinkage.

8.2 Hydration heat

An exponential function used in Norway for many years for expressing heat generation in concrete is given in Equation 11. The function was first introduced by Freisleben-Hansen [27] in Denmark, and, for instance, the present simulation programs "4C-Temp&Stress" and "b4-Cast" use this function.

Equation 11
$$Q(t_{eq}) = Q_{\infty} \cdot \exp\left[-\left(\frac{\tau}{t_{eq}}\right)^{\alpha}\right] \qquad \text{(Danish model)}$$

where $Q(t_{eq})$ [J/kg] is the heat generation as a function of maturity time (=equivalent time) t_{eq} [h], Q_{∞} [J/kg] is the final heat generation after 'infinite' time and is a curve-fitting parameter together with τ [h] and α[–].

An exponential function developed in Sweden is given in Equation 12. The Swedish simulation program "ConTeSt-Pro" applies this function.

Equation 12
$$Q(t_{eq}) = W_{\infty} \cdot e^{\left(-\lambda_1 \cdot \ln\left(1+\frac{t_{eq}}{t_1}\right)\right)^{-\kappa_1}} \qquad \text{(Swedish model)}$$

where $Q(t_{eq})$ [J/kg] is the heat generation as a function of maturity time (=equivalent time) t_{eq} [h], W_{∞} is the final heat generation after 'infinite' time and is a curve-fitting parameter together with λ_1, t_1, κ_1. The parameter λ_1 is mathematically coupled with κ_1, therefore $\lambda_1 \equiv 1.0$ is normally used without changing the degree of freedom of the function.

An example of fitting the two models to experimental data is given in Figure 42. The example is for a concrete with a binder consisting of fly-ash (CEM II). As can be seen, the fit between the models and the experimental data are quite good, but the models do not quite "capture" the details of the hydration heat curve. This "limitation" of exponential functions with regard to fit data is typical for concretes where the pozzolanic (silica fume and/or fly ash) addition is considerable. Concrete with little or no pozzolans (CEM I) has a more "S-shaped" hydration heat; which is a behaviour the models are best suited for. In other words, for this particular concrete, it may be adequate to use the experimental data directly in the simulation; some programs give this option (see "discrete data" in the figure). However, the use of discrete data or modelled data does not necessary give any significant effect on the accuracy in temperature simulations. Anyhow, it is worth noting that inaccuracies in the temperature simulation have direct influence on the stress simulation.

In Norway an easy-to-use excel sheet made by Smeplass [68] for converting measured temperatures from semi-adiabatic calorimeters to isothermal heat data has been used for many years. The excel sheet has been updated many times since the original version.

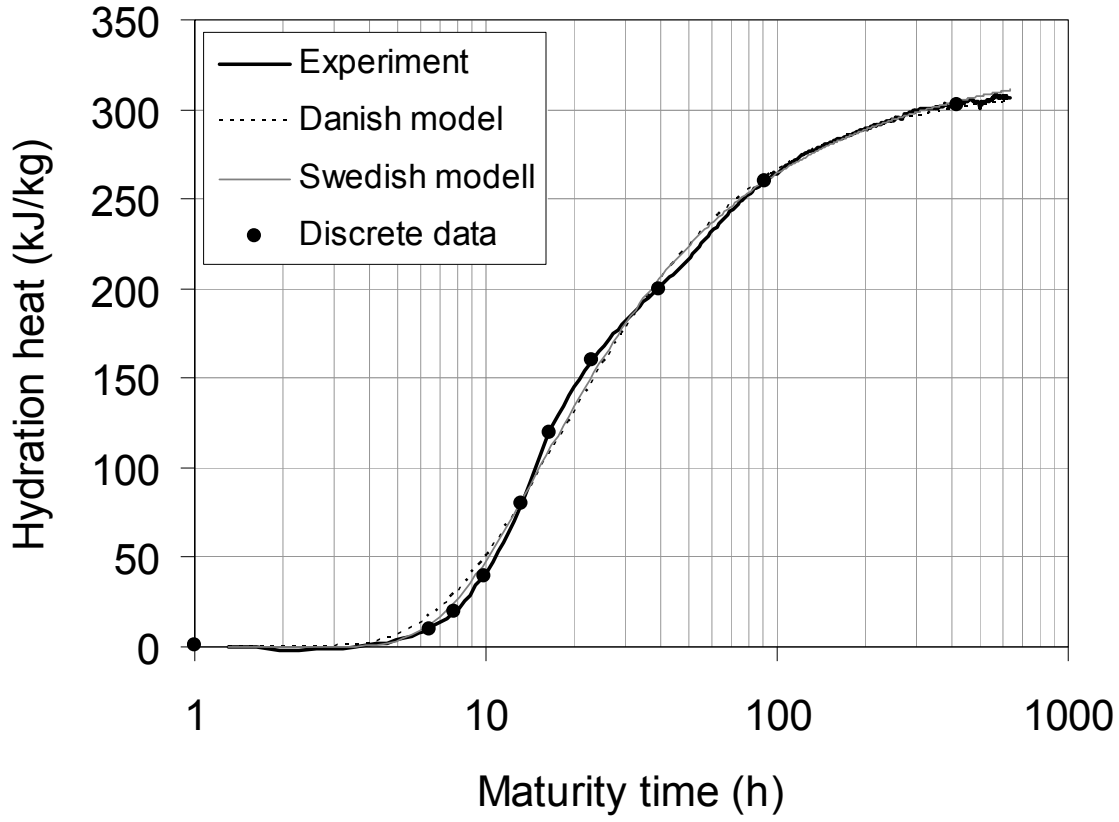

Figure 42 Example of isothermal heat (i.e. heat vs. maturity) generation for a concrete (with Cem II/A-V), and best fit of the two models described above. Discrete data can also be used as input for temperature simulations.

8.3 Coefficient of thermal expansion

The thermal dilation is the product of the temperature changes in the structure and the coefficient of thermal expansion (α_T), as discussed earlier. In Norway (and most other countries) a constant (average) α_T is normally used as input for calculations, even though we know that it may vary during the hardening phase. This simplified input for α_T will not introduce much inaccuracy in structure simulations of the total deformation provided that the deformation data are based on realistic temperature dilation tests and that autogenous shrinkage is deduced according to the procedure described in Section 7.4.

8.4 Autogenous shrinkage

The tradition in Norway has been to implement autogenous shrinkage data for calculations as discrete data (vs. maturity), preferably deduced from experiments performed under a temperature history that is as realistic as possible for the given field condition. Autogenous shrinkage from isothermal tests is first and foremost a reference showing the autogenous shrinkage "potential" for a given concrete, but using such isothermal data for simulations is definitely better than having nothing at all. Applying the maturity principle blindly to autogenous shrinkage (from isothermal tests) is clearly doubtful on a fundamental level, and may be very misleading. If no specific data is available, the approach must then be to use other data on rather similar concretes. Naturally, the quality of the simulation results will then be more uncertain.

A model for autogenous shrinkage based on empirical results from isothermal tests is actually developed in [97]. The general validity of the model appears to be limited as it is an average of different concretes as well as is does not take into account realistic (i.e. variable) temperature effects. It can however serve as a "first approximation" on the autogenous shrinkage behaviour if no other data is available.

Due to the autogenous swelling phenomenon at high and realistic curing temperatures an isothermal test is likely to provide inaccurate information on how autogenous shrinkage will develop on-site. Free dilation tests performed at realistic temperatures therefore provide the most relevant and "safe" data for simulations. When such dilation test(s) shall be carried out this means that hydration heat for the specific concrete must be measured prior to the dilation test, followed by a temperature simulation of a relevant structure. A representative temperature history from this simulation can then be used to control the temperature of the specimen in the dilation test.

8.5 Compressive strength, tensile strength and E-modulus

The "Danish" model for hydration heat discussed above (Equation 11) has also been used to express the mechanical properties: compressive strength, tensile strength and E modulus. If we give these properties the symbol "*X",* the general equation for the model will then be:

Equation 13

$$X(t_{eq}) = X_{\infty} \cdot exp\left[-\left(\frac{\tau}{t_{eq}} \right)^{\alpha} \right]$$

where $X(t_{eq})$ is the given mechanical property as a function of maturity time (=equivalent time) t_{eq} [h], X_{∞} is the property after 'infinite' time and is a curve-fitting parameter together with τ [h] and α.

At the Norwegian University of Science and Technology (NTNU) a function containing a t_0-parameter was introduced [81][99][101], see Equation 14. The model is a modified CEB-FIP model code formulation and is adapted, for instance, in the programs DIANA and in ConTeST-Pro:

Equation 14
$$X(t_{eq}) = X_{28} \cdot \left\{ exp\left[s \cdot \left(1 - \sqrt{\frac{672 - t_0^{(*)}}{t_{eq} - t_0}} \right) \right] \right\}^n$$

where X is the mechanical property as a function of maturity time t_{eq} [h] ($>t_0$), X_{28} is the property at 28 days (=672 hours), s and n are curve-fitting parameters and t_0 is the maturity time when the properties start to develop. The t_0-parameter marked $t_0^{(*)}$ ($=t_0$) was not present originally in [81], but later introduced in ConTeSt Pro [115].

The Equation 14-formulation for compressive strength f_c, tensile strength f_t and E modulus E_c, respectively, then becomes as follows:

Compressive strength:
$$f_c(t_{eq}) = f_{c28} \cdot \left\{ exp\left[s \cdot \left(1 - \sqrt{\frac{28 - t_0^{(*)}}{t_{eq} - t_0}} \right) \right] \right\}^{n_c}$$ where n_c=1

Tensile strength:
$$f_t(t_{eq}) = \mathrm{f_{t28}} \cdot \left\{ exp\left[s \cdot \left(1 - \sqrt{\frac{28 - t_0^{(*)}}{t_{eq} - t_0}} \right) \right] \right\}^{\mathrm{n_t}}$$

E modulus:
$$E_c(t_{eq}) = \mathrm{E_{c28}} \cdot \left\{ exp\left[s \cdot \left(1 - \sqrt{\frac{28 - t_0^{(*)}}{t_{eq} - t_0}} \right) \right] \right\}^{\mathrm{n_E}}$$

Note that the s-parameter is common to all properties, while the n-parameter varies with property [99][101].

In contrast to hydration heat (which is continuous) it takes a certain time for the concrete to develop mechanical properties. Therefore, the parameter t_0 is common in the above functions and it is very useful for stress calculations since it ensures a consistent (and realistic) starting point for the properties and, thus, the stress development in simulations. The maturity time at which mechanical properties start to develop (i.e. at t_0 from which stresses start to develop) corresponds typically to a degree of hydration of 10-20% [101][103].

In addition to the t_0 parameter, the parameter s is also common, and it can therefore in principle be determined from compressive strength tests. Note that the compressive strength is not part of stress simulations, but it is generally used as a "tool" to determine the temperature sensitivity (activation energy) of the concrete and, thus, for all the other properties.

For tensile strength f_t and E-modulus E_c it then remains to determine their 28-day value and the associated curve-fit parameter n_t and n_E [99][101].

Figure 43 is based on experiments and shows the relative mechanical property development over time expressed by the above functions. Relative development means that the properties are related to their 28-day value and all are therefore 1.0 after 28 days. We see that t_0 is 10 hours for this

concrete. The figure illustrates a typical feature for concrete: the relative development of the E-modulus (E) is fast, the tensile strength (f_t) somewhat slower and the compressive strength (f_c) is the slowest. In principle this is unfortunate in that an early deformation is multiplied by an early E to produce a stress that may challenge the slower f_t.

Examples of the "Danish" model (Equation 13, Model I) and the 'NTNU' model (Equation 14, Model II) fitted to experimental E-modulus data are shown in Figure 44. It is clear that the models are quite different – particularly at the start. The disadvantage of Model I is that it has no t_0-parameter and therefore expresses E-modulus values in the fresh phase – which is not correct, and stresses will be overestimated in the early phase and this will then result in a permanent inaccuracy throughout the entire calculation period. Model II (Equation 14), on the other hand, expresses to a larger extent the real concrete behaviour.

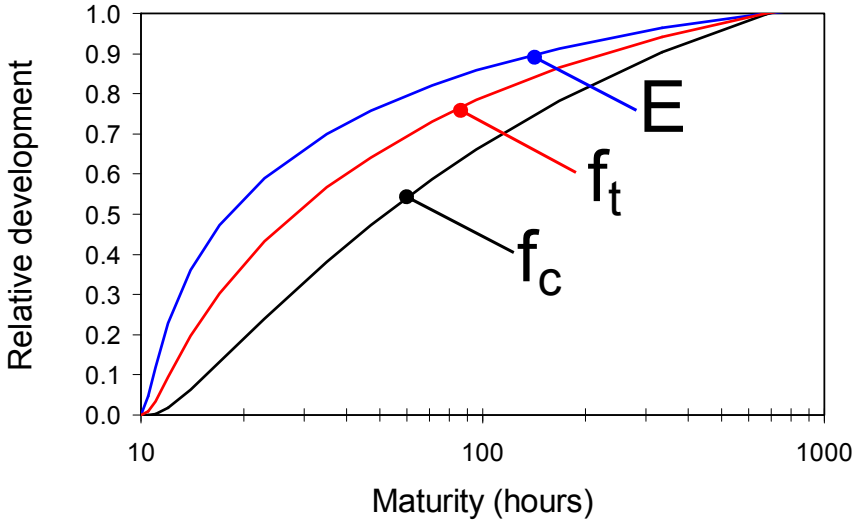

Figure 43 Example of the relative development of E modulus (E), tensile strength (f_t), and compressive strength (f_c). The properties have been normalised with regard to their 28-day value, i.e. all properties are 1.0 at 28 days (= 672 hours). The curves are based on experimental data.[99]

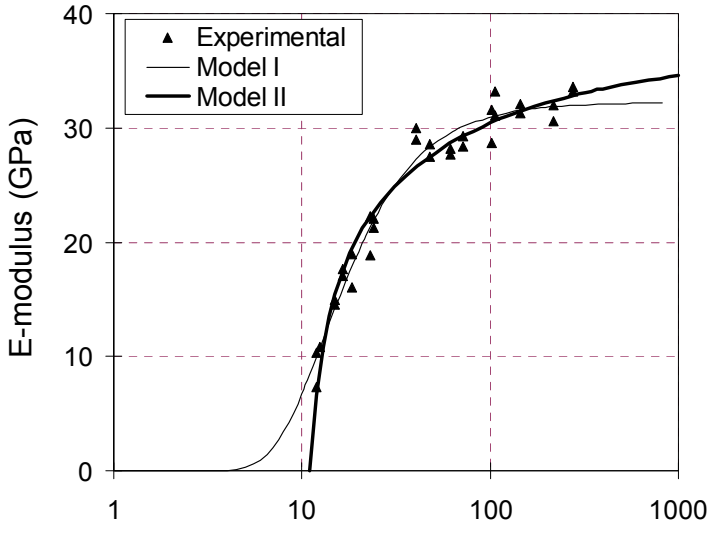

Figure 44 Example of curve-fitting to experimental E-modulus data. Model I=Equation 13 and Model II=Equation 14.

8.6 Uniaxial tensile strength versus splitting strength

The tensile strength of concrete is normally determined by either splitting tests or uniaxial (direct) tension tests, see Figure 45. Uniaxial tensile strength are considered to be the most true tensile failure property, hence in uniaxial tests the failure load directly reflects the tensile strength. Splitting tests is an indirect method and the compressive failure load (P) from the test must be transferred to splitting tensile strength by use of the formula shown in Figure 45. It is important to note that the results from the two methods may be quite different.

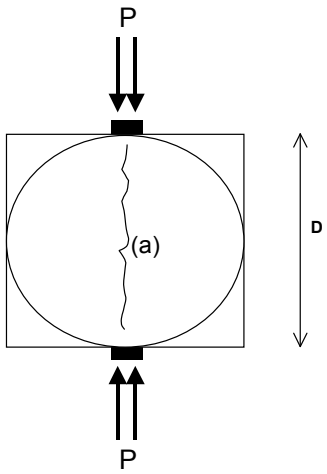

$$f_{ts} = \frac{2P}{\pi DL}$$

Figure 45 Set-up for testing tensile strength. Uniaxial strength test on prisms (left) and splitting strength test on cubes or cylinders (right)

A number of parallel uniaxial and splitting tests on various concretes were reported at NTNU in [99]. The uniaxial tests were on 100x100x600 mm prisms, while the splitting tests were on both 100x200 mm cylinders and 100 mm cubes. Applying linear regression analysis, the following relations between uniaxial tensile (f_t) and splitting strength (f_{ts}) were found:

Equation 15 $f_t = 0.79 \times f_{ts} + 0.53$ (100x200 mm cylinders)

Equation 16 $f_t = 0.77 \times f_{ts} + 0.21$ (100 mm cubes)

Only splitting strength values larger than 1.5 MPa were included, since lower values gave somewhat different trends and considered less certain as well as less practically relevant. The results are shown in Figure 46. If all results above 1.5 MPa are included, the standard deviation of the curves was 0.36 MPa both for the cylinders and the cubes. This is true under the assumption that the results have a normal distribution. Thus, either type of splitting test may be used to estimate the uniaxial tensile strength.

With increasing strength (i.e. increasing maturity) the trend is that splitting strength gives higher values than uniaxial strength. The trend is most pronounced for splitting strength from 100 mm cubes, giving more than 20% higher strength value than uniaxial strength for high strength values. Consequently, when calculating the crack index in crack risk assessments the use of splitting strength results directly will underestimate the cracking risk.

The results shown were based on concretes with w/b=0.40 (mainly CEM I) and standard Norwegian laboratory aggregate (from Årdal). It is likely that the correlation between splitting strength and uniaxial strength depends on w/b-ratio, binder- and aggregate type, hence the correlation may be different for other concretes than shown here. The lesson to be learned from this is that uniaxial tensile strength should be used when calculating the crack index, but the uniaxial strength can be deduced from splitting tests if a correlation is established. The most relevant tensile strength values in crack risk assessments are in the period when the critical time for cracking occurs, for many cases corresponding to a time of somewhere around 1-2 weeks of realistic curing temperature.

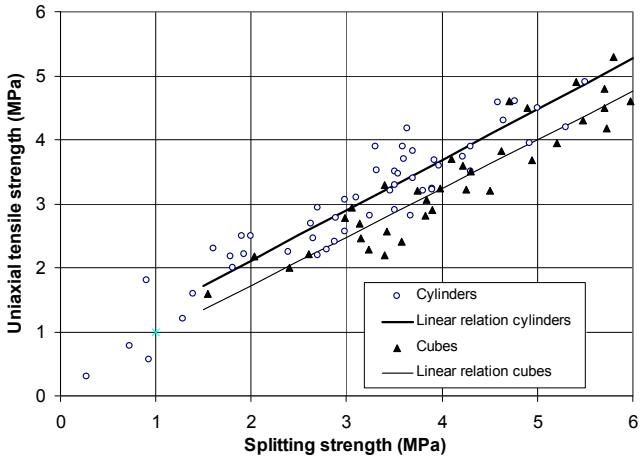

Figure 46 Uniaxial tensile strength versus splitting strength of 100x200 mm cylinders and 100 mm cubes. Each mark represents the mean strength of two or three specimen. [99]

8.7 Creep

Early age creep of concrete is generally measured in the laboratory by applying a constant load to specimens after different curing times and under isothermal conditions. In computer programs for time-dependent analysis of concrete structures, the creep modelling is usually based on linear visco-elasticity for ageing materials. For a general stress history, the strain ε (and stress σ) can in principle be determined from:

Equation 17

$$\varepsilon(t) = \int_0^t J(t,t') \times d\sigma(t') + \varepsilon_{as}(t) + \varepsilon_T(t)$$

Where t is the concrete age and t' the concrete age when the actual stress increment is applied, while ε_{as} represents the autogenous shrinkage and ε_T the thermal dilation. $J(t,t')$ is the compliance function (stress-dependent deformation).

The simple "Double power law" (DPL) has proven useful to express the creep development φ in hardening concrete (though many other formulations also exist). The compliance function $J(t,t')$, the creep ratio $\varphi(t,t')$, and the modulus of elasticity (E_c) can then be given by the following equations:

Equation 18

$$J(t,t') = \frac{1+\varphi(t,t')}{E_c(t'_e)} \quad \text{and} \quad \varphi(t,t') = \varphi_0 t'^{-d} (t-t')^p$$

Equation 19

$$E_c(t_e) = E_{t28}\left\{exp\left[s\left(1-\sqrt{\frac{28}{t_e - t_0}}\right)\right]\right\}^{nE}$$

Where t_e is the maturity (or equivalent time), t_e' is the maturity time at loading. t is the actual time, t' is the actual time when the stress increment is applied, and φ_o, d and p are the DPL model parameters. The expression for the E-modulus is the modified version of the CEB-FIB model, as shown earlier.

Figure 47 compares the compliance function $J(t,t')$ to compressive creep test results at NTNU. The values of the DPL creep model parameters φ_o, d and p were optimized to obtain the good agreement in the figure. The vertical part of each curve up to the indicated dots is defined as the elastic strain, while the rest is time-dependent creep strain.

Early age creep (visco-elasticity) of concrete has been a subject of much attention for many years. For Norwegian research, see for instance [84][83][85]. It is probably the most complex property to understand on a fundamental level. Creep results from simple isothermal laboratory tests and curve-fitting, such as shown in Figure 47, have however shown to give an acceptable basis for estimation of the time-dependent strains/stresses in structure simulations. This is in despite of the fact that creep depends on, for instance, type of stress (compression or tension), stress level, time of loading, temperature changes and temperature level. The implication of this is that all these effects are secondary (or self-compensating?) compared to the "basic" creep that is measured during standard laboratory conditions. This is comforting since these "extra"-effects are very challenging to verify accurately by experiments.

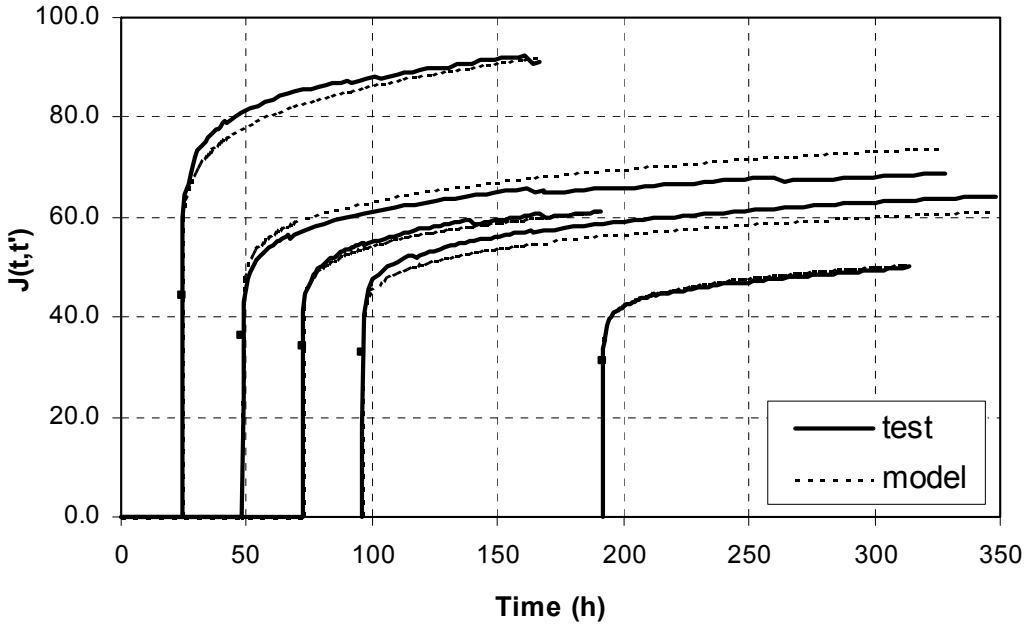

Figure 47 Compressive creep, test results and Double Power Law (DPL) model [84]

9 Simulation programs and input

9.1 Simulation programs

Simulation of the heat-flow in 1D, 2D and 3D simulations is illustrated in Figure 48. In 2D-simulations the temperature field in the mid-section (x-y plane) is calculated, assuming that all cross-sections in the structure have the same temperature field. This approximation is in most cases very accurate since only the end parts of the structure is subjected to heat exchange from the end surfaces. Thus, 2D simulates heat in the x-y plane and stresses out of the plane (z). In 3D simulations both heat flow and stress calculations are in the x, y and z direction (Figure 48 shows only half of the 3D-structure)

2D-programs usually model only a slice (the 2D cross-section) of the structure. The temperature development in the structure and temperature gradients over the cross-section can be accurately predicted. However, in order to calculate the principal (longitudinal) stress out of the plane, which is normally the important issue regarding through-cracking, simplifications must be done (compensation plane method, or Navier-Bernoulli hypothesis for infinitely long structure assumptions [118]). This ability to make assumptions on the structural response in the 3rd dimension is the reason why 2D programs are often denoted "2½D" programs. Consequently, the adequate use of 2D programs requires knowledge of the total 3D structural response and the transformation into 2D and 2½D models.

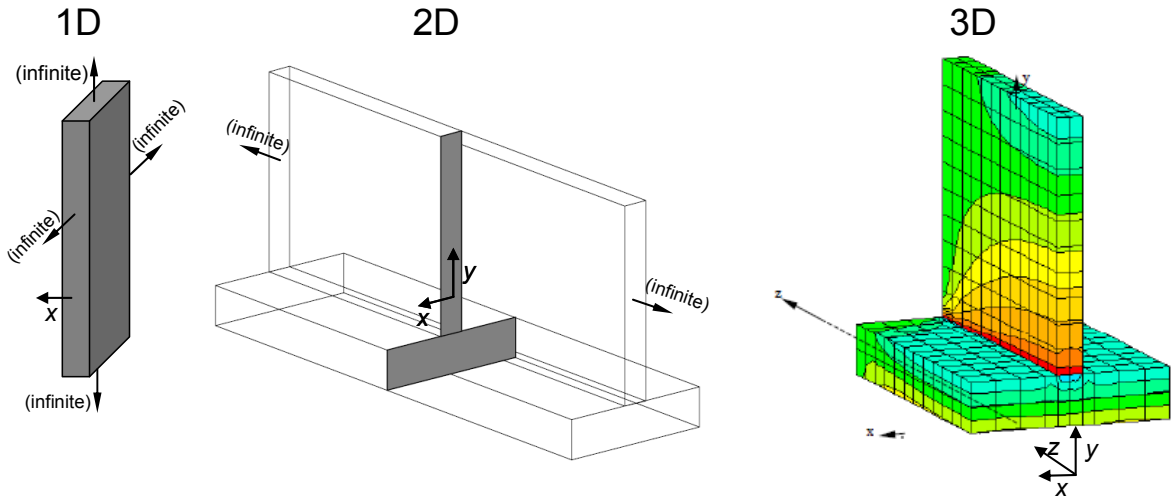

Figure 48 Illustration of directions of heat-flow in 1D (x), 2D (x-y) and 3D (x-y-z) simulations. In both 2D and 3D simulations the critical stress in the longitudinal z-direction can be calculated

Below is a list of some available 1D, 2D and 3D commercial simulation programs commonly used in the Nordic countries.

HETT97 (1D): Swedish (Cementa) user-friendly software that NORCEM has adapted to Norwegian conditions. The program is 1-dimensional (1D) and simulates temperature and compressive strength development, i.e. it is a "traditional curing technology program" and do not calculate stresses. Can be downloaded free of charge from the Norcem internet website.

4C-Temp&Stress (2½D): Danish user-friendly program for temperature and stress simulations. Available from the Danish Technological Institute (DTI).

ConTeSt (2½D): User-friendly program for temperature and stress simulations. The program is in regular use by consultants and contractors in Sweden, and also in other countries. Available from JEJMS Concrete AB.

CrackTeSt-COIN (2½D): This is a modified version of the ConTeSt-program, adjusted to Norwegian modelling tradition and concrete mix design. The making of this program version was initiated by the COIN-project and the modification work was done in 2011. The program will be available commercially from 2012.

b4cast (3D): Specially designed 3D temperature and stress simulation program. The program uses the same materials models as in 4C-Temp&Stress. Available from ConTech Analysis ApS.

DIANA (3D): The program is originally designed for general structural applications. A special module for hardening concrete is developed (In Norway, previously used only at NTNU). The original program is made at TNO Building and Construction, The Netherlands.

A number of other simulation programs also exist on the world market. The main difference between programs is the input-formulations of concrete properties, as well as the complexity (2D, 3D). All are in principle just as applicable if they are used in a sensible manner (important: good fit with experimental data, 3D-program for particular 3D-problems, 2D for 2D-problems or adequate transformation of 3D-problems to 2½D-simulations). When it comes to process time it is roughly a question of seconds for 1D-simulations, minutes for 2D and hours/days for 3D.

9.2 Input data for 2D and 3D programs, brief overview

Some programs contain complete sets of input materials data for the property development for specific "default" concretes which previously have been documented experimentally. In a building project, the actual concrete will generally differ from the "default"-concretes in a program, even though they may look quite similar. In some projects all necessary input properties have been determined experimentally for the actual concrete. In any case, for increasing number of properties that are determined experimentally the simulation results get more reliable. Below is given the various input data that is required in temperature and stress simulations, involving concrete properties, boundary conditions and structural response.

Input data: Concrete properties - hardening concrete

- Hydration heat, density, specific heat, cement (binder) content, thermal conductivity
- Coefficient of thermal expansion
- Autogenous shrinkage
- E-modulus
- Creep
- Tensile strength
- Compressive strength
- Poisson ratio

Input data: Concrete properties - old/mature (restraining) concrete

If the older structure is completely cooled, hydration heat and autogenous shrinkage is set to be zero, and for the mechanical properties a constant value are often used (for instance the 28-days values) and creep may be set to be zero, but the values should be evaluated in each case. If the old structure is not completely cooled (which is beneficial) at casting of the new element, one alternative is to utilize a sequential simulation where both structural elements are given full input data sets for hardening concrete where the casting sequence is reflected in the simulation.

Geometry of structure
Definition of cross-section of old and newly cast structures (2D), including ground conditions. For 3D the entire geometry of the structure must be defined.

Boundary conditions
- Air temperature
- Wind velocity, as well as thermal conductivity and thickness of formwork and insulation materials (which gives the overall heat exchange across the boundary)
- Definitions of the ground or boundary condition for the surface of the structure that faces towards the ground.
- Time of formwork removal and, if used, insulation properties of subsequent surface cover

Simulation
Initial temperature of ground and old concrete, as well as fresh concrete temperature of newly cast concrete must be set.
In order to simulate the casting process, which may take several hours/days in reality; most programs open for including the casting sequence.

When using cooling pipes in the hardening concrete the number of pipes and their placement in the structure must be defined, as well as the cooling water temperature and the size and thermal conductivity of the pipes.

When using heating cables in the old (restraining) structure the number of cables and their placement in the structure must be defined, as well as their output (heat flux).

The fineness of the finite element net must be defined.
Total process time (hydration time) to be calculated must be defined, normally 2-4 weeks.

The temperature simulation is always performed first: Temperature, maturity and the concrete property development over time is then calculated for the entire cross-section (2D) (or for the entire structure for 3D).

The subsequent *stress simulation* requires static/support conditions, i.e. point support or line support, and the freedom of movement of each support. For 2D-simulations freedom of translation in the longitudinal z-direction and freedom of rotation in x and y direction must be defined, see Figure 49. The stress development over time is calculated for the entire cross-section (2D) (or for the entire structure for 3D).

Optional simulation results can be presented and printed out; for instance:
- temperature development over time for chosen points in the structure, or iso-curves for the cross-section at chosen times.
- maturity, compressive strength, E-modulus and tensile strength development over time.
- stress or crack index (stress/tensile strength-ratio) development over time, or iso-curves for chosen times.

Simulations can easily be repeated with changed boundary conditions to identify, for instance, critical climatic conditions with regard to cracking, or to study the effect of countermeasures such as changing the casting sequence, lowering the fresh concrete temperature, cooling pipes, heating cables etc. The effect of replacing the concrete with another concrete (if data are available) can naturally also be studied.

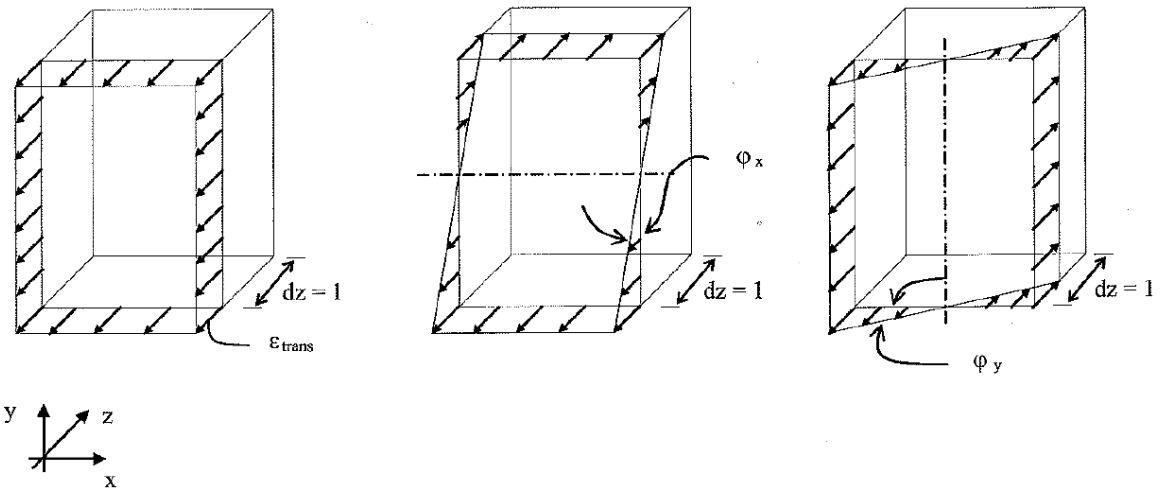

Translation in z-direction Rotation around x-axis Rotation around y-axis

Figure 49 Possible freedom of movement in the model "Compensated Plane" or "Plane Surface Analysis" [106]

10 Simplified simulation methods

10.1 General

The stress generation in hardening concrete can be calculated by simplified hand methods, simplified engineering methods, and advanced 2-dimensional (2D) or 3-dimensional (3D) finite element structural simulations. This chapter gives a brief introduction to stress calculations, but do not go into detail with regard to the numerical solutions that are applied by advanced computer programs – this is not the target of the present report.

To shorten the time-consumption for hardening concrete crack-risk evaluations simplified methods can be useful; at least they can give an estimate of the crack-risk for given concretes/structures or on the effect of countermeasures on-site. Simplified methods must be experience-based, i.e. they must be verified against advanced simulations and/or stress-measurements in the laboratory. When this is done, it is claimed that simplified methods can be used for a variety of structural configurations with satisfactory accuracy [117][118][124]. The accuracy of simplified methods may be questioned, however, for concretes that have very different composition than those used for developing the simplified method parameters. Common for simplified methods is that they need a realistic temperature development for the given structure and also a realistic degree of restraint for the critical area in the structure. Hence, a temperature analysis of the given structure is required, as a minimum, whereas the relevant restraint factor can be estimated using existing diagrams based on previous advanced computer simulations.

Advanced 2D- and 3D finite element calculation programs simulate the entire stress history and predict the critical time for cracking and the critical positions in the structure. The degree of restraint is an integral and "automatic" part of such simulations. Advanced simulations can be time-consuming, but for complex structural geometries the accuracy is better than simplified methods, not surprisingly. It is sensible (and economical) to apply advanced simulation methods for instance when the structural complexity is high or when crack avoidance is of greatest importance for water-tightness and functionality.

Common for all methods is that they require relevant input data for the material properties of the given concrete. A simplified hand method and an engineering method for stress calculations are discussed in the following sections.

10.2 Hand method – Age adjusted effective E-modulus (AEM) method

This method, first time applied to hardening concrete by Larson in 2001 [117][124], neglects the compressive phase (the heating phase) for the externally restrained concrete member, and thus it considers only the period with tensile stress development during the cooling phase. The tensile stress develops from the "second zero stress time" t_2 [in days] and "second zero stress temperature" T_2, see Figure 50. (note that the first zero stress time and -temperature (t_s and T_s) in the figure corresponds to "our" t_0 discussed earlier).

The time t_2 [days] will occur shortly after the temperature has started to cool and can be found according to a k_2-factor, illustrated in Figure 51, which is given as:

Equation 20 $$T_2 - T_0 = k_2 \, x \, (T_1 - T_s)$$

For k_2 the following expression has been proposed [117]:

Equation 21 $$k_2 = 1,41 - 1,36 \times \frac{w}{b}$$

This expression for k_2 was developed in Sweden and is based on typical national concretes. According to this expression k_2 becomes 0.866 for a high performance concrete with water-to-binder (w/b) ratio of 0.40. For "Norwegian" concretes, however, it was found by Kanstad in [118] (see also APPENDIX 3) that k_2=0.92 gave the best agreement with experimental results. This means that t_2 is considerably closer to the temperature maximum than given by Equation 21. The main reason is probably larger autogenous shrinkage in the investigated Norwegian concretes. In the calculation procedure, when k_2 is known, the time t_2 can be determined from the temperature-time curve after T_2 have been determined according to Equation 20. Furthermore it is assumed that the sum (ε_{tot}) of autogenous shrinkage (ε_{as}) and thermal dilation (ε_T) occurring after t_2 is the stress-generating strain at t_3:

Equation 22 $$\varepsilon_{tot}(t_2,t_3) = \varepsilon_{as}(t_2,t_3) + \varepsilon_T = \varepsilon_{as}(t_2,t_3) + (T_3 - T_2) \cdot \alpha_T$$

The stress is applied in one step at t_2, see Figure 52. The effective long-term E-modulus (E_{eff}) used in ordinary structural design methods (calculation of deformations and stresses), $E_{eff} = E_c / (1 + \varphi)$ is based on the assumption that the concrete stress is approximately constant in time. To compensate for the gradual stress development in hardening concrete, which occurs after t_2 in this case, the creep-ratio (φ) in the effective E-modulus expression is multiplied by a reduction factor; termed the aging coefficient X_{AEM}. The age adjusted effective E-modulus, $E_{AEM,}$ is then expressed as:

Equation 23 $$E_{AEM} = \frac{E_c(t_2)}{1 + X_{AEM} \cdot \varphi(t_2,t_3)}$$

Where t_3 is the time [in days] when the crack risk is to be determined, t_2 [days] is the time at zero stress, $E_C(t_2)$ is the E-modulus at t_2, and $\varphi(t_2,t_3)$ is the creep ratio representing the creep at t_3 for stress applied at t_2.

In [126] the following expression for the aging coefficient was used:

Equation 24 $$X_{AEM} = 0,69 + 0,005 \times t_2$$

In the investigation by Kanstad [118] it was not possible to find another expression or a modification of this equation which gave better agreement with the "Norwegian" test results. Finally the stress may be calculated as:

Equation 25 $$\sigma(t_3) = \varepsilon_{tot}(t_2,t_3) \cdot E_{AEM} \cdot R$$

Which then becomes:

Equation 26 $$\sigma(t_3) = (\varepsilon_{as}(t_2,t_3) + (T_3 - T_2) \cdot \alpha_T) \cdot \frac{E_c(t_2)}{1 + X_{AEM} \cdot \varphi(t_2,t_3)} \cdot R$$

where R is the restraint factor

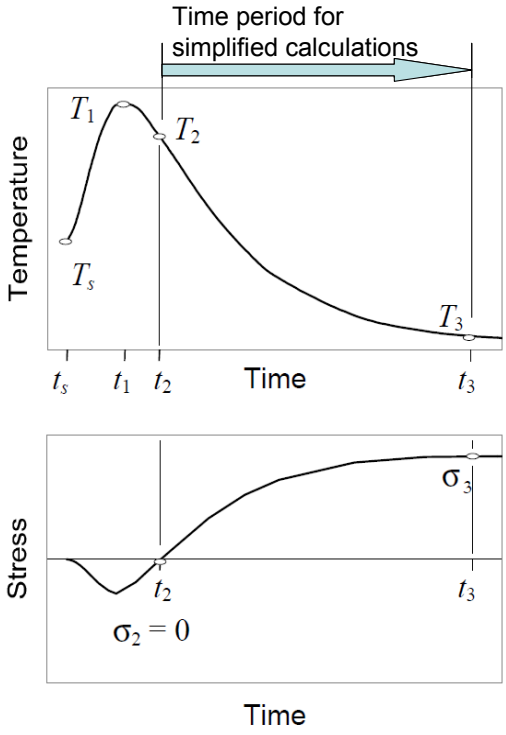

Figure 50 Typical temperature and stress development in hardening concrete subjected to external restraint. Tensile stress starts to develop at the "second zero stress" time t_2 and temperature T_2.

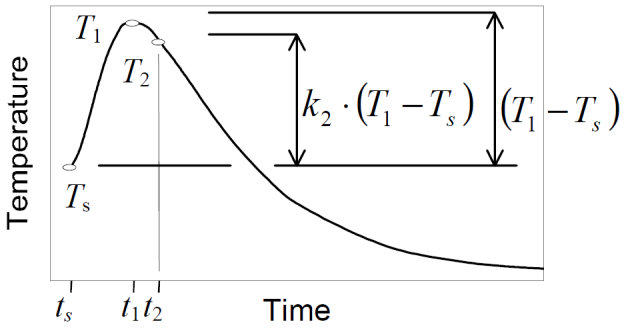

Figure 51 Illustration of the evaluation of T2 and t2 by means of k2.[124]

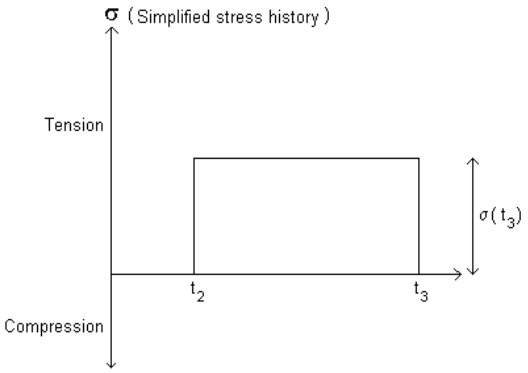

Figure 52 Simplified stress history used in the AEM method [118]

10.3 Hand method (AEM), calculation example

An example of the use of the age adjusted effective E-modulus (AEM) method is shown in the following. The experimental results in Figure 53 were measured for a given concrete with water-to-binder (w/b) ratio of 0.40: Temperature and free deformation (Figure 53-a), E-modulus (Figure 53-b) and creep (Figure 53-c). t_0 was found to be 10 hours for this concrete. Note that the time-scale in Figure 53 is [hours], but the time that should be used in the AEM-calculation is [days]. Our task is to calculate the tensile stress $\sigma(t_3)$ after t_3=7 days (168 hours) for a case were this concrete is subjected to 100% restraint (R=1.0) and a temperature history similar to the one in the test (Figure 53-a). From Figure 53 we can read (and calculate) the following values:
$T_0 = 25\ ^oC$
$T_1 = 40\ ^oC$

$k_2 = 0.866$ (according to Equation 21 for w/b=0.40)
$T_2 = 38\ ^oC$ (according to Equation 20), which gives from Figure 53 that:
$t_2 = 1.29$ days (31 hours)

$\varepsilon_{tot}(t_2) = -27 \cdot 10^{-6}$
$\varepsilon_{tot}(t_3) = 143 \cdot 10^{-6}$
$\varepsilon_{tot}(t_2,t_3) = \varepsilon_{tot}(t_3) - \varepsilon_{tot}(t_2) = 143 \cdot 10^{-6} - (-27 \cdot 10^{-6}) = 170 \cdot 10^{-6}$

$E_c(t_2) = 30.2$ GPa = 30200 MPa

$\varphi(t_2,t_3) = 1.03$
$X_{AEM} = 0.696$ (according to Equation 24 for $t_2 = 1.29$ days)

$E_{AEM} = 17.6$ GPa = 17600 MPa (according to Equation 23)

Finally, we are ready to calculate the stress $\sigma(t_3)$ according to Equation 25:

$$\sigma(t_3) = \varepsilon_{tot}(t_2, t_3) \cdot E_{AEM} \cdot R$$

hence:

$$\sigma(t_3) = 170 \cdot 10^{-6} \cdot 17600\text{MPa} \cdot 1.0 = \underline{3.0\text{MPa}}$$

The calculated stress $\sigma(t_3)$ for this case fits perfectly with what was actually measured experimentally for this concrete in a 100% restraint stress test performed under exactly the same temperature history as given in Figure 53-a. The stress measurement is shown in Figure 54, which also gives the measured tensile strength of the concrete. As can be seen, $\sigma(t_3)$ at t_3=7 days (168 hours) was 3.0 MPa. One important reason for this correspondence between calculated and measured stress is that all materials input to this AEM-calculation is based on experiments.

It can also be seen from Figure 54 that the tensile strength $f_t(t_3)$ after 7 days is 3.1 MPa, thus the crack index (C_i) (Equation 1) is at that time:

$$C_i = \frac{\sigma(t_3)}{f_t(t_3)} = \frac{3.0MPa}{3.1MPa} = 0.97$$

For this case with 100% restraint it is obvious that the concrete is very close to cracking. When simulations are required in projects the calculated C_i must be considerably lower than 1.0 to ensure safety against cracking. For instance, C_i<0.75 have been required sometimes for pre-documentation by calculations. In order to satisfy this requirement for our case this means that the concrete stress $\sigma_{max}(t_3)$ at 7 days cannot exceed: $\sigma_{max}(t_3) < C_i \cdot f_t(t_3) = 0.75 \cdot 3.1\text{MPa} = 2.33\text{MPa}$

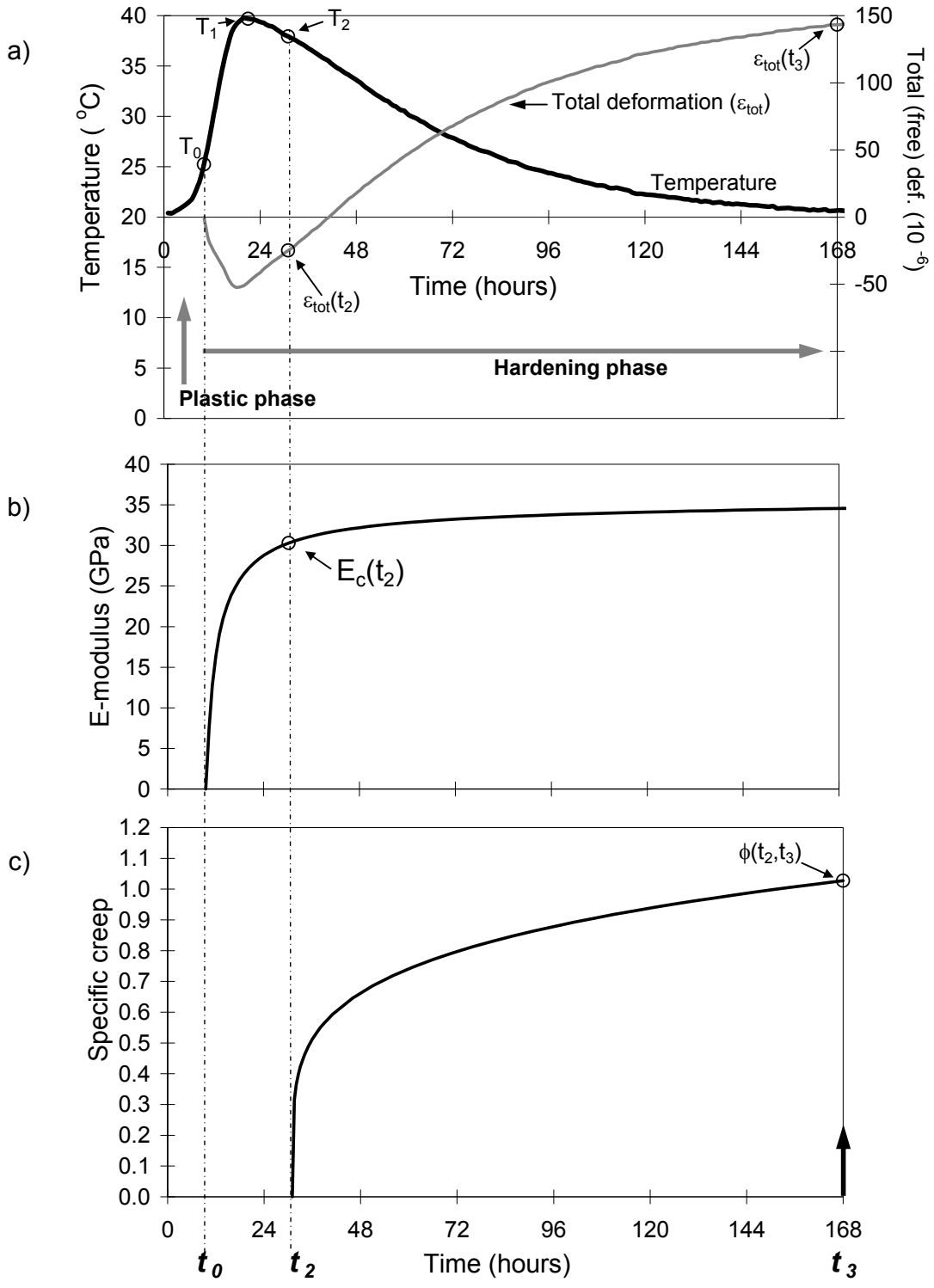

Figure 53 Test results on a concrete (w/b=0.40): Development of (a) Temperature and free deformation, (b) E-modulus, (c) Specific creep. [82][84]

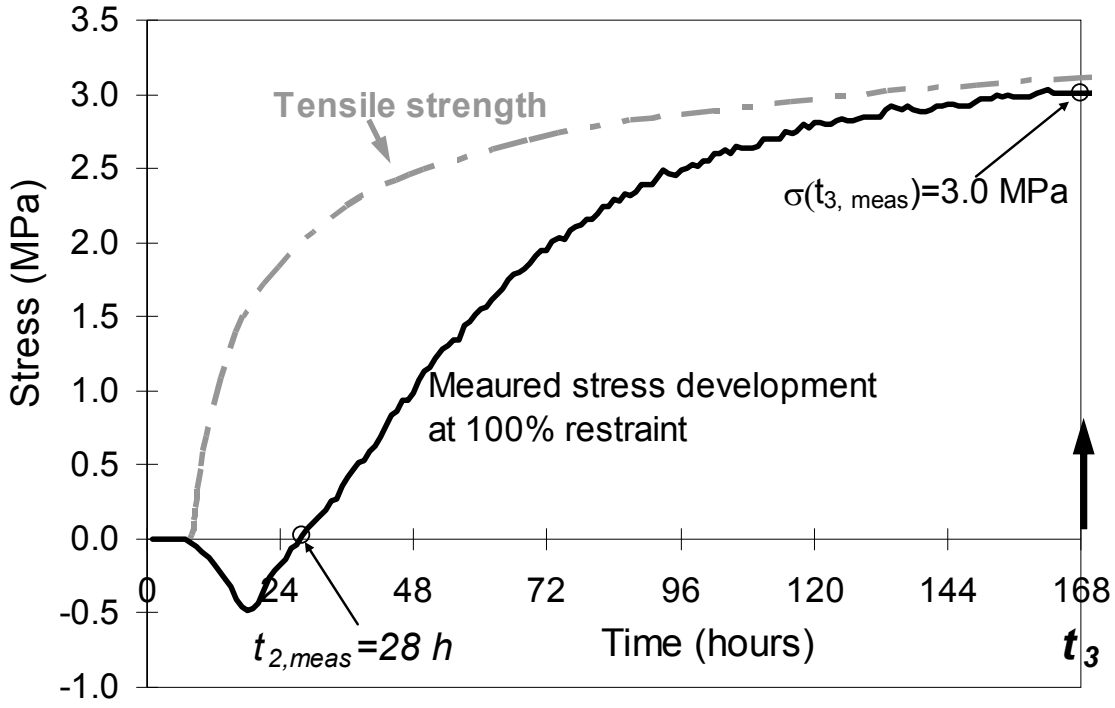

Figure 54 Test results on the same concrete (w/b=0.40) as in Figure 53: Development of restraint stress (R=1.0) and tensile strength. [82]

To proceed further with these numbers; the degree of restraint (R) for a structure that is to be built with the given concrete (and the given temperature history) then cannot be higher than 78%, according to:

$$R < \frac{\sigma_{max}(t_3)}{\sigma(t_3)} = \frac{2.33MPa}{3.0MPa} = 0.78$$

Furthermore, it is notable that the time of second-zero-stress t_2 was 31 hours (1.29 days) according to the AEM-method whereas the stress test in Figure 54 shows that t_2 was 28 hours (1.17 days). If this value (t_2=1.17 days) is used throughout the calculation it will not change $\sigma(t_3)$ much for this particular case. It would however lead to a higher $\varepsilon_{tot}(t_2,t_3)$, a higher $\phi(t_2,t_3)$ and a lower $E_c(t_2)$, but the product of these effects will be no significant change in $\sigma(t_3)$.

Finally, for an "unknown" concrete, imagine that we only knew the w/b-ratio, the temperature history and the structural restraint. This would lead to assumptions regarding ε_T, ε_{as}, E_c and φ which would make the calculation very uncertain. Of course, the better we know these parameters, the better the calculation becomes. This holds for all types of calculations, also 2D and 3D finite element computer simulations.

The space that is given for the 1D hand-method in this section is not proportional to its application in practice where more advanced simulation methods are generally used, but the method is illustrative in the way that it shows the principles of a stress calculation where relevant experimentally-based concrete properties are input.

10.4 Three-step engineering method

The method described in the following is often denoted “the Skanska engineering method”. The basic idea of the method is to make crack risk simulations possible with the use of any commercial finite element programs [98]. The method has been verified against a 3D model, and the accuracy is claimed to be very satisfactory [98][99]. The three steps of the engineering model are, see also Figure 55:

1. Temperature and maturity analysis
2. Restraint analysis
3. Non-linear stress analysis: Simplified model

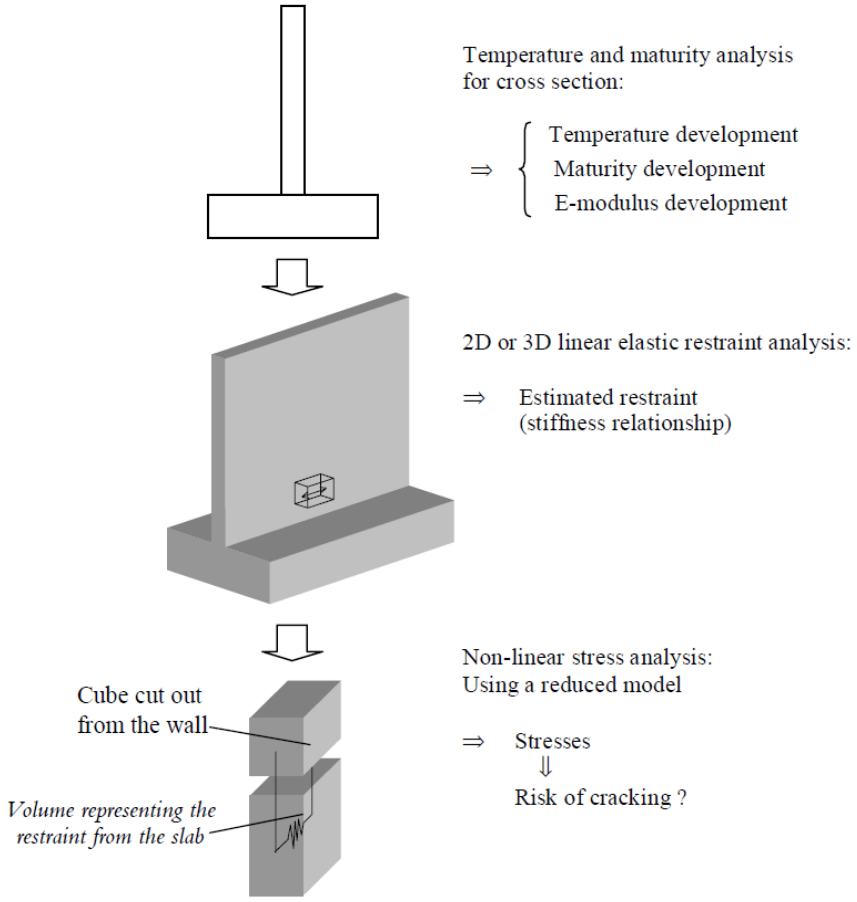

Figure 55 The three principal steps in the engineering method [98]

Step 1:
The temperature analysis must be done for the actual cross section of the structure, for instance by a commercial 2D or even 1D program. Realistic field conditions and concrete properties must be given in the analysis. This analysis gives a relevant temperature history and, thus, the relevant maturity development. This again makes it possible to calculate the appropriate E-modulus development for the hardening concrete structure, for instance expressed by Equation 14, see Section 8.5.

Step 2:
To find the restraint two linear simulations are carried out. The first one is to find the average restraint during the heating phase and the second to find the average restraint during the cooling phase. During these restraint analyses an arbitrary temperature "load" is applied to the newly cast concrete, and temperature is also the only load. The old adjoining/restraining structure is assumed to have a fully developed E-modulus. The restraint simulations (to find R_z) can be either 2D or 3D depending on the geometry of the structure. The linear elastic restraint stress due to the temperature load is then found over time and the stress is compared to the "maximum stress level" defined as the stress level achieved if the restraint had been 100%, i.e. no strain in the longitudinal z-direction:

Equation 27

$$R_z = \frac{\sigma_{zz}}{\alpha_\theta \Delta T_{pre} E_{wall}} \cdot 100$$

where

R_z = Restraint [%]
σ_{zz} = Stress in the z-direction at the studied point [MPa]
α_θ = Thermal expansion coefficient [°C^{-1}]
ΔT_{pre} = Arbitrary prescribed temperature load [°C]
E_{wall} = Elastic modulus of the wall used in the restraint simulation [MPa]

R will be between 0 and 100%, and the point with the highest risk of cracking can then be found from the maximum of the product $\Delta T \cdot R$, where ΔT is found during the previous step 1.

The relation of stiffness between the new (for instance a wall) and the old adjacent concrete that represents the point with the highest risk of cracking can be calculated from a derivation using two parallel-coupled beams where one represents the new concrete and the other the old restraining concrete, and the result becomes:

Equation 28

$$\frac{A_{adj} E_{adj}}{A_{wall} E_{wall}} = \frac{R_z}{1 - R_z}$$

where

$A_{adj} \cdot E_{adj}$ = Stiffness of the adjoining part causing the correct restraint situation [N]
$A_{wall} \cdot E_{wall}$ = Stiffness of the part of the wall studied [N]
R_z = Restraint

Step 3:
In the stress analysis the studied part is a cube cut from the new concrete with the highest risk of cracking, see Figure 56. The size of the old adjoining structure, giving the correct R, is determined according to Equation 28. The temperature of the adjoining structure is normally kept constant in the analysis, if it has cooled to the ambient temperature. All involved concrete properties is then implemented and when the stress is simulated the crack index (C_i) can be calculated.

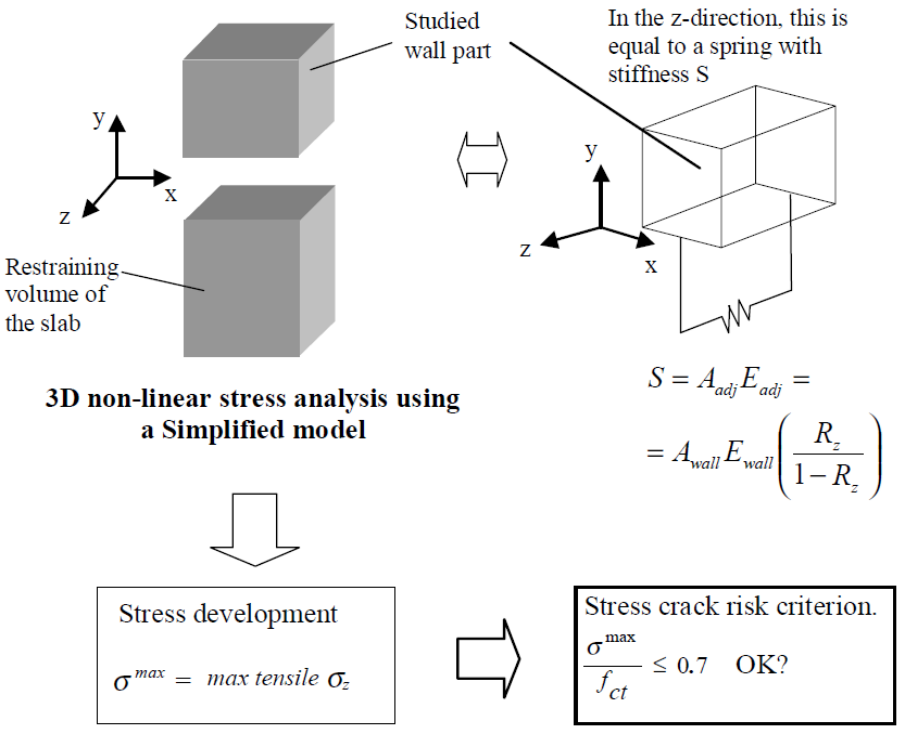

Figure 56 Simplified model, non-linear stress analysis [98]. Maximum allowable crack index, C_i, is 0.7 in the figure.

10.5 Three-step engineering method, calculation example

A 800 mm thick, 5 m high and 25 m long wall is to be cast on a 1 m thick and 5 m wide hardened slab, see Figure 57. In the following example an assessment of the cracking tendency of this structure is performed by using the principles of the three-step engineering method.

The scope is to study the cracking tendency of the wall. We have the choice between two concretes, which have been tested experimentally. Hence, input data for the two concretes are available.

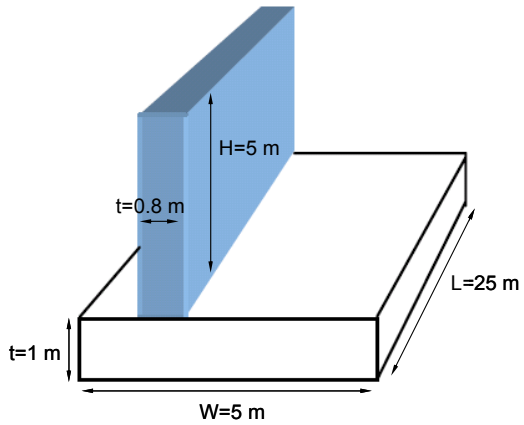

Figure 57 Wall on slab structure to be cast

The used simulation procedure is somewhat simplified compared to the original three-step method described in the previous section:

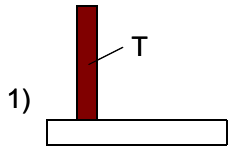

2D-simulation to get T-development

2) Restraint taken from previous 3D-simulations

3) 1D-simulation

Step 1 is identical to the original method. A 2D-temperature simulation is performed to get the relevant thermal "load" in the wall for each concrete.

In Step 2 the restraint is simply picked from 3D-simulation data available in the literature.

Step 3 consists of a 1D-simulation that use the temperature development from step 1 and the restraint from step 2, as well as the input data we have from previous experimental tests.

The two concretes under investigation are:
- Concrete A: a traditional Norwegian structural concrete made with CEM I type cement and mass ratio of 0.40 [82] [84][101].
- Concrete B: a concrete that was developed for one of the projects of the submerged tunnel system in Bjørvika, Oslo, with a high fly-ash content and mass ratio of 0.45 [102][85].

Step 1: 2D temperature simulation:
These kinds of simulations are dealt with in more detail in the following chapters. For this case rather harsh winter conditions were chosen for the 2D-simulation:
Air temperature = -7 °C, wind = 4 m/s
Formwork = 18 mm plywood, removed after 168 hours (1 week)
Fresh concrete temperature = 10 °C
Slab temperature at casting = -3 °C, Ground temperature = 0 °C
And, concrete properties from available sources; based on previous experiments.

The structure as drawn in the 2D-program (4C-Temp&Stress), and calculated average temperature for the wall is shown in Figure 58.

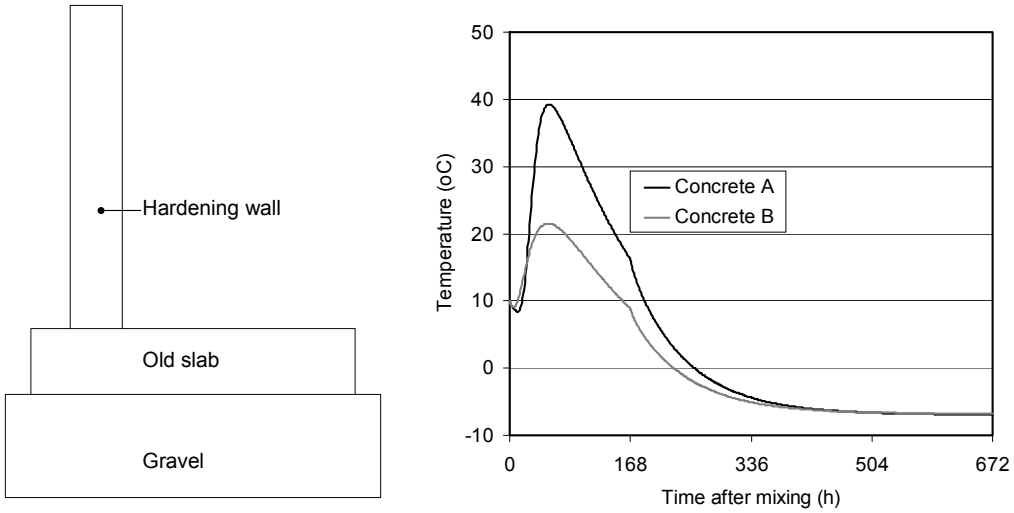

Figure 58 Structure drawn for the 2D-simulation (left) and calculated average temperature development in the wall for *Concrete A* and *Concrete B* (right)

Step 2: Degree of restraint

Previous 3D-calculations for structures very relevant for our case was performed in [116], see Figure 59, where ground stiffness (gravel) was set to k=60 MN/m^2. The critical point with regard to cracking is generally around one wall-thickness up from the joint. The 3D-calculations below are for a wall with thickness=0.65 m, and the restraint (R) in the critical point for this wall is, as shown, R=0.55. In our case the wall is a bit thicker (0.8 m) something that means theoretically that the degree of restraint may be slightly lower than 0.55. However, the slightly conservative and single value **R=0.55** is used further here for our 0.8 m thick wall. The simulations in Figure 59 assume that the average ratio between the E-modulus of the hardening wall to the (constant) E-modulus of the restraining slab is 0.93. This ratio between new and old concrete has shown to be a rather accurate estimate for restraint analyses, provided that both wall and slab is made with the same concrete.

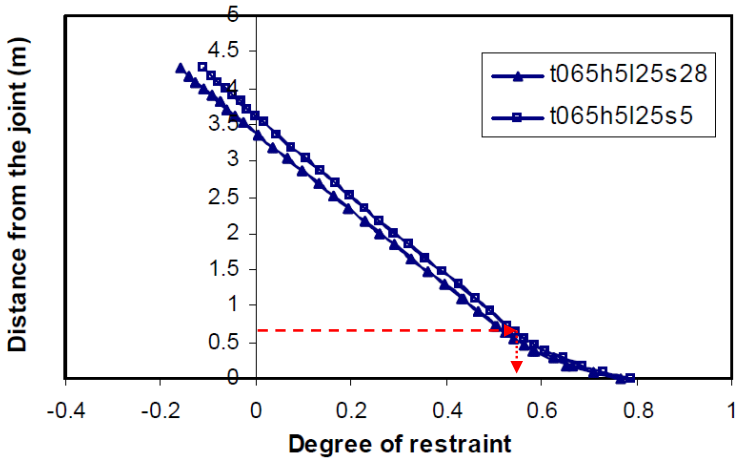

Figure 59 Degree of restraint from 3D-simulations [116] for wall thickness=0.65 m, wall height=5m, wall length=25 m and slab width 5 m (s5) and 2.8 m (s28), respectively.

Step 3: 1D-Stress calculation

The stress calculations performed here are based on linear visco-elasticity for aging materials. The calculation is performed incrementally in an Excel spreadsheet. For a general stress history, the concrete strains are in principle determined as:

$$\varepsilon_c(t) = \int_0^t J(t_e',t,t') \cdot d\sigma(t') + \varepsilon_{Tot}(t)$$

ε_{Tot} is the total free strain (thermal dilation + autogenous deformation) measured during the Dilation Rig test and ε_c is the concrete strain. The compliance function $J(t,t')$ and the creep ratio $\varphi(t,t')$ is defined as:

$$J(t,t') = \frac{1}{E(t_e')}(1+\varphi(t,t')) \qquad \text{and} \qquad \varphi(t,t') = \varphi_0 t_e'^{-d} \cdot (t-t')^p$$

In these equations t is the actual time (concrete age in days), t' the time when a stress increment ($d\sigma$) is applied, and t_e' is the maturity at t'.

The stress (σ) for a full restraint situation is calculated first, hence $\varepsilon_c(t)$ is set to be zero. All concrete properties are implemented according to the available experimental data. The relevant stress for our structural case is then found by multiplying the calculated stress by the restraint factor (=0.55). The 1D system that is calculated is illustrated in Figure 60.

The calculation results for the two concretes, at the given site-conditions given above, are shown in Figure 61; the stress at R=1 and R=0.55 as well as the tensile strength are given in the figure. Figure 62 shows the crack index development for R=0.55. It is obvious that the slow and moderate hydration heat (and also very moderate autogenous shrinkage) of *Concrete B* is beneficial in terms of reducing the crack index, and the maximum crack index value for this concrete is 0.53, while for *Concrete A* the maximum crack index is 0.89. Even though both concretes display crack indices below 1.0, cracking is likely to occur now and then for *Concrete A*. See Chapter 12 for more on reliability of the crack index.

If desired, other site-conditions can now easily be investigated by repeating Step 1 and 3 (the restraint found in Step 2 can be regarded as invariant). If a crack-free structure is of great importance the use of *Concrete A* probably demands for countermeasures such as cooling pipes in the wall or heating cables in the slab. The effect of such countermeasures can be incorporated in the temperature simulation in Step 1. Furthermore, shortening the casting length may be beneficial as it reduces the restraint (step 2 consideration).

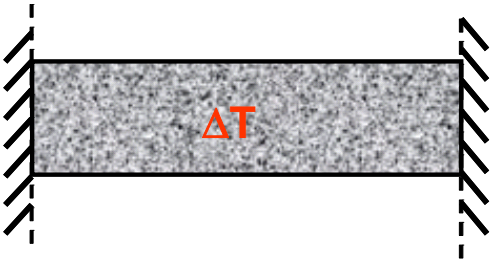

Figure 60 1D-system for initial stress calculation of 100% restraint (R=1.0) stresses. Input: The temperature development from Step 1 and relevant materials input data from previous experimental tests.

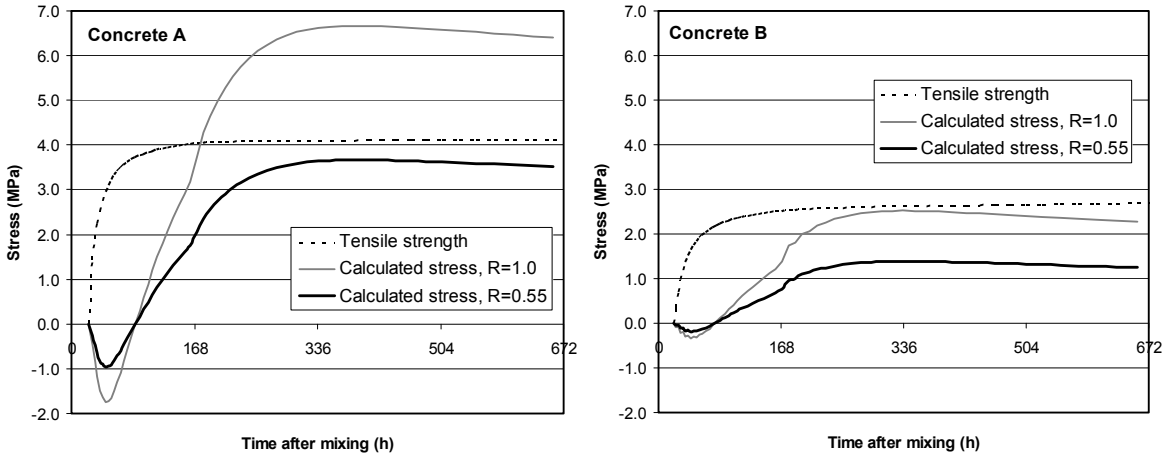

Figure 61 Calculated stress development (1D) for concrete A and B; for full restraint (R=1.0) and 55% restraint (R=0.55).

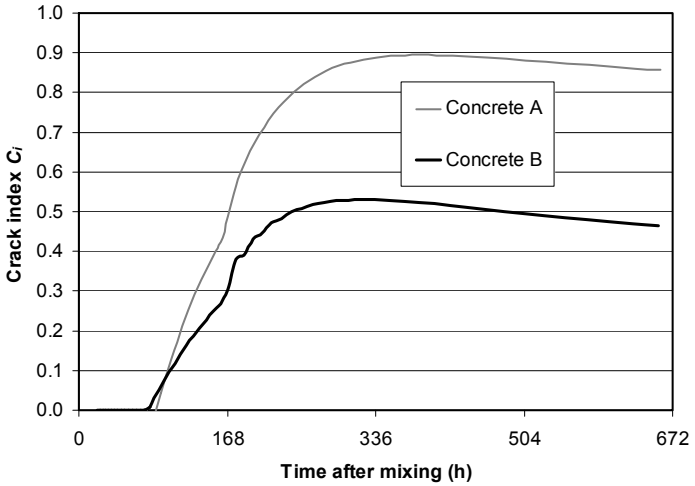

Figure 62 Crack index (ratio concrete stress at R=0.55 to tensile strength) for concrete A and B for the wall temperature relevant for the given site-conditions.

11 Example of a 2D calculation

Examples taken from a simulation by the ConTeSt-Pro program are shown in Figure 63 and Figure 64. The simulated wall structure contains a given concrete and amount of embedded cooling pipes. A crack index < 0.7 was set as criteria for ensuring a crack-free structure. The simulation shows that the applied amount of cooling pipes is not enough to achieve a sufficiently low crack index for the given conditions, see Figure 64 (right figure) where white areas indicates crack indices > 0.7. The volume of cooling pipes must be increased to ensure a crack-free structure, or other actions must be taken. Go ahead, simulate!

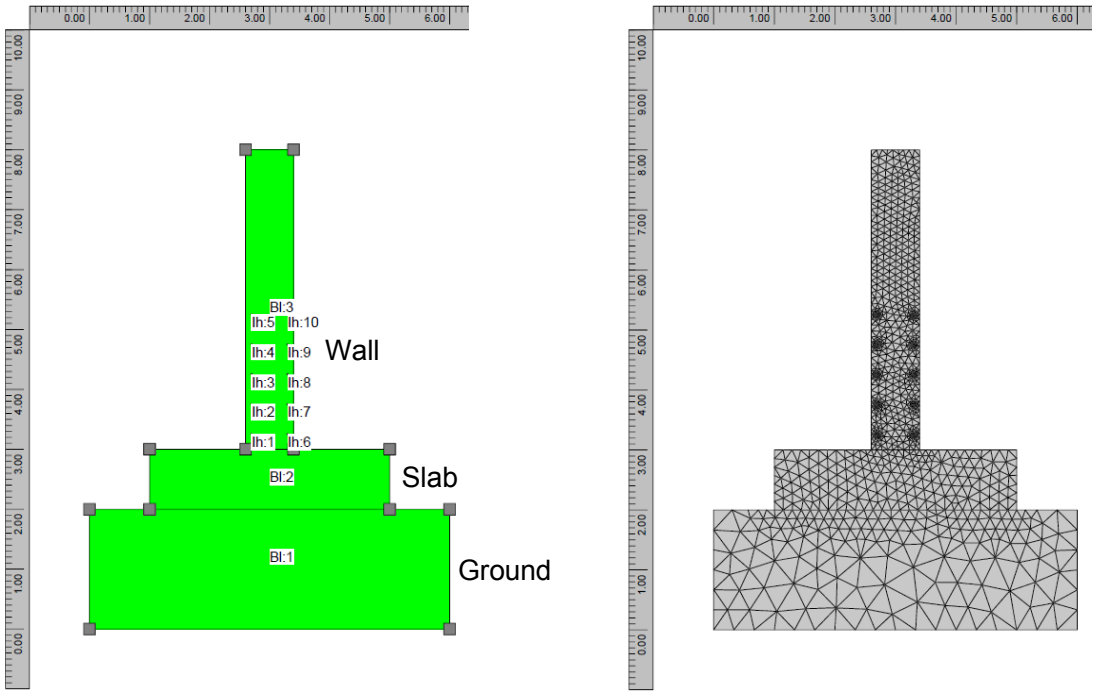

Figure 63 Example from a ConTest-Pro simulation: Sketching of cross-section and structural parts including cooling pipes (left) and generated element net (right). In this case the cooling pipes are fixed to the inner-side of the outer layer of reinforcement.

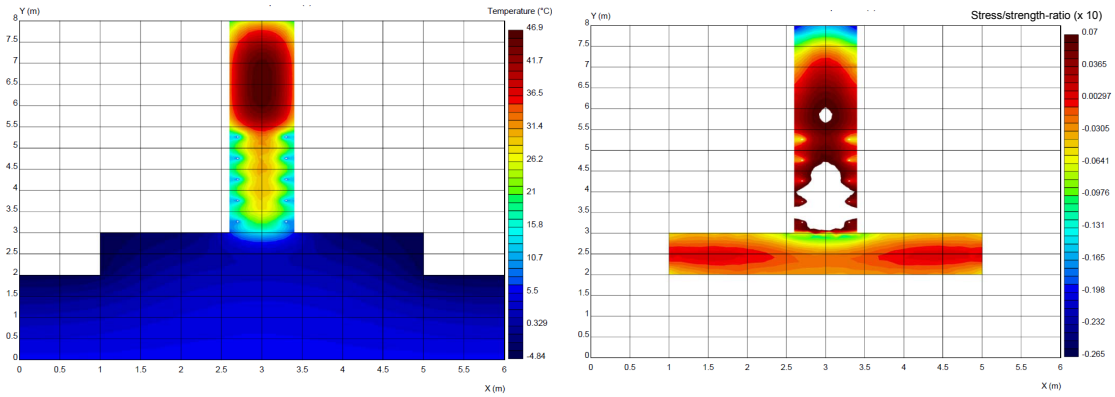

Figure 64 Example from a ConTest-simulation: Iso-curves for temperature at the time of maximum temperature in the wall (left) and iso-curves for the crack index (stress/strength-ratio) at the later critical time of cracking (right), where white areas indicate crack indices > 70% (0.7)

12 Variability and crack risk criteria

All the involved parameters forming the basis for the stress simulations are associated with a certain uncertainty/variability. The properties of concrete are stochastic variables that we simplify by "models" (functions or discrete data) based on average results from experiments, which we then use in the simulations. Regarding the climatic- and on-site (boundary) conditions there are always some uncertainty and the relevant input must be assumed according to the most probable weather for the season and the insulating properties for the formwork materials. The output from simulations is therefore associated with uncertainty, and what we get from simulations is therefore a probability for cracking (or not) within a certain level of confidence. This is illustrated in Figure 65 which assumes that the calculated stress and the measured tensile strength are normally distributed quantities. Furthermore, through counter-measures against cracking we then can simulate the consequence in terms of a decreased probability of cracking.

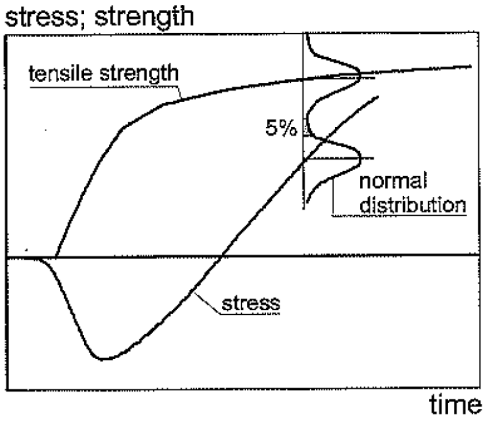

Figure 65 Illustration of uncertainty in stress calulations, and subsequently in the calculation of the crack index.

The level of confidence of simulations is impossible to verify accurately as it is more or less impossible to verify the actual properties and stresses in a real structure. However, through experience different "safety levels" have been proposed, see below.

Cracking occurs when stresses reach the tensile strength capacity of the concrete, hence the Crack Index (C_i = the stress/strength-ratio) becomes 1.0. A crack risk criteria must take the aspects of variation into consideration. Hence, if it is of vital importance to obtain a high safety against cracking in a structure, the simulated C_i should be considerably lower than 1.0.

Assuming normal distributed and independent variables, the upper characteristic value (σ_{ck}) of the calculated stress (σ_c) from a simulation is given as:

Equation 29 $$\sigma_{ck} = \sigma_c + k_\sigma \cdot s_\sigma$$

where k_σ defines the confidence interval and s_σ is the standard deviation for the calculated stress.

The tensile strength (f_t) of concrete has also its variability, hence the lower characteristic value (f_{tk}) of the tensile strength becomes:

Equation 30 $$f_{tk} = f_t - k_t \cdot s_t$$

where k_t defines the confidence interval and s_t is the standard deviation for the tensile strength

A crack risk criteria must therefore be derived from the upper characteristic (calculated) stress and lower characteristic tensile strength, hence:

Equation 31 $$\frac{\sigma_{ck}}{f_{tk}} = \frac{\sigma_c + k_\sigma \cdot s_\sigma}{f_t - k_t \cdot s_t} < 1.0$$

Which can be expressed as:

Equation 32 $$\frac{\sigma_c}{f_t} < 1 - \frac{k_\sigma \cdot s_\sigma + k_t \cdot s_t}{f_t}$$

The ratio σ_c/f_t we recognize as the crack index C_i, which then should be kept below 1.0 to give some certainty against cracking.

In [118] Kanstad compared a number of calculations to experimental tests on restraint specimen tests (TSTM-tests). The calculations were based on individual experiments on all the involved concrete properties, and the actual temperature from the TSTM-specimen was used in the calculation (hence, no uncertainty regarding the boundary condition). The premise for rather accurate calculations were, thus, the best possible in this case. It was found that when using an advanced method including the double power creep law and the principle of linear visco-elasticity for aging materials, the standard deviation of calculated (σ_3) vs. measured ($\sigma_{3,meas}$) stress after around 2 weeks of hardening was (s_σ=) 0.34 MPa. When the calculation was simplified and based on the Burger creep model with default parameters the standard deviation became somewhat higher. In general, the variation in calculated stress s_σ is likely to be higher than the variation of the tensile strength s_t since s_σ consists of multiple materials parameters (E-modulus, creep, thermal- and autogenous deformation, temperature sensitivity).

The determination of tensile strength has also its scatter, as mentioned. According to the work done in connection with [118] the standard deviation s_t of tensile strength was found to be in the range 0.05-0.3 MPa (which is quite low!) for concrete ages corresponding to a tensile strength around 3 MPa, which represent a fairly relevant strength level for the critical time of cracking after 1-2 weeks of hardening for the low w/b concretes that were investigated.

The statistical parameters k_σ and k_t are 1.64 for 5% probability for the (characteristic) upper and lower value of the property to be exceeded. The numbers mentioned above inserted in Equation 32 gives that the crack index C_i should not exceed 0.65–0.79 in order to obtain less than 5% probability for cracking (corresponds to a confidence level of 90%). This then holds for the present case with well-controlled laboratory conditions.

In a field situation there are additional uncertain factors involved; there is uncertainty attached to the boundary conditions, and the input parameters for the simulation are in most cases based on laboratory-mixed concrete while ready-mixed concrete is used in the structure. Ready-mixed concrete is likely to have a larger scatter than “lab-crete”. Obviously the variability (standard deviation) of simulations of structures will be higher than in the well-controlled laboratory conditions discussed above.

These issues have been considered by clients and researchers, but still the chosen crack criteria (C_i) for projects will have a somewhat "philosophic nature" and will also be a result of the fact that the necessary efforts (costs) to secure a crack-free structure should not exceed "common sense". Considering all the uncertainties involved (exact quantification of uncertainty is more or less impossible) less than 5% probability for cracking is probably beyond the limit of common sense. The literature show that the maximum allowable C_i–value set by clients in building projects where a crack-free structure is desired varies from around C_i<0.60 to C_i around 1.0 according to the importance of obtaining a crack-free structure (exposure, importance/complexity of structure etc). For instance the Swedish Transport Administration [107] require for heavy chloride exposed conditions (and normal cement contents) a C_i<0.70 in pre-calculations of stresses. For the submerged structures in the Bjørvika project in Norway C_i<0.75 was required [86]. From the literature it can be seen that the limit value for C_i is set within the interval C_i<0.56 to C_i<0.75 when the target is to reduce the risk of through-cracks to a reasonable "minimum".

A discussion on crack risk criteria from the literature was done by Rostásy et al. in [122], who also gives an illustrative figure which gives the underlying philosophy of crack-control with regard to what resources one should put into it in relation to the importance of obtaining a crack-free structure, see Figure 66. Here, the figure has been made "C_i-neutral" as the "optimal range" with regard to the maximum allowable (calculated) crack index will be very different for different projects. Hence, the "optimal range" does not mean that C_i should be below 1.0 in all cases. For example, for many projects one through-crack or more per casting length have no particular negative effect on the performance of the structure. For other projects, however, water-tightness/durability/very difficult access for maintenance are key factors and investments in stress simulations/counter-measures against cracking (i.e. ensuring a low C_i) are sensible and an absolute necessity to ensure functionality over time.

The principle here is that the repair/maintenance costs (K_{rep}) goes down along with increasing investments in counter-measures against cracking which increases the initial cost of the structure (K_{in}). The sum is the total cost of the structure (K_{tot}). For many structures Figure 66 is probably also very relevant in a service-life perspective, i.e. K_{tot} can be interpret also as the service-life costs.

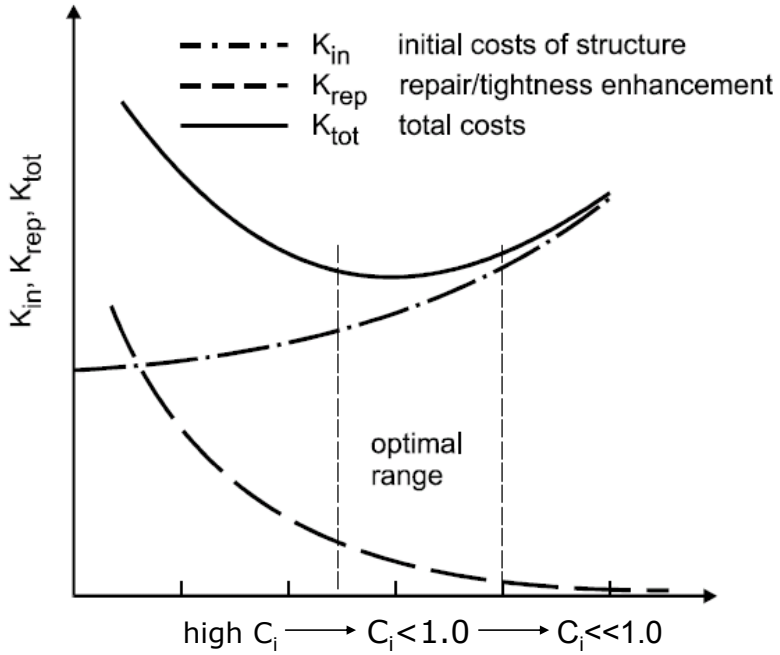

Figure 66 Influence of the crack risk criteria C_i on the cost (K) of a structure (schematic). Originally reported in [122], modified figure (made C_i-neutral)

The crack criterion has also been dealt with by the Japan Society of Civil Engineers (JSCE) [120][121][122]. JSCE gives three ranges relating to the probability of occurrence of through-cracks, see Figure 67. The category "range 1" is where through-cracks are unacceptable, "range 2" is where a few through-cracks are tolerated and "range 3" is where through-cracks are generally tolerated. Range 1 was originally defined with C_i<0.67, range 2 with C_i<0.83 and range 3 with C_i<1.43. After on-site observations [121] it was indicated that these ranges were not strict enough and the limit values for C_i was reduced to 0.56, 0.67 and 1.0 for range 1, 2 and 3, respectively. Figure 67 gives the adjusted C_i-limits. The details behind these considerations are not investigated here, but it is clear that the "stochastic nature" of concrete and stress simulations have been considered.

Experiences from the Bjørvika submerged tunnel project in Oslo, Norway [86] showed that the stress simulations coincided rather well with observations on-site provided that the direct tensile strength was used in the evaluation, and not the splitting tensile strength. After some time of hardening splitting strength f_{ts} may be significantly higher than direct tensile strength f_t, thus using f_{ts} the calculated C_i after a week or two becomes much lower than when using f_t (see Section 8.6 for more on this issue). Since the crack criteria in this project was set to C_i<0.75 the entire 25% (nominal) safety margin against cracking at C_i=1.0 was terminated. Initially (with f_{ts}) the calculations showed C_i-values ≤ 0.75, but on-site there was a moderate cracking tendency. After implementing the lower f_t in the simulations it was shown that cooling pipes had to be used in the massive walls to get the C_i-values below 0.75. After this, through-cracks never occurred in all cases where the cooling system worked as intended.

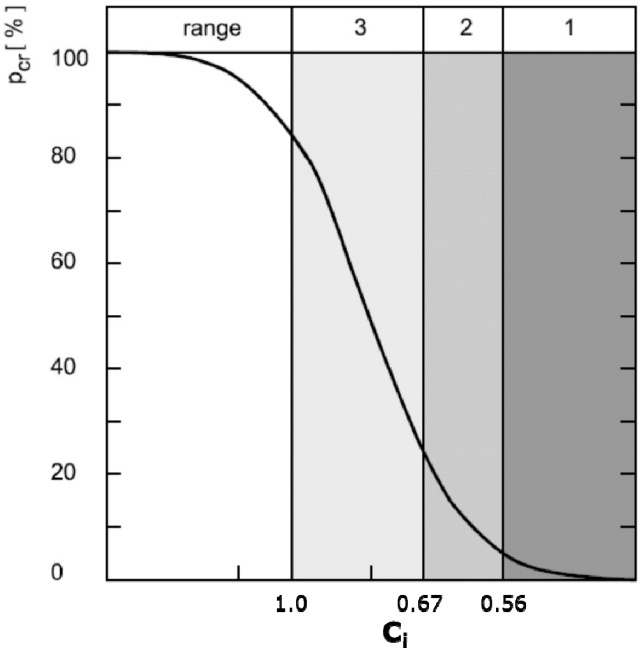

Figure 67 Crack criteria (C_i) dependent on the probability of cracking (P_{cr}), adjusted for on-site observations. Based on [120][121]

Finally, some countries operate with "a safety factor" γ rather than a crack index C_i. γ is simply the inverse of C_i:

Equation 33 $$\gamma = \frac{1}{C_i} = \frac{f_t}{\sigma_c}$$

For example, a C_i-interval 0.60-0.75 then corresponds to a safety factor γ of 1.67-1.33.

13 Effect of reinforcement

The mode of operation for the reinforcement in a hardening concrete structure subjected to external restraint is generally understood as follows: Since the coefficients of thermal expansion of steel and concrete are rather similar it is likely that reinforcing steel bars are more or less stress-less during the temperature changes in a hardening structure. The steel bars only acts to reduce crack widths when cracks are actually formed.

For a structural concrete subjected to external (service) loads an increasing amount of reinforcement decreases the crack widths; this is the basis in standards and codes for structural design. Standards and codes are mainly based on well-controlled laboratory flexural tests, and the requirements generally aim to limit crack widths to 0.2-0.3 mm.

With regard to cracking in hardening structures it is thus expected that the crack widths also will be limited when the amount of reinforcement is increased. However, the structural behaviour of a hardening structure is often complex, and it is not obvious how stresses/strains redistribute when cracks form and how effective the reinforcement will be. To the author's knowledge no systematic registrations have been done with regard to the effect of reinforcement on the crack widths of through-cracks in hardening structures. It is a fact though that extra reinforcement is sometimes used as a measure, in the case of through-cracks, to limit crack widths/increase the probability for water-tightness.

14 Importance of input parameters

The influence of input parameters on the calculated crack sensitivity from stress simulations have been studied in [127][128][129][130]. Based on these studies, and general experience with stress simulations, a ranking of the importance of parameters with regard to stress build-up and crack-risk in a structure is made in the following. It is divided into two categories, material properties and ambient/site-conditions. The various parameters have been ranked into groups with regard to their influence/significance in stress calculations; where group 1 has large significance, group 2 has less etc.

Significance of material properties

Group 1
- heat of hydration (accuracy of temperature calculation)
- coefficient of thermal expansion
- autogenous shrinkage
- end of dormant phase (i.e. t_0)
- final value of tensile strength and modulus of elasticity

Group 2
- time development of tensile strength and modulus of elasticity
- creep/relaxation

Group 3
- activation energy
- heat capacity (specific heat x concrete density)
- thermal conductivity

It should be noted that any sensitivity analysis on the effect of the activation energy (E_T) should be performed by changing the E_T and then determine new pertaining model parameters with this changed E_T. E_T cannot be changed alone.

Significance of ambient/site conditions

Group 1
- temperature of fresh concrete / temperature development of the hardening concrete
- temperature of restraining structure(s)

Group 2
- heat transfer coefficient of formwork
- ambient temperature
- wind

Note that the Group 2 parameters right above will have larger impact for smaller cross sections than for massive structures.

15 Minimum test program and simulation strategy

15.1 Minimum test program

The starting point is that we need input data for temperature- and stress simulations of a given concrete that shall be used in a structure in a building project, i.e. we have a concrete with unknown properties that must be tested experimentally. The proposed programme below is considered to be a minimum for such purpose. The suggested program is partly reported previously and partly an extract of the issues that are dealt with earlier in this report.

In Norway today, all the relevant concrete properties needed for temperature- and stress simulations can only be measured experimentally in the NTNU/SINTEF-laboratory in Trondheim.

Mechanical properties

Based on a number of tests on concretes made mainly of cements of type CEM I it was found in [101] that the relationship between the mechanical properties for the various mixes was quite similar. This observation was utilised to define a minimum test programme for mechanical properties. The proposal below is based on the CEB-FIP model code formulation (see Equation 14) and the following minimum test program was proposed:

- The temperature sensitivity factor (activation energy) can be determined from compressive test results, hence an adequate test programme involving quite frequent testing over time at different curing temperatures must be carried out, see NS 3656 Rate of reaction.

- To determine the parameter t_0 from compressive test results is the simplest method (extrapolation from low early strength values to zero strength). However, the best determination of t_0 is likely to be from stress measurements from a restraint stress test (TSTM-test), if this is available. t_0 can also be indirectly determined, though less accurate, from heat of hydration measurements, or by methods based on ultrasonic pulse velocity.

- E-modulus and tensile strength tests on specimens exposed to isothermal conditions (20 ^{o}C) at two ages: at around 2 days and at 28 days. Uniaxial tensile strength should be used in simulations, either measured directly or deduced from splitting strength results. Note that if the 28-days compressive strength at elevated curing temperature shows a significant strength loss compared to 20 ^{o}C curing, then this issue should also be studied for the tensile strength.

> The parameters s and t_o are determined from the compressive strength test results, while the parameters n_t and n_E are determined from the tensile strength and the E-modulus test results, respectively. Default values based mainly on concretes with CEM I was proposed (n_t =0.59 and n_E =0.37) [101] and might probably be used without significant loss of accuracy, but note that the default values are not necessarily applicable for CEM II, CEM III, fly-ash additions, etc.

Hydration heat

A semi-adiabatic calorimeter test is very simple to perform and one test is generally sufficient to characterize the heat evolution of a concrete. During such test the core temperature of the specimen and the surrounding air temperature must be registered. In principle the determination of the hydration heat is better the larger the semi-adiabatic calorimeter is. 1 m^3 concretes specimens have sometimes been used (on-site), but much less specimens can be used in the laboratory without losing significant accuracy (see NS 3657 Heat of hydration). Semi-adiabatic test results must be

compensated for the heat loss during the test in order to determine the adiabatic temperature rise of the concrete. The adiabatic temperature rise is then converted to isothermal heat development, which is the input for temperature simulations.

- For CEM I-based concretes the hydration heat is rather fast and a 7-15 litres well-insulated cubic specimen (see NS 3657) is believed to give sufficient accurate data since a large portion of the heat is actually accumulated in the specimen and thus measured as a temperature rise.
- For slower binders (CEM II, CEM III, fly ash additions, etc) more time is given for the specimen to loose heat during the hydration period, thus a less portion of the heat is accumulated in the specimen. To counteract for this, one approach has been to place the well-insulated semi-adiabatic calorimeter in a hot room (for instance 35^{o}C) just after casting. This reduces the temperature difference between specimen and room during the test, consequently the heat loss during the test is reduced. Alternatively, the volume of the specimen can be increased for concretes that are made with slow binders; this increases the accumulated heat in the specimen relative to the heat loss.

Adiabatic calorimeters can also be used, naturally, but there is doubt whether it increases the accuracy compared to semi-adiabatic calorimeters [131]. The reason for this is probably that adiabatic calorimeters may suffer from the need for an advanced and very accurate heat compensation system. Every minor malfunction/inaccuracy in this system influences the result. (Isothermal calorimeters are also sensible equipment which can only measure on small specimens, preferably cement paste)

Thermal dilation and autogenous shrinkage

Due to the unsystematic effect of temperature on autogenous shrinkage and thermal dilation, as discussed in Chapter 7, the test temperature will influence the quality of the data for the simulations. The type of tests given below is categorized according to the quality of the output from the test (ranking 1, 2, 3), where tests performed under realistic temperature developments gives the best data. The temperature of the specimen(s) should be measured during any of the tests.

1. Test temperature development realistic/typical for the given structure in the project (taken from a temperature simulation of the structure, for instance the average temperature development of the structure):
   A. Realistic stepwise (saw-toothed) temperature development: The coefficient of thermal expansion (α_T) can be found from each temperature step. The average α_T can be calculated (or expressed by a variable model formulation). Autogenous shrinkage is then the remaining deformation when the thermal part ($\alpha_T \cdot \Delta T$) is subtracted from the measured (total) deformation from the test.
   B. Realistic (smooth) temperature development(s): The coefficient of thermal expansion (α_T) must be assumed (qualified guess). Autogenous shrinkage is then deduced by subtracting the thermal part ($\alpha_T \cdot \Delta T$) from the measured (total) deformation from the test.

2. Isothermal temperature development test(s): Autogenous shrinkage is measured directly during the test as there is no temperature change. For simulations the coefficient of thermal expansion (α_T) must be assumed.

3. No data available. Autogenous shrinkage and the coefficient of thermal expansion (α_T) must be assumed, preferably by using experience from previous tests on concrete(s) of the same quality (same water-to-binder ratio, etc) and rather similar binder composition.

15.2 Simulation strategy

When all involved concrete properties are implemented into the program, either by a model or discrete data, the simulations can start. The ideal case is (A) first to use the given simulation program (2D or 3D) to simulate the situation in one or more TSTM-tests with the concrete in question. If this simulation(s) fit well with the TSTM-test(s) this secures confidence in the materials models and the simulation program.

The actual structure can then be simulated for the given concrete, structural geometry and relevant on-site conditions. If temperature is measured in any previous sections in the project it is advisable first to compare these temperature curves with a temperature calculation (B) using the site-conditions during that particular cast (actual formwork, climate, fresh concrete temperature, etc.).

The temperature- and stress development of structural parts to be cast in the future can now be simulated (C) for relevant on-site conditions, and the probability for cracking can be evaluated; see Chapter 12 for crack risk criteria.

Note that the compressive strength development is also one of the many outputs of such simulations. Hence, simulations can naturally be used also in the production planning, for instance, to avoid freezing of the fresh concrete during cold weather, to determine the earliest time of formwork removal, necessary duration of support of decks, earliest time of post-tensioning, etc.

References

[1] Meddelelse nr. 1, Den Norske Ingeniørforening (1930) Undersøkelse av skader på våre betongdammer og bruddstensdammer i mørtel, årsak og botemiddel. Oslo 1930.

[2] Blanks R.F., Meissner H.S. and Rawhouser C. (1938) Cracking in mass concrete. Journal of American Concrete Institute, March-April 1938, pp. 477-495

[3] Abrams D.A. (1945) Cracking and temperature control of mass concrete. Proc. of the American concrete institute. November 2945, pp. 1-24

[4] http://no.wikipedia.org/

[5] Carlson R.W. (1938) Temperature and stresses in mass concrete. Proc. of the American concrete institute. March-April 1938, pp. 497-515

[6] ACI Committee No 207 (1970) Mass concrete for dams and other massive concrete structures, Journal of the American concrete institute, April 1970, pp. 273-309

[7] Carlson R.W. (1937) A simple method for the computation of temperatures in concrete structures. Proc. of the American concrete institute, Nov-Dec 1937, Vol.34, p.89

[8] Reinius E. (1942) Ytspänningar ock ytarmering i massiva betongkonstruktioner (Eng: Surface stresses and surface reinforcement in mass concrete structures), Swedish cement and concrete research institute, Tidsskrift, no. 3.

[9] Asplund S.O. (1945) Några kriterier för skadelig sprickbildning i armerad betong (Eng: Some criterias for hermful crack formation in reinforced concrete). Swedish cement and concrete research institute, Vol.30, H.1, pp.21-27

[10] Davis R.E., Davis H.E. and Brown E.H. (1937) Plastic flow and volume changes of concrete. Proceedings, American Society for Testing and Materials, Part II, Philadelphia, pp. 317-331

[11] Sjödin O.V. (1936) Mätningar på krympning och swëllning i utförda betongkonstruktioner (Eng.: Measurements of shrinkage and expansion in built concrete structures). Betong, Vol.2, No.2, pp. 76-89

[12] Springenschmid R. (1969) Versuche und Erfahrungen mit Längs- und Querfugen (Eng: Tests and experiences with longitudinal and transversal joints). Zement und Beton, pp. 9-18

[13] Springenschmid R. and Nischer P. (1973) Untercuchungen über die Ursache von Querrissen im jungen Beton (Eng: Investigation of the causes of cracking in young concrete). Beton und Stahlbetonbau, 9-1973

[14] Orr D.M.F. and Haigh G.F. (1971) An apparatus for measuring the shrinkage characteristics of plastic mortars. Mag. of Concr. Res., Vol.23, No.74, March

[15] Paillére A.-M. and Serrano J.-J. (1976) Appareil d'étude de la fissuration du béton, Bull. Liaison Labo (Eng: Apparatus for studying cracking in concrete). Pont et. Ch., 83, May-June, pp. 29-38

[16] Springenschmid R., Gierlinger E. and Kiernozycki W. (1985) Thermal stresses in mass concrete: A new testing method and the influence of different cements. 5th int. conf. on large dams (ICOLD), Lausanne, 57-R. 4, pp. 57-72

[17] Springenschmid R., Breitenbücher R. and Mangold M. (1994) Development of the Cracking Frame and the Temperature-Stress Testing Machine. Proc. of the Int. Symposium Thermal Cracking in concrete in early ages. Rilem proc. 25, Ed. Springenschmid, Munich, Oct. 1994

[18] Mangold M. (1994) State of the art report: Methods for experimental determination of thermal stresses in the laboratory. In the RILEM TC-119 TCE Technical recommendation report based on the Int. symp. Thermal cracking in concrete at early ages, Oct. 10.-12.

[19] Nylander H. (1944) Några spänningsoptiska undersøkningar (Eng.: Some stress-optical investigations). Tekniska Skrifter, no 101.

[20] Reinius E. (1945) Temperatur ock krympspänningar i betongskivor, som stå på fast underlag (Eng.: Temperature and contraction-stresses in concrete walls which are fixed to the base)., Vol. 30, H.1, pp.1-20

[21] Hansen T.C. (1960) Ytsprickbildning hos massiva betongkontruktioner vid tidlig formrivning (Eng.: Surface cracking of mass concrete structures at early formremoval). Utredningar no. 4, Stockholm 1960, pp. 119-132

[22] Cannon R.W. (chairman) et al (1973) Effect of Restraint, volume change, and reinforcement on cracking of massive concrete. ACI Journal, July 1973, pp. 445-470

[23] Bernander S. (1973) Kylning av hårdnande betong med kylslingor (Eng.: Cooling of hardening concrete by means of embedded cooling systems). Nordisk betong 2-1973, pp.21-30

[24] Buö F.O. (1973) Sprickbildning i betongväggar til följd av cementets hydratasjonsvärmeutvikling (Eng: Crack formation of concrete walls due to evolution of heat of hydration). Nordisk betong 2-1973, pp. 12-20

[25] Bernander S. (1981) Egenspänningar i ung betong pga temperaturförlopp under hydratationen (Eng: Eigenstresses in young concrete due to temperature developments under hydration). Nordisk betong 2-1981, pp. 25-31

[26] Saul A.G.A. (1951) Principles underlying the steam curing of concrete at atmospheric pressure. Magazine of Concrete Research, Vol.2, No.6, pp. 127-140

[27] Freisleben Hansen P. (1975) Matematisk simulering af temperaturefordeling og egenskabsudvikling i hærdnende betonkontruktioner (Eng: Mathematic simulation of temperature distribution and property development in hardening concrete structures). Proc. of the Nordic seminar: Termiske problemer ved udførelse af massive betonkonstruksjoner (Eng: Thermal problems during execution of massive concrete structures), Copenhagen, 11th September 1975, Nordisk Betonforbund, Published by Danish Concrete Federation (Dansk Betonforening), November 1975 1975

[28] Proceedings of the Nordic seminar: Thermal problems during execution of massive concrete structures (in Danish: termiske problemer ved udførelse af massive betonkonstruksjoner), Copenhagen, 11th September 1975, Nordisk Betonforbund, Published by Danish Concrete Federation (Dansk Betonforening), November

[29] Freisleben Hansen P. (1977) Måleinstrument til control af betongens hærdning (Eng: Maturity Computer for controlled curing and hardening of concrete). Nordisk betong 1-1977, pp. 21-25.

[30] Freisleben Hansen P. (1978) Hærdeteknologi-2, Dekrementmetoden (in Danish), Åalborg Portland og BKF-centralen

[31] Freisleben Hansen P. and Pedersen E.J. (1982) Winter-casting of concrete (in Danish: Vinterstøbing av beton). Danish Building Research Institute (Statens byggeforskningsinstitut), SBI-anvisning 125

[32] Sellevold E.J. and Knudsen T.S. (1979) Cement research in Scandinavia. Advances of concrete technology – Cements research progress 1979. pp. 263-279

[33] Pedersen S. (1976) Dansk Betongdag 1976 (Eng: Danish concrete day 1976). Nordisk Betong, 6-1976, p. 19

[34] Jonasson J.-E. (1977) Datorprogram för icke-lineära beräkningar i betong med hänsyn til svinn, krypning ock temperatur (Eng: Computer program for non-linear analyses of concrete in view of shrinkage, creep and temperature), Swedish Cement and Concrete Institute, Fo 7:77, Stockholm 1977, pp. 161

[35] Jonasson J.-E. (1988) HETT, et datorprogram för beräkning av hollfasthet, ekvivalent tid ock temperatur (Eng: HETT, a computer program for calculation of strength, equivalent time and temperature). Swedish Cement and Concrete Research Institute, Stockholm, 1988, pp. 53

[36] Emborg M. (1989) Thermal stresses in concrete at early ages. Doctoral thesis, Division of structural engineering, Luleå University of Technology.

[37] Le Chatelier H. (1900) Sur les changements de volume qui accompagnement le durcissement des ciments. Bull. Soc. Encour. Ind. Natl., 5th series, pp. 54-57

[38] Powers T.C. (1935) Absorption of water by Portland cement paste during the hardening process. Industrial and engineering chemistry, Am. Chem. Soc., Vol.27, No.7, pp.790-794

[39] Lynham C.G. (1935) Growth and movement in Portland cement concrete. Oxford Univ. press, London, Humphrey Milford, Chapter III, pp. 25-45

[40] Davis H.E. (1940) Autogenous volume changes of concrete. Proc. Am. Soc. for testing and materials. Philadelphia, Pa, The Society, pp. 1103-1110

[41] Swayze M.A. (1942) Early age volume change and their control. Proc. ACI, Vol. 38, No. 5, April 1942, pp. 425-440

[42] Houk I.E. and Borge O.E. (1969) Studies of autogenous volume change in concrete for Dworshak Dam. ACI Journal, July 1969, pp. 560-568

[43] Proceedings of the int. conference on concrete of early age, RILEM report, Paris, France, 1982, ISBN 2-85978-038-6

[44] Proceedings of the int. conference: Thermal Cracking in Concrete at Early Ages, Ed. by R.Springenschmid, Published 1994 by E & FN Spon, 2 - 6 Boundary Row, London SE1 8HN, UK. ISBN: 0 419 18710 3, pp. 449-456

[45] Proceedings of the int. NTNU/SINTEF workshop: Early volume change and reactions in paste-mortar-concrete, Trondheim, Norway, 1996

[46] Proceedings of the int. workshop: Autogenous Shrinkage of Concrete. Organized by the Japan Concrete Institute, Hiroshima, Japan, 1998, Ed. by E.Tazawa, © 1999 E & FN Spon, ISBN 0-419-23890-5.

[47] Proceedings of the int. research seminar: Self-desiccation and its importance in concrete technology. Lund, Sweden, 1997, Ed. by B.Persson and G.Fagerlund, ISBN 91-630-5528-7

[48] Proceedings of the second int. research seminar: Self-desiccation and its importance in concrete technology. Lund, Sweden, 1999, Ed. by B.Persson and G.Fagerlund, ISBN 91-630-8230-6

[49] Proceedings of the third int. research seminar: Self-desiccation and its importance in concrete technology. Lund, Sweden, 2002, Ed. by B.Persson and G.Fagerlund, ISBN 91-631-1993-5

[50] Proceedings of the fourth int. research seminar: Self-desiccation and its importance in concrete technology. Gaithersburg, Maryland, USA, June 2005, Ed. by B.Persson, D.Bentz and L-O.Nilsson, ISBN 91-631-7102-3

[51] Proceedings of the int. RILEM workshop: Shrinkage of Concrete, Shrinkage 2000. Paris, France, 2000, Ed. by V.Baroghel-Bouny and P.-C. Aïtcin, PRO 17

[52] Proceedings of the int. workshop: Control of cracking in early-age concrete. Sendai, Japan, 2000

[53] Proceedings of the RILEM int. conference on early age cracking in cementitious systems (EAC'01). Israel, 2001. Ed. by K.Kovler and A.Bentur.

[54] Rilem Technical committee TC 195-DTD Recommendation for Test Methods for autogenous deformation and thermal dilation of early age concrete (2007) Round Robin documentation report: Program, test results and statistical evaluation. Final draft, presently unpublished as a RILEM-report.

[55] RILEM Technical committee TC 196-ICC (2007) Internal curing of concrete, state-of-the-art report. ISBN 978-2-35158-009-7, p. 161

[56] Proceedings of the Nordic workshop: Crack risk assessment of hardening concrete structures, Ed. by Bjøntegaard Ø. and Kanstad T., Trondheim, March 31.–April 1. 2005, Nordic Concrete Federation, ISBN 82-91341-97-4

[57] Proceedings (CD) of the second int. RILEM Symposium: Advances in Concrete Through Science and Engineering at Quebec City, Canada, Ed. by Marchand J, Bissonnette B., Gagne R, Jolin M. and Paradis F., Sept. 11-13, 2006

[58] Sellevold E.J. and Bjøntegaard Ø. (2006) Driving forces to cracking in hardening concrete: Thermal and autogenous deformations. Proc. (CD) of the second int. RILEM Symposium: Advances in Concrete Through Science and Engineering at Quebec City, Canada, Ed. by Marchand J, Bissonnette B., Gagne R, Jolin M. and Paradis F., Sept. 11-13, keynote paper.

[59] Separate session at ACI Fall Convention 2002, Phoenix, Arizona. Papers were later published in: ACI SP-220: Autogenous deformation of concrete. Ed. by O.M.Jensen, D.P.Bentz and P.Lura, 2004, ISBN 0-87031-143-3

[60] Proceedings of the int. conference (2003) Advances in Cement and Concrete. Copper Mountain, Colorado. Ed. by D.A.Lange, K.L.Scrivener, J.Marchand, Copyright © 2003 University of Illinois

[61] Proceedings (CD-rom) of the ACBM/RILEM int. symposium (2004) Advances in concrete through science and engineering. Evanston, Illinois

[62] Bjøntegaard Ø. (2005) The Nor-Crack project 2001-2005: Project information, results and materials data base. Proc. of the Nordic workshop: Crack risk assessment of hardening concrete structures, Ed. by Bjøntegaard Ø. and Kanstad T., Trondheim, March 31 – April 1, The Nordic Concrete Federation, pp 8-16

[63] Private correspondence with Steinar Helland, Skanska, regarding the early developments of curing technology in Norway.

[64] Sandvik M. (1984) Matematiske modeller av betongens fasthetsutvikling og anvendelse på betong med og uten tilsetning av silikastøv (Eng: Mathematical models of concrete strength development and application on concrete with and without silica fume additions). Dr. thesis, NTH, Division of building materials. Report BML 84.101, Sept. 1984

[65] NTNU-course (1988) "Betongens herdeteknologi" (Eng: Curing technology for concrete). Norges Tekniske Høgskole, Institutt for Byggningsmateriallære

[66] Helland S. (1986) Curing control by Microcomputer. Nordisk Betong, Vol. 1-2, pp. 63-70

[67] Helland S. (1987) Temperature and strength development in concrete with w/c less than 0.40. Proc. of the Symp. Utilization of High Strength Concrete, Stavanger, Norway, June 15-18, 1987, Ed. Holand I., Jakobsen B., Helland S. and Lenschow R., ISBN 82-519-0797-7, pp. 473-485

[68] Smeplass S. (1988) Kalor, programdokumentasjon (Eng: Calor, program documentation). Sintef FCB-report, STF65 A88031, ISBN 82-595-5096-2 (in Norwegian)

[69] Kompen R. (1991) DP 3-1 Produksjonsteknologi, fersk betong. Materialutvikling høyfast betong, Aker Entreprenør a.s., memo to meeting 01.08.1991

[70] Kompen R. (1993) Low water-to-binder ratio concrete for bridges: Experiences from full-scale construction. Proc. of the Symp. Utilization of high strength concrete, Lillehammer, Norway, June 20-23, 1993, pp. 512-516

[71] Kompen R. (1994) High performance concrete: Field observations of cracking at early ages. Proc. of the int. conference: Thermal Cracking in Concrete at Early Ages, Ed. by R.Springenschmid, Published 1994 by E & FN Spon, 2 - 6 Boundary Row, London SE1 8HN, UK. ISBN: 0-419-18710-3, pp. 449-456

[72] Piene E.G. (1992) Tøyningskapasitet og ultralydhastighet for betong i tidlig alder (Eng: Strain capacity and ultra-pulse velocity in concrete at early ages). NTH-report, Report N8 from the project "Cracking of high strength concrete at early ages", 01.06.1992

[73] Piene E.G. (1992) Resultater fra måling av volumendringer for forseglede sementpastaprøver (Eng: Results from measurements of volume changes in sealed cement paste samples), NTH-memo, 1992

[74] Sellevold E.J. and Piene E.G. (1992) Volumendring pasta: Kjemisk svinn, bulk volumsvinn, RF-utvikling, porevanntrykk (Eng: Volume change paste: Chemical sjrinkage, bulk volume shrinkage, RH-development, pore water pressure). NTH-report, Report N10 from the project "Cracking of high strength concrete at early ages", 10.12.1992

[75] Radocea A. (1990) Water pressure in fresh and young cement paste. Nordic Concrete Research, No. 9, Dec. 1990, Oslo

[76] Bjøntegaard, Ø. (1992), Plastic cracking sensitivity of concrete with water-binder ratio of 0.40. Msc thesis, The Norwegian University of Technology (NTNU), Trondheim, No. 071264.00, Dec. 1992 (in Norwegian).

[77] Bjøntegaard, Ø. (1993), Opprissing av brubetong i tidlig, plastisk fase (Eng.: Cracking of bridge concrete in early, plastic phase), NTH-report, Report N14 from the project "Cracking of high strength concrete at early ages", 06.10.1993

[78] Johansen R. (1980) Tendency of cracking due to plastic shrinkage. Sintef-report STF 65A 80016, FCB 1980 (in Norwegian)

[79] Hammer T.A. (2007) Deformations, strain capacity and cracking of concrete in plastic and early hardening phases. Doctoral thesis, NTNU, ISBN 978-82-471-5191-4

[80] Sellevold E.J. (1992) Macroscale measurement methods, status. Report on a trip to Paris and München. NTH-report, Report in the project "Cracking of high strength concrete at early ages", 10.12.1992

[81] Kanstad T. (1994) Early age behaviour of concrete and reinforced concrete structures. NTNU-report. 12-09-1994.

[82] Bjøntegaard, Ø. (1999) Thermal Dilation and Autogenous Deformation as Driving Forces to Self-Induced Stresses in High Performance Concrete. PhD thesis, NTNU, Dept. of Structural Eng., Dec. 1999, ISBN 82-7984-002-8.

[83] Bosnjak D. (2000) Self-Induced Cracking Problems in Hardening Concrete Structures. Doctoral thesis, NTNU, Dept. of Structural Eng., Dec. 2000, ISBN 82-7984-151-2.

[84] Atrushi D. (2003) Tensile and Compressive Creep of Early Age Concrete: Testing and Modelling. Doctoral thesis, NTNU, Dept. of Structural Eng., March 2003, ISBN 82-471-5565-6.

[85] Ji G. (2008) Cracking Risk of Concrete Structures in the Hardening Phase: Experiments, Material Modelling and Finite Element Analysis, Doctoral thesis, NTNU, Dept. of Structural Eng., ISBN 978-82-471-1079-9

[86] Smeplass S., Bjøntegaard Ø., Kompen R., Haram E. (2010) Bjørvika submerged tunnel, experiences. Crack-control in the concrete's hardening phase. (in Norwegian: Senketunnelen i Bjørvika, erfaringsrapport. Kontroll med opprissing i betongens herdefase). Technology report no. 2580, Norwegian Public Roads Administration, Road Directorate. 2010-03-05, ISSN 1504-5005

[87] Temadag: Bjørvikaprosjektene – erfaringer med lavvarmebetong og risskontroll (Eng: The Bjørvika projects – experiences with low-heat concrete and crack control), oral presentations, no proceedings. Arr. by the Norwegian Concrete Association, Ingeniørenes Hus, Oslo, April 27., 2010.

[88] Hoff A. (1980) Temperature stresses/Heat of hydration. Part 3: Parameter studies at FCB. FCB-report STF65 F80064, Trondheim, Norway

[89] Gemert A. van and Verboven F. (1993) Chemical shrinkage of cement pastes, Msc thesis, Katholieke Universiteit Leuven and NTNU, Trondheim 1994

[90] Reyniers B. and Van Loo D (1993) Chemical shrinkage of cement, Msc thesis, Katholieke Universiteit Leuven and NTNU, Trondheim 1993

[91] Ardoullie B. and Henrix E. (1997) Chemical shrinkage of cementitious pastes and mortars", Msc thesis, Katholieke Universiteit Leuven and NTNU, Trondheim 1997

[92] Justnes H., Van Gemert A., Verboven F., Sellevold E.J. (1996) Total and external chemical shrinkage of low w/c-ratio cement pastes", Adv. in Cement Research, Vol. 8, No. 31, pp. 121 - 126, 1996

[93] Bjøntegaard Ø. and Sellevold E.J. (2001), Autogenous and Thermal Deformations, IPACS-report, TU Luleå, Sweden, ISBN 91-89580-20-6.

[94] Dettling H. (1964) Die Wärmedehnung des Zementstaines, der Gesteine und der Betone (thermal dilation of cement paste, aggregate and concrete), Deutscher Ausschuss für Stahlbeton, Heft 164, Berlin 1964 (in German)

[95] Maruyama I. and Teramoto A. (2011) Impact of time-dependant thermal expansion coefficient on the early-age volume changes in cement pastes. Cement & Concrete Research 41 (2011), pp.380-391

[96] Hashida H. and Yamazaki N. (2002) Deformation composed of autogenous shrinkage and thermal expansion due to hydration of high-strength concrete and stress in reinforced structures. Proc. of the 3rd Int. Res. Seminar: Self-desiccation and its importance in concrete technology. Ed. by Persson B. and Fagerlund G., Lund Institute of Technology, June 14-15, 2002, pp. 77-92

[97] Hedlund H. (2000) Hardening concrete: Measurements and evaluation of non-elastic deformation and associated restraint stresses. Ph.D. thesis, TU Luleå, ISBN 91-89580-00-1

[98] Kjellmann O. and Olofsson J. (2001) 3D structural analysis of crack risk in hardening concrete. Verification of an engineering method. IPACS report, TU Luleå, ISBN 91-89580-53-2

[99] Olofsson J., Bosnjak D. and Kanstad T. (2000) Crack Control of Hardening Concrete Structures - Verification of a Three-step Engineering Method. 13th Nordic Seminar on Computational Mechanics (NSCM-13)

[100] Kanstad T., Hammer T.A., Bjøntegaard Ø. and Sellevold E.J. (2003) Mechanical Properties of Young Concrete: Part I - Experimental Results related to Test Methods and Temperature Effects, Materials and Structures, Vol. 36, May 2003, pp 218-225.

[101] Kanstad T., Hammer T.A., Bjøntegaard Ø. and Sellevold E.J. (2003) Mechanical Properties of Young Concrete: Part II - Determination of Model Parameters and Test Programme Proposals, Materials and Structures, Vol. 36, May 2003, pp 226-230.

[102] AF Spesialprosjekt, materialdokumentasjon: Dahl P.A (2006) Bjørvikaprosjektet, entreprise Sørenga: Dokumentasjon av egenskaper for lavvarmebetong. Sintef Prøvningsrapport, 2006-03-14

[103] Krauss M., Hariri K. and Rostasy F., Non-Destructive Assessment of Mechanical Properties of Concrete at Very Early Age by US Techniques - Methods, Results and Modelling, IPACS-report BE96-3843/2001:12-5

[104] Øverli J.A., Calculation methods. Temperature- and stress analysis by use of FEM (in Norwegian). Part of Tekna-course 2010-01-05: Young concrete – crack-control with curing technology.

[105] Nilsson M. (2000) Thermal cracking of young concrete: Partial coefficients, restraint effects and influence of casting joints. Licentiate thesis, Luleå Univ. of Technology, ISSN 1402-1757.

[106] Jonasson J.-E., Wallin K. and Nilsson M. (2009) Casting of wall on slab. Study of risk of cracking due to hardening phase temperature development (in Swedish: Gjutning av vägg på platta. Studier av sprickrisker orsakat av temperaturforlöppet vid härdningen). Luleå Tech. Univ., Report, ISSN 1402-1528, ISBN 978-91-86233-73-0

[107] Handbook, Bro 2004 (2004) Swedish National Road Authorities, Chapter 4-11 Temperature cracks in concrete – cracking risk

[108] Sellevold E.J. and Bjøntegaard Ø. (2006) Coefficient of Thermal Expansion of Cement Paste and Concrete: Mechanisms of Moisture Interaction. Materials and Structures, 39, 9, pp. 809-815.

[109] Bjøntegaard Ø. and Sellevold E.J. (1998) Thermal Dilation-Autogenous Shrinkage: How to separate?, Proceedings of the Int. Workshop : Autogenous Shrinkage of Concrete, Ed. by Ei-ichi Tazawa, © 1999 E & FN Spon, ISBN 0-419-23890-5.

[110] Selmer Olsen R. and Brock E. (1983/84) Engineering geology – Rock (in Norwegian: Ingeniørgeologi – Fjell), Compendium in Subject 21515, NTNU.

[111] Bjøntegaard Ø., Fosså K.T., Atrushi D., Sellevold E.J., Kanstad T., Hammer T.A and Smeplass S. (2003) Stress development and cracking tendency in hardening concrete: Test methods at NTNU, NOR-CRACK report #2.1, Subtask 2 Fundamental studies, STF22 A03607, ISBN 82-14-02582-6.

[112] Various documentation reports in Norwegian from the Bjørvika Project, the Bjørvika Tunnel Consortium (Skanska, Bam, Volker Stevin), The Bjørvika Project – The sea part, 2005-2007.

[113] Collection of 12 reports on various experiments on low-heat concrete (2004). The Bjørvika Project, E18 between the Festningstunnelen and the Ekeberg tunnel, The Norwegian Public Roads Administration, November 2004.

[114] 4C-Temp&Stress calculation program, user manual (1998) DTI Building and Technology, Denmark

[115] ConTeSt Pro (1999) User manual

[116] Kanstad T., Bosnjak D. and Øverli J.A. (2001) 3D Restraint Analyses of Typical Structures with Early Age Cracking Problems, IPACS report, TU Luleå, ISBN 91-8958-32-x

[117] Larson M. (2003) Thermal crack estimation in early age concrete – Models and methods for practical application. Doctoral thesis 2003:20, TU Luleå, ISBN 91-89580-04-4

[118] Kanstad K. (2005) Verification of three different calculation methods for early age concrete. Proc. of the workshop: Crack risk assessment of hardening concrete structures, Ed. by Bjøntegaard Ø. and Kanstad T., Trondheim, March 31.–April 1. 2005, Nordic Concrete Federation, pp. 101-110, ISBN 82-91341-97-4

[119] Kanstad T., Hammer T.A., Bjøntegaard Ø. and Sellevold E.J (2001) Mechanical properties of young concrete: Evaluation of test methods for tensile strength and modulus of elasticity. Determination of model parameters. IPACS report, Tu Luleå, ISBN 91-89580-49-4

[120] Japan Society of Civil Engineers: Standard specification for design and construction of concrete structures. Second edition, 1995. Referred and evaluated by [122].

[121] Nishida H., Ushioda K., Dobashi Y ans Matsui K. (1995). Evaluation of thermal cracking index in slab-concrete under certain parameters. Trans. of Japan Concrete Inst. Vol. 17, pp. 127-140. Referred and evaluated by [122].

[122] Rostásy F.S., Krauß M. and Gutsch A.-W. (2001) Computation of Stresses and Cracking Criteria for Early Age Concrete, Methods of iBMB, IPACS report, Tu Luleå, ISBN 91-89580-35-4

[123] Kjellman O. and Olofsson J. (2001) 3D Structural Analysis of Crack Risk in Hardening Concrete - Verification of an Engineering Method. IPACS report, Tu Luleå, ISBN 91-89580-53-2

[124] Larson M. (2001) Improved hand calculation method. IPACS report, Tu Luleå., ISBN 91-89580-56-7

[125] Jonasson J.-E., Nilsson M., Larson M. and Hedlund H. (2001) Manual Method with Diagrams for Crack Risk Estimation and Restraint Curves. IPACS report, Tu Luleå. ISBN 91-89580-90-7

[126] Nilsson, M. (2003) Restraint factors and partial Coefficients for Crack Risk Analyses of Early Age Concrete Structures. Doctoral Thesis 2003-19. TU Luleå.

[127] Krauss M., Rostasy F.S., and Budelmann H. (2005) Probabilistic concept for the validation of the effectiveness of countermeasures against early age cracking in massive concrete structuresProc. of the Nordic workshop: Crack risk assessment of hardening concrete structures, Ed. by Bjøntegaard Ø. and Kanstad T., Trondheim, March 31 – April 1, The Nordic Concrete Federation, pp 34-43

[128] Krauss M. (2004) Probabilistic concept for the validation of the effectiveness of measures against early-age cracking in massive structures. Doctoral thesis, Technical University of Braunschweig.

[129] Lura P. and van Breugel K. (2001) Thermal properties of concrete: Sensitivity studies. IPACS report, Tu Luleå. ISBN 91-89580-15-x.

[130] Kanstad T. and Bjøntegaard Ø. (2001) Chapter 5: Materials behaviour, material data base. Part of IPACS Recommendation report. TU Luleå (the full report was never fully completed)

[131] Morabito P., Bjøntegaard Ø., Breugel K. van., Dalmagioni P., Gram H.-E., Gutsch A., Hedlund H., Jonasson J.-E., Kanstad T., Lura P., Pellegrini R., Rostasy F. and Sellevold E. (2001) Round Robin testing programme: Equipment, testing methods, test results. IPACS report, Tu Luleå. ISBN 91-89580-42-7.

APPENDIX 1 Thermal Dilation-Autogenous Shrinkage: How to separate?

Paper

Bjøntegaard Ø. and Sellevold E.J. (1998) **Thermal Dilation-Autogenous Shrinkage: How to separate?**. Proceedings of the Int. Workshop: Autogenous Shrinkage of Concrete, Ed. by Ei-ichi Tazawa, © 1999 E & FN Spon, ISBN 0-419-23890-5.

THERMAL DILATION – AUTOGENOUS SHRINKAGE: HOW TO SEPARATE?

Ø. BJØNTEGAARD AND E.J. SELLEVOLD

The Norwegian University of Science and Technology (NTNU)
Trondheim, Norway

Bjøntegaard Ø. and Sellevold E.J. (1998) *Thermal Dilation-Autogenous Shrinkage: How to separate?*, Proceedings of the **Int. Workshop : Autogenous Shrinkage of Concrete**, Ed. by Ei-ichi Tazawa, © 1999 E & FN Spon, ISBN 0-419-23890-5.

Abstract
Thermal dilation (TD) and autogenous shrinkage (AS) generate stresses in concrete members hardening under restraint. The sum of TD and AS may readily be determined in the laboratory for realistic temperature histories, and may serve as an accurate basis for stress calculations in structures. However, for general calculation programs it is desirable to have individual material models for TD and AS. An experimental strategy is proposed to obtain a basis for such models. Preliminary results are given, which demonstrate that AS depends strongly on temperature history, and cannot be realistically estimated from isothermal tests.
Keywords: Autogenous shrinkage, high performance concrete, temperature dependence, thermal dilation

1 Introduction and background

Hardening concrete will generate stresses if the movements caused by hydration reactions are restrained. There are two active mechanisms producing movements: Thermal Dilation (TD) and Autogenous Shrinkage (AS). Traditionally, only thermally induced stresses have been considered when estimating cracking risk in young concrete. However, with increased use of high performance concrete (water-to-binder ratio below 0.45) it has become clear that AS may contribute significantly to stress generation, and any serious approach to estimate cracking risk by calculations must take both TD and AS into account as “driving forces” to stress generation.

In a realistic case, where the concrete goes through a natural heating-cooling cycle the first days, of course TD and AS occur simultaneously, and the sum of the two deformations may easily and accurately be measured in the laboratory for the given

temperature history. This total deformation is the driving force to stress generation, and from a calculation point of view, there is no need to separate TD and AS. However, a more general stress calculation procedure applicable to any temperature development requires a mathematical model for each mechanism. To achieve this goal it is necessary to design and perform experiments that makes a separation of TD and AS possible. Our effort to do this is the topic of the present paper.

To our knowledge there is, surprisingly, no systematic attempt to formulate general models for TD and AS reported in the literature. Information is available on the Thermal Dilation Coefficient (TDC), and a large number of papers have been published in recent years on AS, but the vast majority on isothermal tests at 20°C.

AS is the external consequence of the chemical shrinkage associated with the hydration reactions, which amounts to about 25% by volume of the chemically bound water. The first few hours the concrete behaves as a liquid, and as chemical shrinkage takes place it is directly reflected in the AS measured externally. During setting a solid skeleton is formed, which allow empty pores to form (self-desiccation) and, as a consequence, AS becomes much smaller than the chemical shrinkage. Thus, initially AS (measured volumetrically) is equal to the chemical shrinkage, while AS is reduced strongly through setting. To measure AS accurately (both linearly and volumetrically) at early times (before and during setting) is very difficult. It is of practical importance, however, since Norwegian experience shows that high performance concrete is sensitive to cracking during this period [1]. The problems associated with AS and very early cracking is a topic discussed separately [2] at this conference.

The present paper only considers AS in the period after setting, i.e. when the elastic modulus is sufficiently developed so that stresses are produced in the Stress-Rig (TSTM). Even in this period there are experimental pitfalls, mainly associated with water supply. If bleeding has taken place before setting, then the bleed water will be reabsorbed by the concrete as self-desiccation occurs, resulting in reduced shrinkage or even expansion. Similarly, water available in the aggregates may play a role, since very little water is required to “refill” the self-desiccation pores and thereby eliminate AS. For instance, in a concrete with 400 kg cement, a 50% degree of hydration corresponds to a volume of self-desiccation pores of: $400 \cdot 0.24 \cdot 0.25 \cdot 0.5 = 12$ l/m^3. This amount of water can easily be available in the aggregates. We have demonstrated that AS is eliminated in concretes with lightweight aggregate [6]. We believe that variations both in amounts and availability of water in aggregates may explain the large differences in AS found in published reports.

The information on TD in the literature is also very limited, but provides certain expectations to the TDC development during the hardening phase. In the fresh (liquid) state the water phase dominates and TDC is very high compared to solids (possibly $60 \cdot 10^{-6}$/°C). When a skeleton is formed we expect solid behavior with much lower TDC. Wittman [3] found that for cement paste (w/c=0.40, saturated) that TDC increased from about $10 \cdot 10^{-6}$/°C at 3 days hydration fairly linearly up to about $18 \cdot 10^{-6}$/°C at 60 days. The moisture content is also important. For mature cement paste Meyers [4] found that TDC depend strongly on ambient Relative Humidity (RH), in that TDC increased from $12 \cdot 10^{-6}$/°C at 100% RH, to about $18 \cdot 10^{-6}$/°C at 70% RH, decreasing to $12 \cdot 10^{-6}$/°C again at 40% RH. It should be added that both publications do present contradictions and inconsistencies, but we conclude that a minimum TDC is expected after setting, followed by a gradual increase over time both due to increased

hydration and reduced RH because of self-desiccation. The determination of TDC also depends strongly on experimental conditions and rate of temperature change. Cement paste contains pore water in different states: interlayer-, gel-, adsorbed-, capillary- and "free" water in the largest pores. Temperature changes will induce redistribution of water between the different phases, for example, heating will drive water from small pores (gel-adsorbed water) to larger pores (capillary water) since the entropy of water in small pores is lower than in large pores. Thus, depending on the time scale, the observed thermal dilation will consist of a "pure" temperature effect (fast), a moisture redistribution effect (slower) and finally both superimposed on a basic AS as long as the hydration reaction is going on.

Based on the preceding considerations the following approach was taken to obtain generalized models for TDC and AS during concrete hardening under realistic temperature conditions. The steps outlined below developed as consequence of the results obtained "on the way". The work has by no means reached the final stage yet. Hence, this paper is a report on work in progress, for the purpose of clarifying the present situation for ourselves as well as for colleagues involved in the same process. Note that all the experiments are carried out using one particular high performance concrete mix.

1. AS at a series of isothermal temperatures from mixing. Purpose: to establish if a simple maturity concept can be used to describe AS. This proved to be impossible.
2. AS at a series of isothermal temperatures, but with fixed starting temperatures (13°C and 20°C) from mixing until 8 hours. At 8 hours the temperature was increased in steps of 7-10°C until the desired isothermal temperatures were reached. This series is referred to as "Poly-isothermal".

The results of steps 1 and 2 demonstrated that a simple generalized description of AS in terms of maturity is not possible. The next step was therefore to determine TDC as directly as possible during isothermal and realistic temperature histories.

3. TDC measured "directly". The principle is to superimpose steps of ±3°C for some hours duration on either isothermal or realistic temperature developments. This scheme allows the calculation of TDC at each step, and then to calculate AS by removing the TD-contribution to the total measured movement. This series is referred to as "Saw-toothed".

Work with this latter approach is presently going on, and the resulting TDC and AS are being analyzed with a view to obtaining generalized descriptions. The work is discussed below.

2 Experimental

2.1 Test method

The experimental work is based on the use of a concrete dilatometer which measures the free length change of a prismatic specimen with dimension 100 mm • 100 mm •

500 mm (length), see Fig. 1. At each end of the specimen an inductive displacement transducer measures the length change. The signals are recorded separately and added to obtain the total length change. The transducers are connected to the specimen by thin invar rods reaching 10-15 mm into the specimen and, hence, the "active" length of the specimen is 470-480 mm. At the end of each invar rod a thin steel disc is fixed as "anchorage". A thermo-couple measures the temperature in the center of the specimen. Registrations of both length change and temperature start within 1 hour after concrete mixing. The temperature control of the specimen is provided by water that is circulated in copper tubes fixed outside 5 mm thick copper plates forming the inner walls of the mould. The plates are heavily insulated on the outside. The water temperature is controlled by a computer.

When the fresh concrete is placed in the mould it is covered with a Al/plastic foil impermeable to moisture. The 5 mm copper plate cover is placed on top and weighted down to provide a seal against moisture loss. The ability of the equipment to prevent moisture loss during the experiments is presumably high, however, not yet determined by measurements. This important question will be resolved by experiments in the near future.

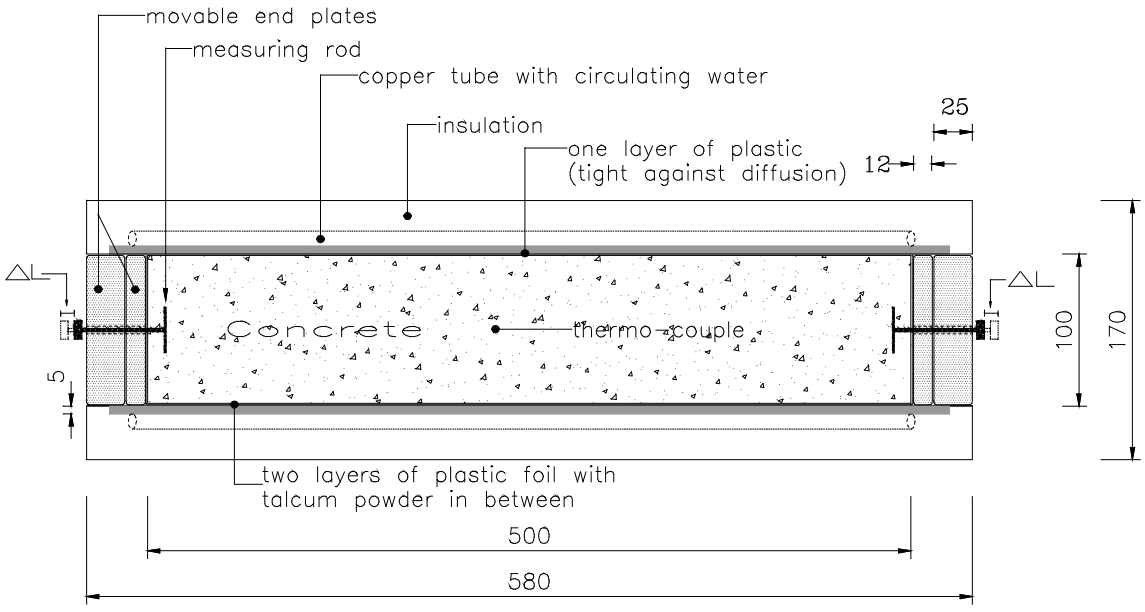

Fig. 1 The concrete dilatometer

2.2 Temperature histories

All the experiments reported here were carried out using one particular high performance concrete mix. Up till now a total of 19 tests have been performed, of which 16 with different temperature histories. Table 1 shows the different temperature histories employed. The initial temperature at each test is given in the left column of the table and the subsequent temperature "treatment" is indicated in the other columns. As can bee seen from the table, most of the tests are performed with initial temperatures of 20°C. Fig. 2 shows measured temperatures during some of the tests with initial temperature of 20°C.

Table 1. Survey of temperature histories (°C)

Initial temperature	Isothermal	Isothermal (saw-toothed) ±3	Poly-isothermal Final temperature 20	27	35	45	Realistic (smooth) Max.temperature 29	32	47	62	Realistic (saw-toothed) Max.temperature 50	60
5	XX											
13	X		X		X							
20	XXX	X		X	X	X	X		X	X	X	X
26								X				
45	X											

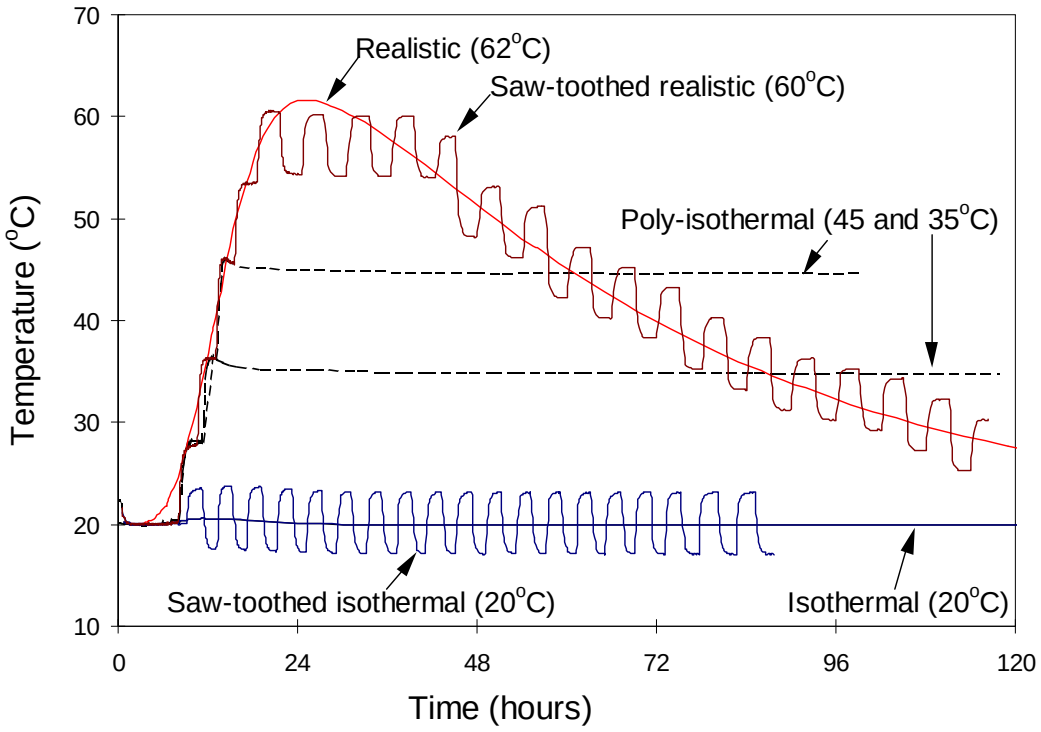

Fig. 2 Examples of different temperature histories (measured)

3 Mix proportions

The same mix is used in all tests. The water-to-binder ratio is 0.40 and the silica fume content is 5% of cement weight. The concrete represents a typical Norwegian concrete used for bridge constructions. Mix proportions are given in Table 2. The slump had a mean value of 18 cm with a coefficient of variation of 15% for the 12 batches at 20°C. The air content varied from 2% to 3.1% for the 19 concrete batches.

Table 2 Mix proportions (kg)

Cement (CEM I-52.5 LA)	368
Water	155
Silica fume	18.4
Sand 0-2 mm	150
Sand 0-8 mm	767
Stone 8-11 mm	636
Stone 11-16 mm	318
Plasticizer (Scancem P)	1.93
Superplasticizer (Mighty 150)	3.09

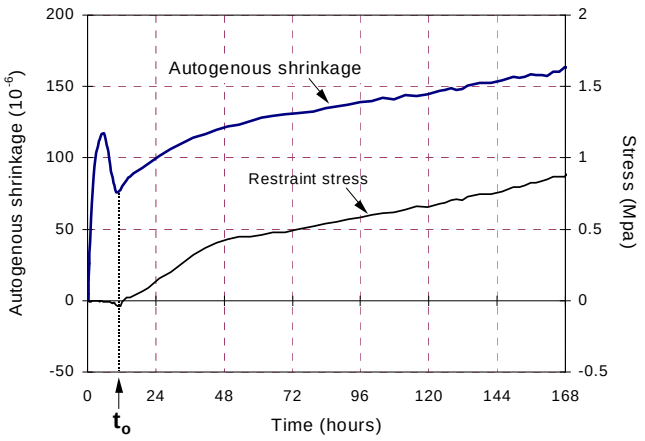

Fig. 3 Autogenous shrinkage and generated stresses (100% restraint) during 20°C isothermal tests. t_o indicates where AS is zeroed.

4 Results

4.1 General behavior of autogenous shrinkage

Fig. 3 shows typical 20°C isothermal results both for AS and the corresponding stress development under full restraint in the TSTM. AS is recorded from time zero, i.e. about ½-1 hour after mixing. The TSTM only provides full restraint after the feedback system is activated at 6 hours after mixing (the feedback system requires a certain concrete stiffness before it is activated). The AS curve shown in Fig. 3 is quite typical: The initial strong contraction (whose physical reality is questionable) is followed by expansion. The expansion is real as evidenced by the (small) compressive restraint stress, and is possibly caused by reabsorption of bleed water. We have chosen to zero the AS curves at the end of the expansion (10 hours age at 20°C). This is indicated as t_o in Fig. 3, and, as can bee seen, AS developing beyond t_o generates significant stresses in the TSTM. The behavior before t_o is discussed in detail at this conference [2].

4.2 Reproducability

As shown in Table 1 a number of repeat tests have been made. Fig. 4 shows such data for isothermal tests at 5°C and 20°C. There is deviation between the curves, but the main features of the behavior are reproduced. Note that within the IPACS-program [5] there is a Round-Robin test under way both concerning AS and stressgeneration under full restraint.

4.3 Isothermal tests

The concretes were mixed at temperatures as close to the test temperatures as possible. Fig. 5 shows the AS results at 5, 13, 20 and 45°C. The desired temperatures were in all cases reached within one hour after placing the concrete in the temperature controlled

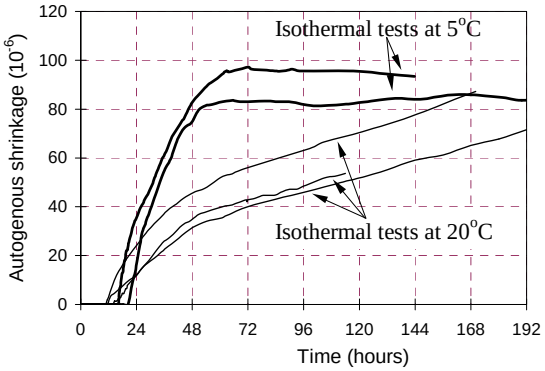

Fig. 4 Repeated isothermal tests at 20°C and 5°C

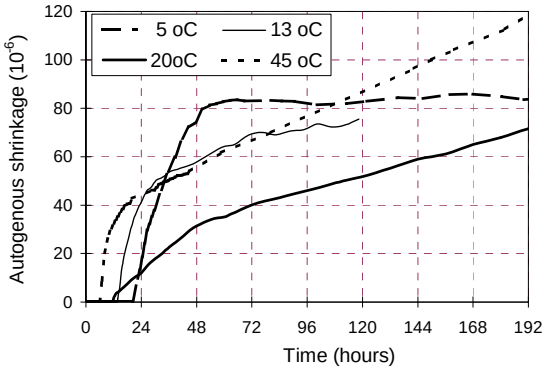

Fig. 5 Autogenous shrinkage during isothermal tests at different temperatures

dilatometer i.e. long before the zero-time for the AS-plots. The figure shows very unsystematic behavior; particularly the first 48 hours. Clearly, a simple time shift using the maturity principle will not be able to characterize the results coherently. From a practical point of view, fully isothermal tests are not very relevant, hence we abandoned this approach and proceeded to the more realistic "poly-isothermal", see below.

4.4 Poly-isothermal tests

This series was intended to be more realistic in terms of practical concreting, using fixed temperatures of 13°C and 20°C the first 8 hours, and then increasing the temperature in steps to the desired level, see Fig. 2. Fig. 6 gives the results vs real time. In Fig. 7 a "normal" activation energy (ΔE) for strength development is used to transform real time to maturity. Note that the expression $\Delta E=A+B(20-T)$ is used. In Fig. 8 a much higher ΔE value is used. The thermal dilations due to the temperature steps are not shown in the figures, they are eliminated by a curve fitting procedure. Note also that the temperatures are not "realistic", in the sense that a given final temperature is maintained till the end of the test, and not reduced after the heating phase as would be the case in a structure.

The raw data given in Fig. 6 is fairly systematic for each initial temperature, increased temperature leads to increased magnitude and rates of AS. The time shift provided by the normal activation energy is not enough to make them coincide (Fig. 7). The very high ΔE-value used in Fig. 8 makes the curves coincide in the period up to about 1 week maturity time, but with significant deviation after that. Furthermore, the two different initial temperatures (13 and 20°C) give quite different results both for the rate of AS development and total AS after a certain time. In practical terms, a generalized description of AS using maturity can be given, but only for a given initial temperature and up to about 1 week maturity time. Note that with this high ΔE-value 1 hour at 45°C correspond to 19 hours at 20°C, hence agreement up to 1 maturity week means only about 9 hours at 45°C, something which is much to short time to be practically useful. This is not a very general, nor a very practical result, and a different approach was chosen for the next stage.

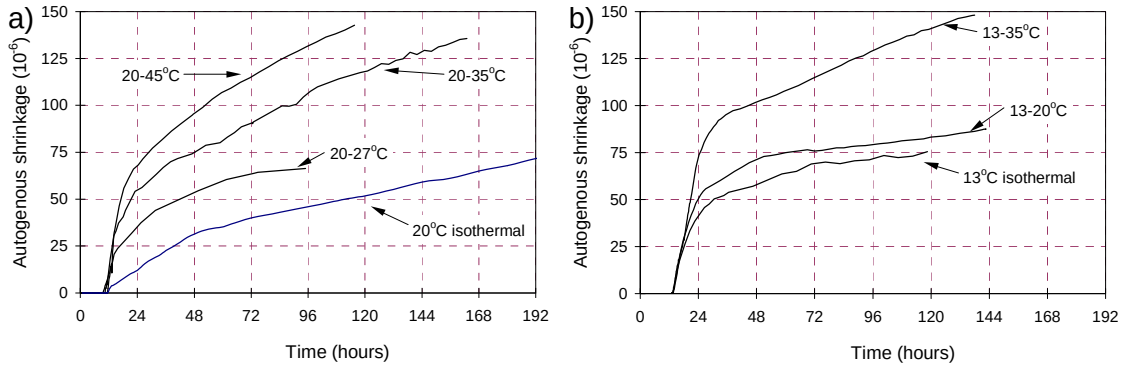

Fig. 6 Autogenous shrinkage vs real time during poly-isothermal tests with initial temperature of (a) 20°C and (b) 13°C.

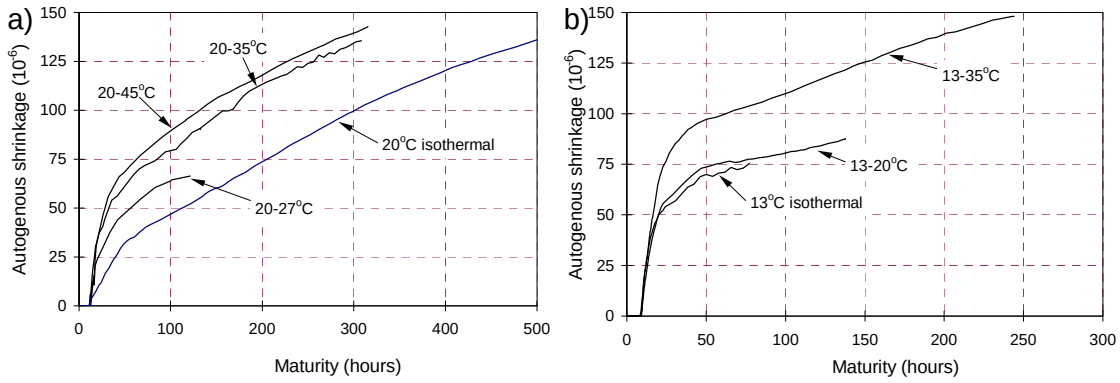

Fig. 7 Autogenous shrinkage vs maturity time during poly-isothermal tests with initial temperature of (a) 20°C and (b) 13°C. Maturity time is the equivalent time at 20°C isothermal conditions (A=33500 J/mole and B=1470 J/mole·°C)

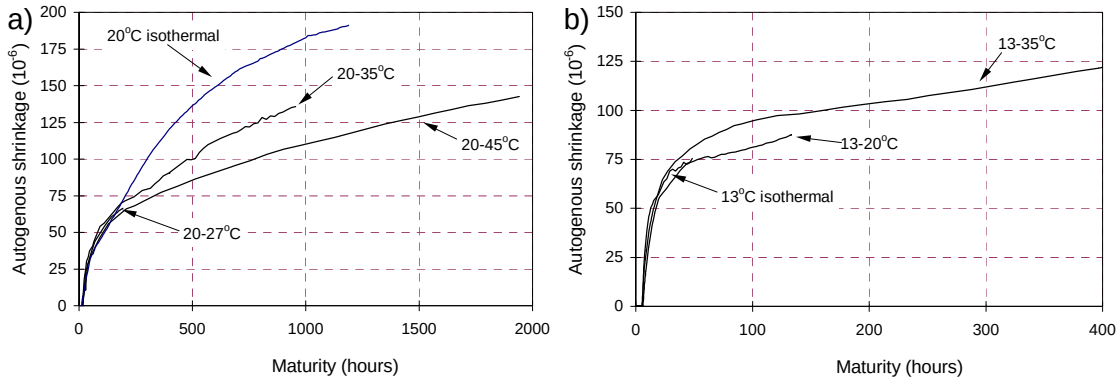

Fig. 8 Autogenous shrinkage vs maturity time during poly-isothermal tests with initial temperature of (a) 20°C and (b) 13°C. Maturity time is the equivalent time at 20°C isothermal conditions (A=91500 J/mole and B=0)

AS is clearly a very complicated concrete “property”, in that what is measured in the laboratory is the overall result of a large number of physical processes: a) the various hydration reactions and their dependence on temperature, time and the state of stress existing in the various phases; b) the state of internal stress generated by self-desiccation through a combination of capillary and Gibbs-Bangham mechanisms; and 3) the viscoelastic response of the skeleton matrix which changes very strongly both with degree of hydration, temperature level and the rate of temperature change.

Thus there is no reason to expect simple behavior of AS even under the relatively simple isothermal and poly-isothermal conditions discussed so far. In a realistic case where the temperature development is analogous to the one shown in Fig. 2, the situation is even more complicated and to base a model on the isothermal and poly-isothermal results is clearly not reasonable. The next step was therefore to determine AS as directly as possible under realistic conditions. This was done by determining the TDC during an experiment using the “saw-tooth” principle illustrated in Fig. 2, see below.

4.5 Realistic- and saw-tooth temperature tests

The detailed temperature program for the saw-tooth tests are given in Fig. 9, together with the set of smooth realistic temperature curves which have also been applied in the AS and TSTM equipment. Fig. 10 gives the saw-tooth results in terms of calculated TDC vs real time. Fig. 11 shows an example of the relationship between total measured deformation and the two contributing parts TD and AS, as calculated. Fig. 12 shows three sets of AS curves, each set comparing AS calculated from smooth and saw-tooth temperature developments shown in Fig. 9.

The isothermal results form a consistent picture; Fig. 12 shows that the AS for smooth and saw-tooth correspond well, demonstrating that the ±3°C steps did not change the overall AS. The TDC (Fig. 10) behave as expected; strong initial decrease followed by slow increase as the skeleton matrix dominates and RH is decreased by self-desiccation.

It is worth noting the following consistent observation in the isothermal saw-tooth test: In each step the temperature in the concrete reached thermal equilibrium after about 1 hour and the temperature was maintained, at least 1 more hour before the next step. In a COOL-step (23-17°C) the second hour produced a AS slope similar to the 20°C isothermal “background”; while in a HEAT-step the initial expansion was followed by a very high rate of contraction each time, several time as high as the “background”. Thus, if moisture redistribution is the main mechanism for the time dependence it is slower during HEAT (gel→capillary) than the opposite way during COOL. The fact that the mean saw-tooth AS curve corresponds to the smooth isothermal demonstrates that no extra irreversible structural changes are introduced by the temperature steps. These results also demonstrate that there is no “unique” TDC for concrete; its magnitude depends on the time allowed for the time dependent part. Much more work is clearly required to reach a better understanding of TD.

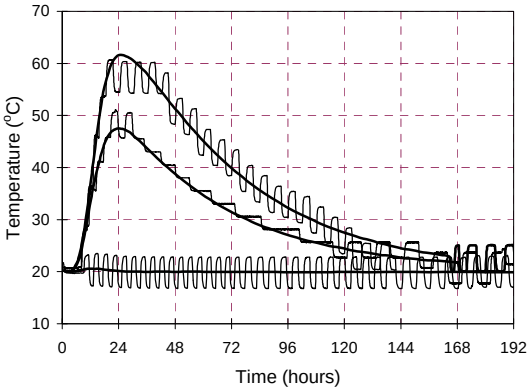

Fig. 9 Measured concrete temperatures: realistic (smooth and saw-toothed) and isothermal (smooth and saw-toothed)

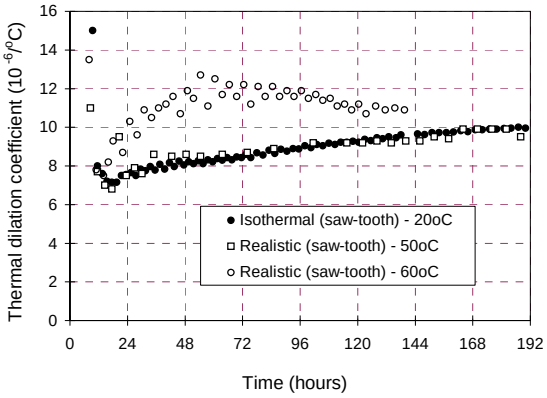

Fig.10 Development of the TDC at 3 different saw-toothed temperature histories, see Fig. 9

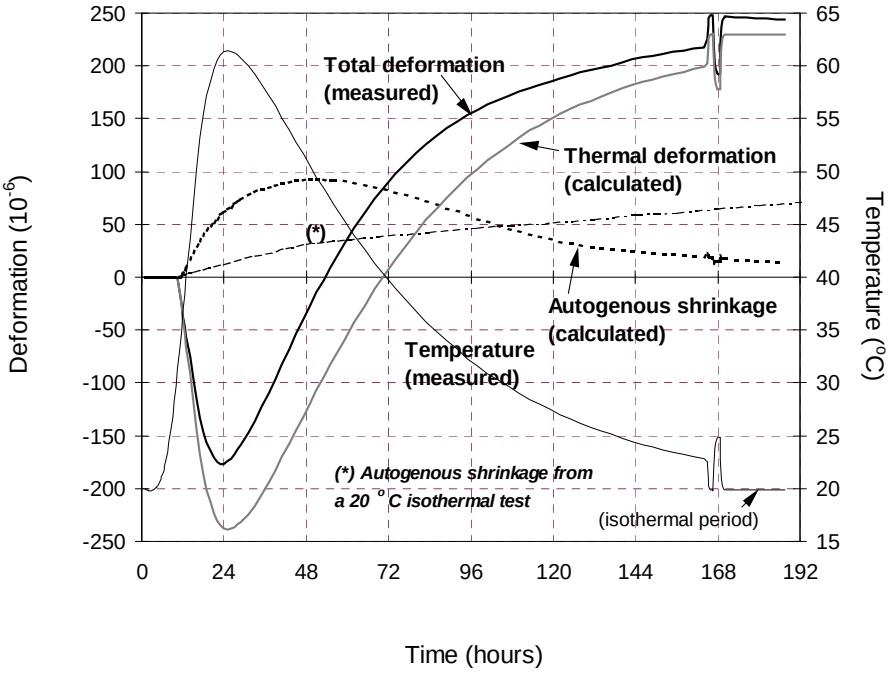

Fig. 11 Example of the relationship between total measured deformation and the two contributing parts TD and AS (smooth temperature, 62°C maximum)

The results in Fig. 10 for the two saw-toothed realistic temperature histories given in Fig. 9 are less consistent. The TDCs for the 50°C maximum curve correspond very directly to the isothermal, but the 60°C maximum curve is different. It is, however, clear from Fig. 9 that the saw-tooth pattern also is different in the two tests. These are the only saw-toot tests run so far; the need for more work is obvious. In Fig. 12 the AS are calculated for the two sets of realistic tests using the TDC given in Fig. 10. The principle of calculation is illustrated in Fig. 11 for the smooth realistic case with 62°C maximum. Fig. 12 shows fairly bad agreement for the two sets of smooth and saw-tooth curves. Relatively small changes in the TDCs have been shown to be able to produce much better correspondence. The main point, however, is that each set of

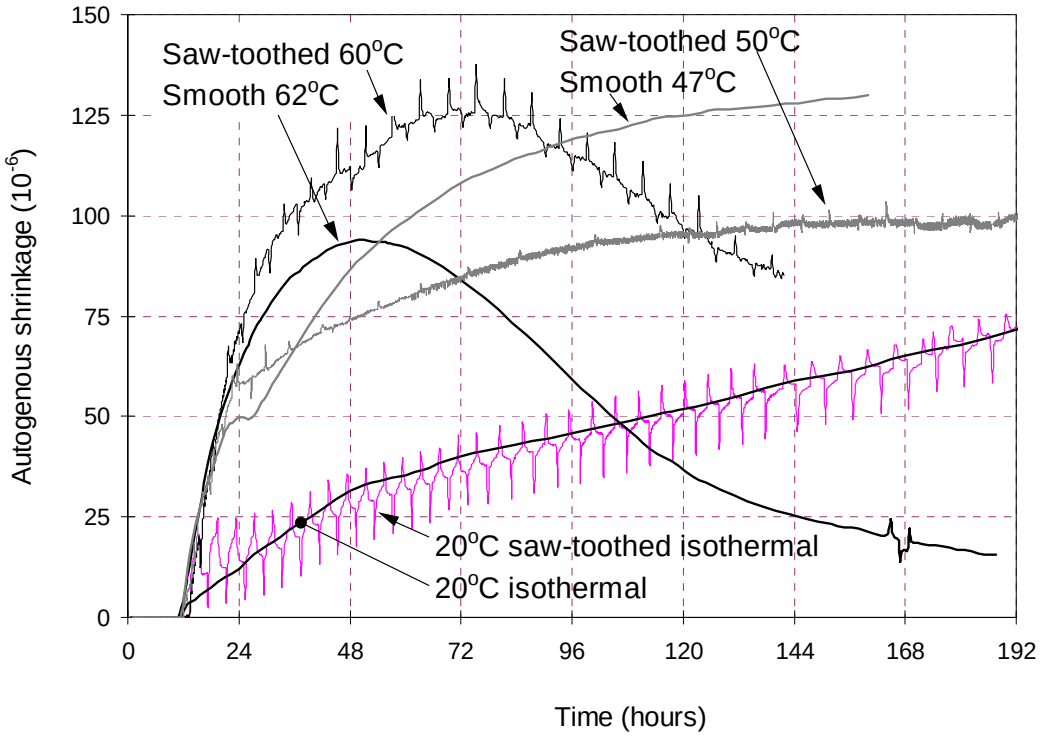

Fig. 12 Development of AS at realistic- (smooth and saw-tooted) and isothermal (smooth and saw-toothed) temperatures.

curves display the same major features: The 50°C maximum curves show that AS flatten out after about 4 days. The 60°C maximum curves show that AS becomes negative (i.e. expansion!) after 2 to 3 days.

The latter observation is surprising, but possible real as indicated in Fig. 11 after 168 hours: Here the temperature is constant and the total measured deformation is expansion. This has been shown in two experiments, but not yet by the stress development in the TSTM, since the specimens break very early in the cooling phase with 100% restraint. A system is now ready to provide less than 100% restraint to enable stresses to be measured over long times. The expansion after 2-3 days is of practical importance, since the critical time for cracking in many cases occurs later than this.

5 Conclusions

These preliminary results demonstrate very clearly a few main points:

- At our present state of knowledge the only certain way to estimate deformations in order to predict stresses in a structure by calculations, is to measure thermal dilation (TD) + autogenous shrinkage (AS) in the laboratory at the relevant temperature development. Any generalized TDC and AS models are not trustworthy today.

- The method (saw-tooth pattern etc) to determine TDC experimentally must be refined through further experiments.
- The determination of AS as the difference between the total measured deformation and the calculated TD (based on TDC from saw-tooth tests) appears the most promising at the moment. Efforts should be concentrated on this area first, using realistic temperature histories. The primary questions to be answered are:
  - Does increased maximum values in realistic temperature histories lead to decreased AS after a few days culminating at around 60°C in AS-expansion?
  - Is this a general phenomenon or dependent on binder components?
- A basic isothermal AS-test at 20°C is considered useful as reference point for a given mix. However, the primary questions should, in our opinion, be answered in as broad a way as possible (internationally), before realistic material models can be formulated.

6 Acknowledgement

The present work is part of the Norwegian project NOR-IPACS supported by NFR (Norwegian Research Council) with the following partners: Selmer ASA (project leader), Elkem ASA Materials, Norcem A/S, Fesil ASA and NTNU. The national project is from mid 1997 integrated with a new European Brite-Euram project (IPACS) with Sweden (Scancem) as project leader and partners from Norway, Germany, Italy and The Netherlands.

7 References

1. Kompen, R., (1994) High performance concrete: Field observations of cracking tendency at early age. *Proceedings of the International Rilem Symposium: Thermal Cracking in Concrete at Eearly Ages,* Munich, Rilem Proceedings 25, Oct. 1994
2. Hammer. T.A. (1998) Test method for linear measurement of autogenous shrinkage before setting. *Paper submitted to this conference*
3. Wittman, F. and Lukas, J. (1974) Experimental study of thermal expansion of hardened cement paste. *Materals and Structures*, no. 40, pp. 247-52
4. Meyers S.L. (1951) How temperature and moisture changes may effect the durability of concrete. *Rock Products*, pp. 153-7, Chicago, Aug. 1951
5. Bjøntegaard Ø., Sellevold E.J. and Hammer T.A. (1997) High performance concrete at early ages: Selfgenerated stresses due to autogenous shrinkage and temperature. *Third CANMET/ACI International Symposium on Advances in Concrete Technology*, Auckland, New Zeeland, Aug. 25-27
6. Hammer T.A., Bjøntegaard Ø. and Sellevold E.J. (1998) Cracking tendency of high strength lightweight aggregate concrete at early ages. *CANMET/ACI/JCI Fourth International Conference on Recent Advances in Concrete Technology*, Tokushima, Japan, June 7-11

APPENDIX 2 CTE of Cem. Paste and Concrete: Mechanisms of Moisture Interaction

Paper

Sellevold E.J. and Bjøntegaard Ø. (2006) **Coefficient of Thermal Expansion of Cement Paste and Concrete: Mechanisms of Moisture Interaction**. Materials and Structures, 39, 9, pp. 809-815

Materials and Structures (2006) 39:809–815
DOI 10.1617/s11527-006-9086-z

ORIGINAL ARTICLE

Coefficient of thermal expansion of cement paste and concrete: Mechanisms of moisture interaction

E.J. Sellevold · Ø. Bjøntegaard

Received: 1 August 2004 / Accepted: 29 November 2005 / Published online: 11 July 2006

Abstract Crack sensitivity calculations for young concrete are strongly influenced by the coefficient of thermal expansion (CTE) values for the concrete. This paper demonstrates the strong effect of moisture content on CTE, and discusses the mechanism(s) based on experimental results on mature cement paste. The temperature variation of the relative humidity (RH) exerted by the pore water is quantified and used to explain the high CTE of partly dried specimens. The relevance for early age crack sensitivity is that the concrete should be kept as wet as possible. This minimizes CTE and will largely eliminate autogenous shrinkage. However, trustworthy procedures to separate autogenous- and thermal deformations require a better fundamental understanding of moisture effects and the nature of delayed deformations.

Résumé *L'évaluation de la sensibilité à la fissuration des bétons au jeune âge est grandement influencée par le coefficient de dilatation thermique (CDT). Cet article démontre l'influence majeure de la teneur en eau des bétons sur le CDT, et propose/présente le(s) mécanisme(s) élaboré(s) sur la base de résultats expérimentaux obtenus sur des pâtes de ciment matures. L'influence de la température sur l'humidité relative du système poreux par l'eau interstitielle est quantifiée et utilisée pour expliquer le haut CDT mesuré sur les éprouvettes partiellement séchées. En conséquence, pour minimiser la sensibilité à la fissuration des bétons au jeune âge, le béton doit être maintenu humide aussi longtemps que possible. Cela a pour double effet de réduire le CDT et de largement diminuer le retrait endogène. Cependant, pour être valides, les méthodes de calcul permettant de séparer les déformations de retrait endogène et les déformations thermiques doivent reposer sur une meilleure compréhension fondamentale de l'effet de l'humidité et de la nature des déformations différées.*

E.J. Sellevold · Ø. Bjøntegaard
The Norwegian University of Science and Technology,
Department of Structural Engineering, Trondheim, Norway

1. Introduction

The current worldwide interest in early age cracking problems in structures with High Performance Concrete (HPC) has led to intensive work on autogenous deformations. This concentration has resulted in neglect of the normally even more important thermally induced deformations. The coefficient of thermal expansion (CTE) is often just given a constant default value in calculation programs, while we know that it varies strongly both with concrete mix constituents (particularly aggregate type) and time (degree of self-desiccation). Figure 1 [1, 2] shows typical behavior from early times for a pure cement paste (a) and a concrete (b) containing the same paste as binder (28 vol%). Note that "DCS" in the figure means degree of capillary saturation, which is the degree of water saturation in the pore system excluding the air/macro pores. Both

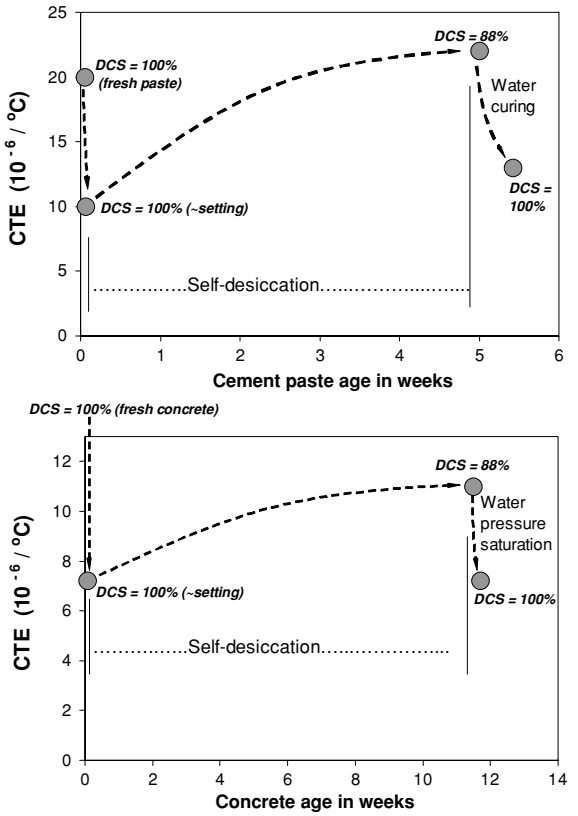

Fig. 1 Effect of the degree of capillary saturation (DCS) on the Coefficient of Thermal Expansion (CTE) of: (a) cement paste (w/b = 0.40 and 5% silica fume) and (b) concrete containing the same paste as binder (28 vol%). $[10^{-6}]$ = microstrain = μs. Bjøntegaard [1]

curves are for sealed hydration up to the time when the specimens are immersed in water. Before setting both cement paste and concrete have very high CTE values (20 μs/°C was measured both for the cement paste and the concrete [1]) since no solid framework exists and the continuous water phase controls. CTE reduces as solids form, reaching a minimum value around the final set, which points are shown in Fig. 1. From then on CTE increases as self-desiccation proceeds. The increase for paste is about from 10 μs/°C to 22 μs/°C, and the reduction after water immersion is back to 13 μs/°C. For concrete the equivalent numbers are about from 7 μs/°C to 11 μs/°C, and back to 7 μs/°C. These numbers demonstrate clearly the dominant influence of the water content on CTE; for the concrete CTE returns to the exact same value it had on setting after full saturation at an age of 11 weeks, i.e. the hydration has no net effect on the CTE in saturated state (!). The moisture effect is clearly very important from a practical point of view, and simple in the sense that the CTE value of a given concrete can be controlled by controlling the moisture content. Minimum CTE is obtained in a wet state, so that by supplying an internal water source during curing two important benefits are obtained: the autogenous deformation is reduced or eliminated and CTE is minimized.

This dramatic effect of moisture content on CTE has been demonstrated repeatedly for mature cement pastes since the classic work by Meyers 1951 [3]. Powers 1958 [15], Helmuth 1960 [4], Dettling 1964 [5] and Bazant 1970 [6] have made significant contributions to our, yet incomplete, understanding of the underlying mechanisms. This brief paper gives the authors' current view of the mechanisms as a basis for discussions.

CTE cannot be uniquely defined for concrete, since an imposed temperature change produces time dependent deformations. It is therefore a choice what is called immediate deformations (ID) and counted as CTE, and what is considered delayed deformation (DD) and, thus, not included in the CTE. The DD will include both a direct temperature gradient effect, and a part of more complex character – for example, caused by moisture redistribution, see later.

In practice thermal equilibrium in a test sample is reached much faster than deformation equilibrium, but still 1/2 to some hours are needed in most experimental setups before the temperature gradient is largely eliminated and ID is defined. ID will of course then include some fundamental time-dependent deformation component active during the temperature equilibrium period. Often in the literature CTE is found from dynamic experiments, i.e. deformations are recorded during heat-cool cycles. If there is no hysteresis then CTE is uniquely defined as the slope of the curve in a T vs. deformation plot; however, in practice there is hysteresis that depends both on the specimen size, the rate of temperature change and the magnitude of DD, producing a CTE value that may depend strongly on all the experimental conditions, as well as on any fundamental time-dependent fenomena.

For hardening concrete an additional complication exists. Under realistic temperature development (heating followed by cooling) the total deformation can be measured relatively easily. To separate the total deformation into its thermal and autogenous components the best procedure is to calculate the thermal part by using the temperature history and the relevant CTE [1, 2].

The thermal part is then subtracted from the total to produce the autogenous part. However, the autogenous part determined this way will also include the time-dependent components, i.e. DD. The consequence is that definition of the "pure" autogenous deformation under realistic temperature conditions is very complex, if not impossible. This "DD-complication" is expected to depend strongly both on moisture state, degree of hydration and temperature history. Hence, it is probably a main reason why the autogenous deformation determined this way behaves very unsystematically with respect to temperature history, as discussed in [1, 2, 7].

2. Mechanisms

There appears to be general agreement in the literature that both the strong dependence of CTE on moisture content and the existence of DD are related to temperature-induced redistribution of moisture in the pore system. We share this view and will discuss the mechanisms in three categories, roughly (but not entirely) corresponding to those proposed by Bazant [6].

1. Pure thermal dilation
2. Thermal shrinkage or swelling
3. Relative humidity change

Particular attention will be paid to the two major observations: (1) CTE increases strongly as the moisture content is reduced from saturation, and (2) the DD is large in saturated samples but reduces strongly with decreasing moisture content. The DD in saturated samples is in opposite direction to the immediate thermal (ID); for partly saturated samples the DD has been found to be in either direction or almost absent.

2.1. Pure thermal dilation

Each constituent material (solid particles, adsorbed water, pore water etc.) has a CTE value. CTE of water is much higher than CTE of solids. Thus, a very fast temperature increase followed by an isothermal period will lead to fast expansion (ID), followed by a time dependent contraction (DD) as the induced excess pressure in filled pores is dissipated by flow to the outside or to partly empty pores. Scherer [8] and Ai et al. [9] have used this phenomenon to measure water permeability in saturated cement pastes. They have also demonstrated that the phenomenon is "symmetrical", i.e. a sudden cooling of a saturated paste leads to a sudden contraction followed by a time-dependent expansion as water is sucked in from outside. Depending on the permeability of the paste and the distance to available "sinks", the pressure release may be fast or slow, i.e. it may appear as ID and hence be counted in CTE, or as DD. The literature shows that DD is much larger in saturated samples than in partly dried. Thus, for concrete in practice where the most normal moisture state is "natural self-desiccated condition" (80–90% degree of capillary saturation) less DD is found, and any pressure relief mechanism is presumably very fast and counted as ID and part of CTE. This mechanism consequently is consistent with the observations that DD is greatest in saturated samples and that DD is in opposite direction to the ID. However, it does not account for the strong CTE increase found as the moisture content is reduced from saturation.

2.2. Thermal shrinkage and swelling

Pore water can roughly be divided into two types. Gel water, a collective term for water which is strongly influenced by its proximity to solid surfaces; i.e. interlayer water, adsorbed water and water in very small pores (gel pores). Capillary water is water in larger pores (smallest dimension over a few nm), and it is commonly treated as bulk water under the influence of capillary tension when the sample is not fully saturated, i.e. when curved water-air menisci exist. At saturation there is no capillary tension, but the water in these "larger" pores is still commonly referred to as capillary water, and the pores as capillary pores.

Equilibrium requires that the chemical potential (molar Gibbs free energy) of coexisting water phases is equal both before and after a temperature change. The rate of change of the chemical potential of a water phase with respect to increasing temperature is the negative of the entropy. The entropy of gel water is lower than that of capillary water as shown in Fig. 2, Radjy, Sellevold and Hansen [10]. Thus, a sudden increase in temperature leads to a higher chemical potential in gel water than in capillary water, setting up a driving force for an internal redistribution of water from gel to capillary pores. This is expected to lead to shrinkage, i.e. sudden heating of a cement paste sample is expected to produce a sudden expansion followed by a time dependent contraction. On cooling the opposite effect is expected; a sudden contraction followed by a

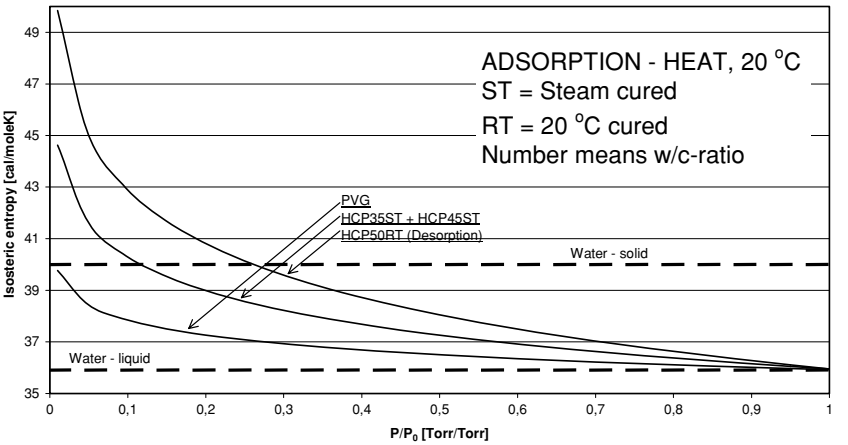

Fig. 2 Entropy of adsorbed water (relative to saturated vapor). HCP = Hardened Cement Paste, PVG = Porous Vycor Glass. Low relative vapor pressure is associated with gel water, higher values with capillary water. Note that large ordinate values mean large change from vapor state, i.e. low absolute entropy – as also demonstrated by the ref. water and ice lines. Radjy, Sellevold and Hansen [10]

time dependent expansion as water moves from capillary pores to the gel. It is perhaps difficult to visualize how water can redistribute in a saturated sample, i.e. when there is no available space. The theory is that, for example, cooling will force water to the gel pores in an amount necessary to increase the local pressure (disjoining pressure) enough to establish equilibrium in chemical potential with the water in capillary pores. This pressure in the gel water will produce expansion.

In less than saturated samples the situation is that the gel pores are full, but the capillary pores partly empty and with the water under capillary tension. The redistribution takes place as for saturated samples, in theory, implying the possibility of a situation after cooling when the gel water is under pressure (disjoining) while the capillary water is under tension. This situation produces chemical potential equilibrium, but the physical reality of the situation is perhaps questionable. It should be added that it is impossible to calculate the magnitude of any of the redistribution effects with any reasonable certainty. The thermodynamic arguments tell us in which direction water moves, but quantification requires much more basic data than we have presently.

Note that in saturated samples water redistribution results in changed gel water pressure and hence dimensional change. In partly dried samples changing air-water meniscus radii in capillary pores also comes into play; for example on heating water moves from gel to capillary pores, reducing disjoining pressure (contraction) in gel, but in the capillaries the increase in water content leads to increased RH (expansion). Thus the gel-capillary mechanism is to some extent coupled to the RH-mechanism discussed in the next section.

Powers [15] and Helmuth [4] explained DD results for saturated specimens only in terms of this gel-capillary redistribution mechanism, and did not consider the excess pressure mechanism due to high CTE of water discussed above. This is consistent since gel-capillary mechanism also produces DD in opposite direction to the ID for saturated specimens. However, since the transport is internal only no effect of specimen size is expected. In fact a strong size effect is found [9], hence the gel-capillary mechanism must be rejected as the main explanation of the strong DD effect in saturated samples. Helmuth also considered the gel-capillary mechanism responsible for the moisture effect on CTE, arguing that at 82% degree of capillary saturation there was "...not enough capillary water to allow redistribution" – i.e. it is the absence of redistribution that is responsible for the high CTE at 82% saturation. We do not share this view. The porosity of a w/c = 0.45 mature paste is about 41 vol%. At 82% saturation the situation is: 19 vol% is water-filled gel pores, while the 22 vol% is capillary pores with 15 vol% water-filled and 7 vol% empty. With these numbers in mind it is difficult to accept Helmuth's explanation, particularly since moisture redistribution *must* take place in order to re-establish equilibrium in chemical potential after a temperature change.

Thus, in our view, the gel-capillary mechanism is unable directly to explain the two major observations on CTE: (1) the strong moisture dependence and (2) the large DD in saturated specimens and the reduction/elimination as the moisture content decreases. Directly, the disjoining pressure changes in the gel pores implicit in the mechanism will influence the DD to an

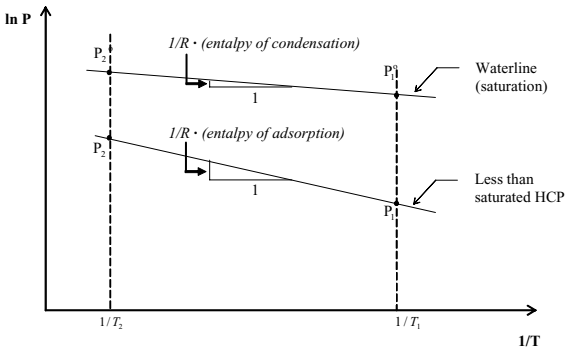

Fig. 3 Vapor pressure exerted by pore water in hardened cement paste vs. inverse of temperature for different constant water contents. Principle sketch. HCP = Hardened Cement Paste

unknown extent in all relevant moisture states, and the direction will always be opposite to the pure thermal effect (ID). Indirectly, the moisture redistribution mechanism may play an important role in the RH-mechanism to be discussed next; but in the same direction as the pure thermal (ID).

2.3. Relative humidity change

The raw data in the project to obtain enthalpy and entropy of pore water [10] was vapor pressure vs. temperature for a given cement paste at different moisture contents. Figure 3 shows such data in a principle sketch. A characteristic of the results is that the curves are nearly straight lines, and that the slopes increase as the moisture contents are reduced, i.e. that the enthalpy of the pore water decreases with decreasing moisture content, see Fig. 4, where this is shown to be true for all the adsorbent/adsorbate systems. Figure 3 illustrates clearly a very important aspect: If the lines were parallel then the RH would be independent of temperature (easy to prove mathematically, remembering that at any given temperature, RH equals the vapor pressure exerted at a certain moisture content divided by the saturation vapor pressure). When the lines are not parallel as in Fig. 3 the result of heating from T1 to T2 is that RH increases, since:

$$\frac{p_2}{p_2^o} > \frac{p_1}{p_1^o} \quad \text{hence RH2} > \text{RH1}$$

This effect has been measured by several researchers [6, 10–14], and has important consequences for CTE. The effect is shown in Fig. 5, which is taken from [10]. The scatter between the three data sources is large, but the magnitude of the effect is at least indicated. It should be noted that the data from [10–12] were obtained using very different principles of measurement. New data by Nilsson [14] is roughly in line with the plot, but also shows a clear w/c-effect; the %RH/°C-factor decreases as the w/c increases. The phenomenon is further discussed in [10].

The consequences of the RH-increase on heating for CTE may be estimated using Fig. 5 and isothermal shrinkage data, for example Hansen [13]. A mature paste (w/c = 0.4) cured isolated may self-desiccate to 85% RH (the value depends on the cement). The %RH/°C-factor may be about 0.2%/°C (Fig. 5), and the slope of the shrinkage-RH curve about 60 μs (microstrain) per %RH [13]. Then the apparent CTE from this mechanism becomes $0.2 \times 60 = 12\ \mu$s/°C. Figure 1 showed CTE to be 22 μs/°C for the 88%

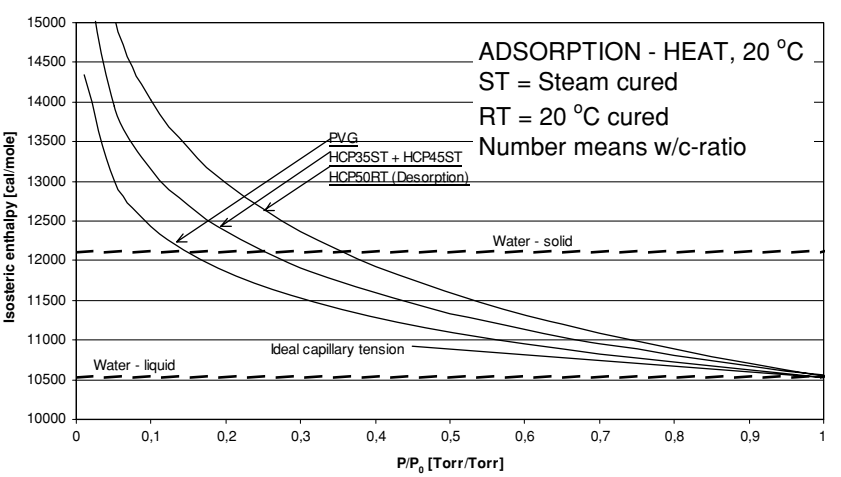

Fig. 4 Enthalpy of adsorbed water (relative to saturated vapor). HCP = Hardened Cement Paste, PVG = Porous Vycor Glass. P/P_s [Torr/Torr] = RH(%)/100. Radjy and Sellevold [10]

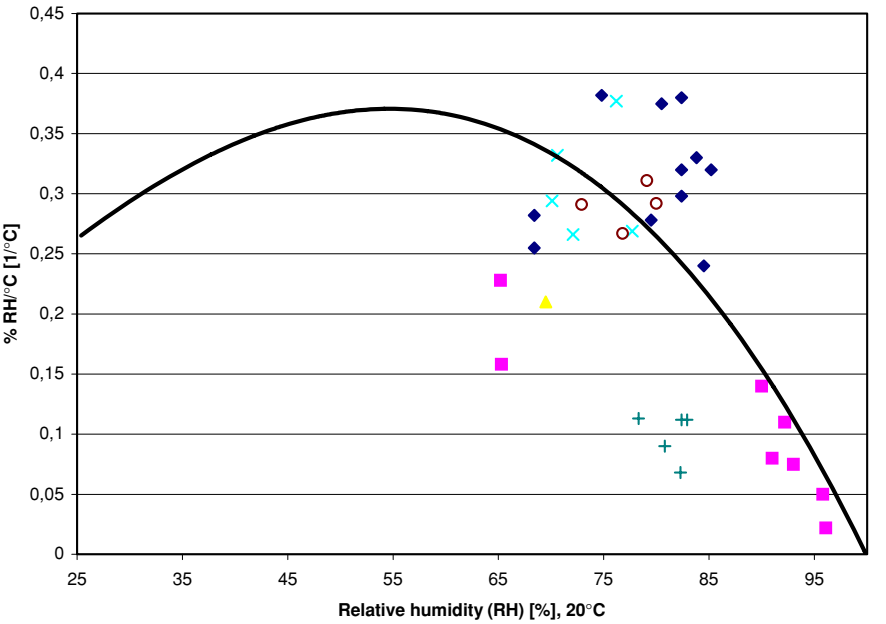

Fig. 5 The change in RH per °C at different RH-values exerted by the pore water in cement pastes. Solid line is for HCP50RT = a mature cement paste with w/c = 0.50 cured at 20°C [10]. Points are from Nilsson [11] and Persson [12]

saturated paste (roughly corresponding to RH = 85%), of which then maybe 12 μs/°C are caused by the RH-effect.

Thus, the RH-mechanism alone is able to explain the whole moisture content effect on CTE. However, note the uncertainty in the value 0.2%/°C taken from Fig. 5, i.e. the explanation should only be considered a reasonable possibility since it works in principle and has the right order of magnitude. It is of course implied that the RH-effect is fast and the resulting deformation is ID – and hence recorded as part of the CTE. This seems reasonable since the RH-increase is a direct result of the T-increase and thus a local phenomenon requiring no long range mass transport. Note that in contrast to the other two mechanisms already discussed, the RH-mechanism produces deformation in the *same* direction as the pure thermal expansion/contraction (ID). It is necessarily coupled with the gel-capillary mechanism for less than saturated samples: heating produces gel-capillary transport which leads to increased meniscus radius and increased RH. There are also other possible contributing explanations of how in physical detail the RH-increase on heating is produced. One model is sketched here: At DCS = 88% the paste certainly contains water under capillary tension due to existence of air-water menisci. Possibly is each meniscus the interface between the air and a significant volume of pore water ("ink-bottle" – effect). A temperature increase will lead to expansion of this water, which again can result in increased radius of the meniscus as the waterfront moves outward. The increased radius leads to an increased RH according to the Kelvin equation. The increased temperature also leads to reduction of the air-water interfacial tension – again increasing the RH. The model is discussed in more detail in [1] and [10], but we note that the model is one of principle only – it has too many degrees of freedom to allow quantitative tests, as was the case for the gel-capillary mechanism.

3. Conclusions

The paper demonstrates the strong effect of moisture content on CTE, and discusses the mechanism(s) behind. From a practical point of view crack sensitivities may be reduced by keeping the concrete as wet as possible during the early phase. This minimizes CTE and will largely eliminate autogenous shrinkage.

From a fundamental point of view the situation is less clear. It is satisfactory that the RH-mechanism apparently alone is able to explain the large effects of moisture content on CTE, and that the large delayed deformation (DD) in saturated samples may be explained by pore water pressure due to differences in CTE of the solid and water phases. The source(s) of the RH-variation with temperature, the rate and magnitude of

the gel-capillary redistribution mechanism and the nature and magnitude of the DD-effects in less than saturated samples are not resolved today. In our view the most urgent need is for more systematic experimental data, starting with mature hardened cement paste in well-defined moisture states subjected to different and well-controlled temperature changes. This is a necessary first step before introducing the complexities of changing temperatures in hydrating cement pastes.

It should be kept in mind that our primary goal is the practical one of understanding CTE in order to separate thermal deformations from autogenous deformations for concrete hydrating under realistic temperature regimes. This is necessary in order to be able to formulate models for each type of deformation to be used in early age crack risk calculations.

Acknowledgements

This paper is a product of the Norwegian NOR-CRACK project. The financial contribution of the Norwegian Research Council and the project partners are gratefully acknowledged. The partners in the project are the Norwegian Public Roads Administration, Skanska Norway AS, Norcem A.S., Elkem ASA and Fesil A.S., and NTNU Department of Structural Engineering (project leader).

References

1. Bjøntegaard Ø(1999) Thermal dilation and autogenous deformation as driving forces to self-induced stresses in HPC, *Doctoral thesis*. The Norwegian University of Science and Technology, Dept. of Structural Eng., ISBN, 82-7984-002-8.
2. Bjøntegaard Ø, Sellevold EJ (2001) Interaction between thermal dilation and autogenous deformation in HPC. Materials and Structures, 34:266–272.
3. Meyers SL (1951) How temperature and moisture changes may affect the durability of concrete. Rock Products, 153–178.
4. Helmuth RA (1960) Dimensional changes of hardened portland cement pastes caused by temperature changes. Highway Research Board pp. 40:315–336.
5. Dettling H (1964) Thermal dilation of cement paste, aggregate and concrete (only available in German). *Deutscher Ausschuss für Stahlbeton*, Heft 164, Berlin.
6. Bazant ZP (1970) Delayed thermal dilatations of cement paste and concrete due to mass transport. Nuclear Eng. and Design, 308–318.
7. Bjøntegaard Ø, Sellevold EJ (2001) Thermal dilation and autogenous deformation. Proc. of the RILEM Int. Conf. on Early Age Cracking in Cementitious Systems, Ed. by K Kovler, A Bentur, Haifa, Israel, March 12–14, pp. 63–70.
8. Scherer GW (2000) Measuring permeability of rigid materials by a beam-bending method: I, Theory. J. Am. Ceram. Soc., 83(9):2231–2239.
9. Ai H, Young JF, Scherer GW (2001) Thermal expansion kinetics: Methods to measure permeability of cementitious materials: II, application to hardened cement pastes. J. Am. Ceram. Soc., 84(2):385–391.
10. Radjy F, Sellevold EJ, Hansen KK (2003) Isosteric vapor pressure – temperature data for water sorption in hardened cement paste: Enthalpy, entropy and sorption isotherms at different temperatures. Report BYG-DTU R-057, Techn. Univ. of Denmark, Lyngby. Available at http://www.byg.dtu.dk/publicering/rapporter/R-057.pdf.
11. Nilsson L-O (1987) Temperature effects in RH measurements on concrete – some preliminary studies. The Moisture Group, Report :1, BFR, 84.
12. Persson B (2001) Compatibility between flooring material on concrete and moisture, volatile organic compound, and adhesion. Working Report, Division of Building Materials, Lund Institute of Technology, Lund p. 29. (in Swedish).
13. Hansen W (1987) Drying shrinkage mechanisms in portland cement paste. J Am Ceram Soc 70(5):323–328.
14. Sjøberg A, Nilsson, L-O, Rapp T (2002) Publikation P-o2:1, Measuring moisture in heated concrete floors. Step 1: Prestudy (available only in Swedish), Inst. for Byggnadsmaterial, Chalmers Tekn. Høgskola, Gøteborg, Sweden.
15. Powers, TC (1958) The physical structure and engineering properties of concrete. Research Dep. Bulletin 90, Portland Cement Association, Chicago.

APPENDIX 3 Verification of three different calculation methods for early age concrete.

Paper

Kanstad K. (2005) **Verification of three different calculation methods for early age concrete**. Proc. of the workshop: Crack risk assessment of hardening concrete structures, Ed. by Bjøntegaard Ø. and Kanstad T., Trondheim, March 31.–April 1. 2005, Nordic Concrete Federation, pp. 101-110

Proc. of the Nordic workshop: Crack risk assessment of hardening concrete structures, Ed. by Bjøntegaard Ø. and Kanstad T., Trondheim, March 31 – April 1, Printed in 2006 by The Nordic Concrete Federation (www.tekna.no/NCF), pp. 101-110

Verification of three different stress calculation methods for early age concrete

Terje Kanstad
Ph.D, Professor
Department of Structural Engineering, NTNU
N-7491 Trondheim
E-mail: terje.kanstad@ntnu.no

ABSTRACT

Three different methods for crack risk assessment of early-age concrete based on stress-strain based criterions are considered; (1) advanced and (2) simplified solutions based on linear viscoelasticity for aging materials and (3) a method based on the age-adjusted effective E-modulus method. Regarding the reliability of the methods, the agreement between calculated results and results from several experimental series is investigated. It is shown that the agreement is best for the most advanced method, but that it also is satisfactory for the more simplified methods.

Key words: early age concrete, calculation, simplified methods, degree of restraint.

1. INTRODUCTION

Methods to determine the risk of early-age cracking should be based on stress-strain based criterions and consider the many crucial factors involved; material properties as hydration heat development, thermal conductivity, mechanical properties, creep, autogenous shrinkage, thermal dilation, and external factors as ambient air temperature, wind speed, formwork-stripping, fresh concrete temperature and finally structural restraint from adjoining structures and subgrade. To obtain reliable calculation results, and to achieve an efficient methodology to prevent such cracking, were two major objectives by the Brite-EuRam Project IPACS (Improved Production of Advanced Concrete Structures) with partners from Sweden, Norway, The Netherlands, Germany and Italy (1997-2001). Although this project and several other comprehensive research projects have been conducted the latest years, the reliability of results from such analyses is still not generally accepted to be satisfactory. This might partly be due to lack of common understanding of the theoretical approach, but also to the fact that only few researchers have tried to work with a broader range of experimental data, and results obtained at different laboratories. Comparison of results obtained at different laboratories should be a major topic in this context because it is impossible that the different calculation methods can agree if they are adapted to experimental results with large deviations.

A major objective by this paper is to investigate the agreement between different calculation methods and results from several comprehensive experimental series. Three different methods for crack risk assessment of early-age concrete based on stress-strain based criterions are considered. Two of them are based on linear visco-elasticity for aging materials (advanced and simplified solution), while the third one is a method based on determination of the structural degree of restraint and the age-adjusted effective E-modulus method.

2. SIMPLIFIED METHOD BASED ON DETERMINATION OF THE DEGREE OF RESTRAINT AND THE AGE-ADJUSTED EFFECTIVE E-MODULUS

2.1 Structural systems and application of the term: Degree of restraint (R)

Due to time consuming calculations and the large variety of external conditions which have to be investigated, simplified models and methods can be very useful. In these methods the term degree of restraint is commonly used. It can be defined as the stiffness of the restrained structure divided by the total stiffness of the system as illustrated in figure 1. It is usually denoted by *R,* and may vary between 0 and 1 (0 and 100%). It can also be explained as the degree of free movement prevention.

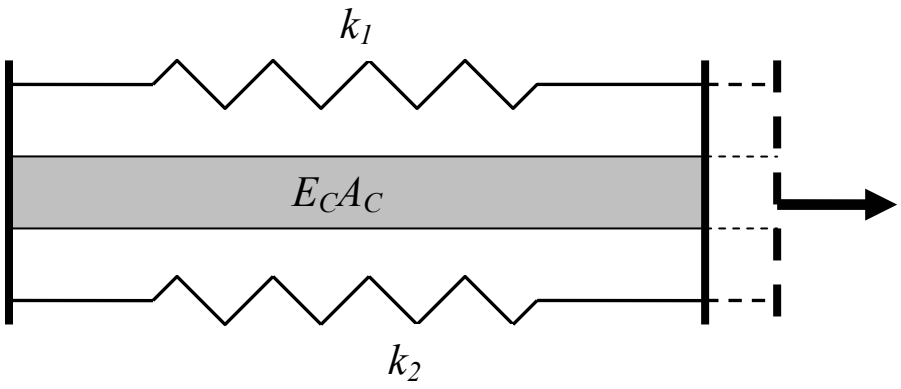

$$R = \frac{E_C A_C}{E_C A_C + k_1 + k_2}$$

Figure 1 - Illustration of the degree of restraint

In all types of concrete structures the degree of restraint can be determined by linear elastic analyses. An arbitrary constant temperature load ($\alpha_T \Delta T$) can be applied on the hardening (or the considered) part of the structure, and the resulting stresses calculated. The largest tensile stress, which in most cases is parallel to the structures length-axis, and located in the lower central part of the hardening concrete, is then compared to the stress level for 100 % restraint, i.e. with no strain. The degree of restraint is calculated as:

$$R = \frac{\sigma}{\alpha_T \Delta T E} \qquad (1)$$

σ = Stress in the length direction for the hardening part of the structure [MPa]
α_T = Thermal dilation coefficient [°C^{-1}]
ΔT = Prescribed temperature load [°C]
E = Elastic modulus of the hardening concrete [MPa]

The restraint factor will in principle be different for the expansion and the contraction phase due to the different E-modulus, but experience has shown that the difference is small. It is therefore recommended that the same degree of restraint can be used for both phases. For further discussion see f.i. [1-4].

2.2 Examples

Figure 2 shows how the degree of restraint varies with the height coordinate in a hardening concrete wall on a strip foundation for three different geometries. Typical values for other types of structures are found in [1-4].

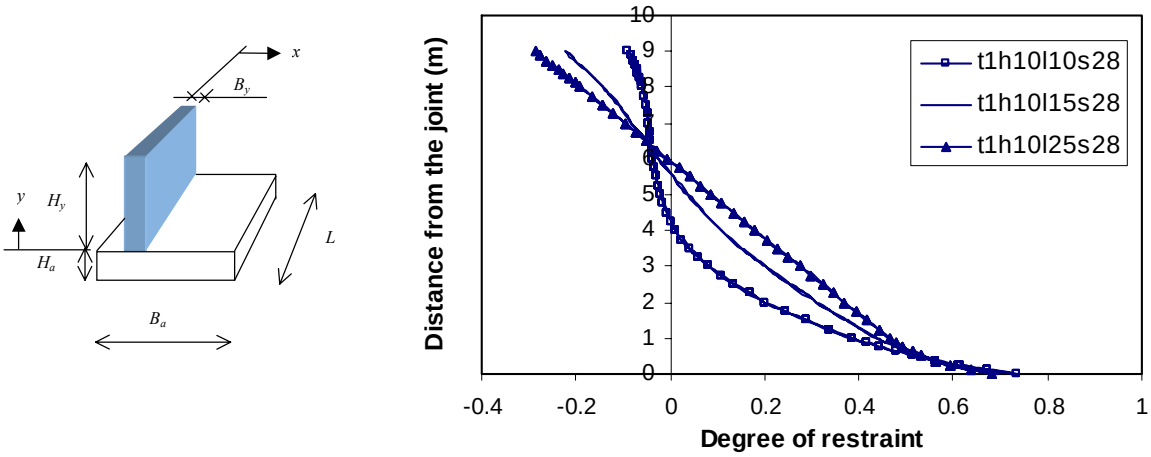

Figure 2 - Hardening concrete wall cast on strip foundation. Degree of restraint versus height-coordinate for different wall length; L=10m, 15 m and 25 m [2].

2.3 The Age adjusted effective E-modulus method (AEM)

This method, which originally was proposed by H.Trost, was first used on early age cracking problems by Larsson [5]. While this work was limited to an ordinary Swedish bridge concrete, it has now been verified towards results from a series of Norwegian bridge concretes with different binder types as part of the Norwegian Nor-Crack project [6,12].

The background and the different model parameters are illustrated in Figure 3a. As seen in the figure, the most realistic stress history has a similar shape as the temperature history, with an initial compressive phase (heating) and a subsequent tensile phase (cooling). An accurate stress calculation method requires that the complete stress history has to be described, which in most cases have been done using descriptions based on the theory of linear visco-elasticity for aging materials. For simplified methods, however, this is not convenient due to the need for numerical

solutions, and one alternative is to use a method based on the AEM. In this case one might neglect the compressive phase, and assume that the tensile stresses are constant in time, starting at the decisive point of time t_2, which is the time when the stress is zero as illustrated in figure 3b.

a)

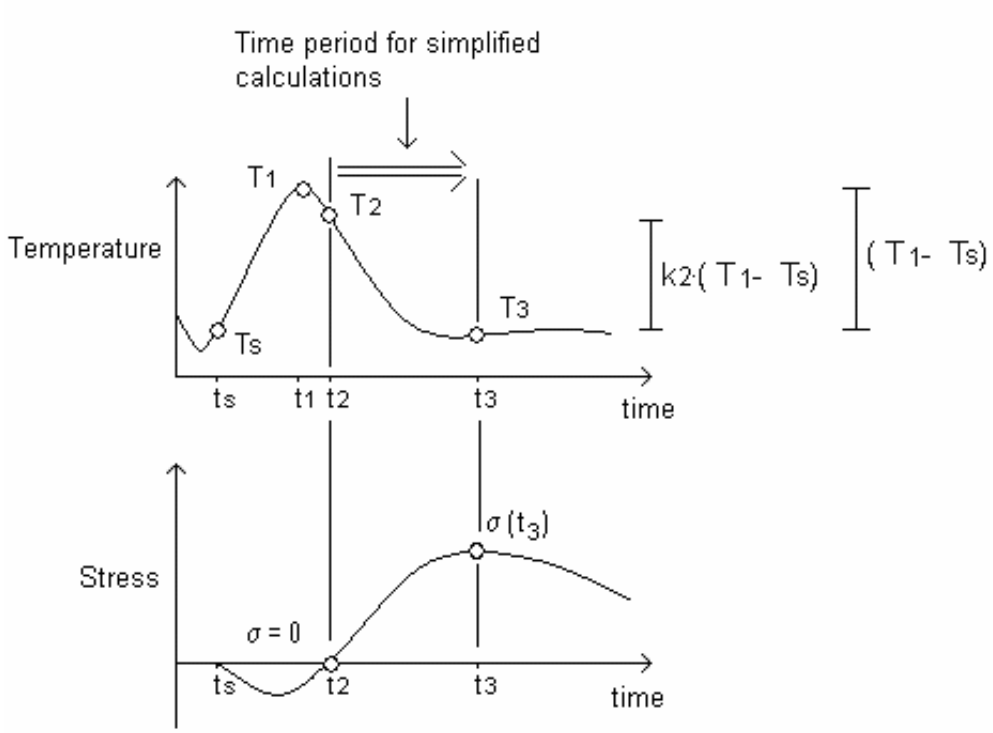

b)

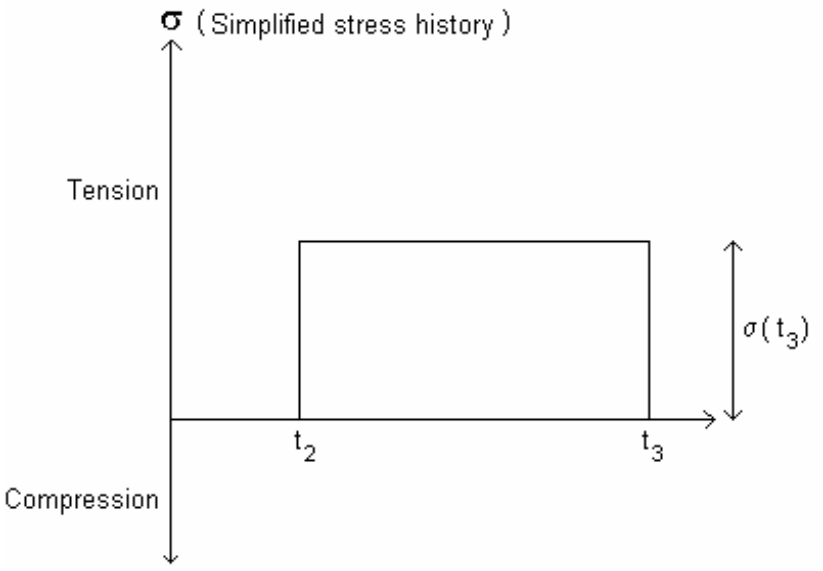

Figure 3 - (a) Typical temperature- and stress development versus time used to illustrate the Age adjusted effective E-modulus method. (b) Simplified stress history used in the AEM-method.

The time, $t_2$will occur shortly after the temperature reaches its maximum. It can be related to the part of the cooling temperature, Ie the temperature reduction after t_2 as:

$$T_2 - T_0 = k_2 \times (T_1 - T_0)$$

For k_2 Larson [5] used the following expression: $k_2 = 1,41 - 1,36 \times \frac{w}{b}$

In the Nor-Crack project it was found that t_2 lied considerably closer to the temperature maximum than predicted by Larson's equation. The main reason is probably larger autogenous shrinkage in the Norwegian concretes, and it was shown that k_2=0,92 gave the best agreement with the experimental results. In the calculation procedure, the corresponding time t_2 can be determined from the temperature-time curve after k_2 and T_2, have been determined. Furthermore it is assumed that the sum of autogenous deformation and thermal strain occurring after t_2 is the stress giving strain (initial strain), and that the whole stress is applied in one step at t_2:

$$\varepsilon_0(t_2, t_3) = \varepsilon_{AD}(t_2, t_3) + \varepsilon_{TD}(t_2, t_3) = \varepsilon_{AD}(t_2, t_3) + (T_3 - T_2) \times \alpha_T$$

The effective longtime E-modulus used within ordinary structural design methods (calculation of deformation, stresses and crackwidth), $E_{eff} = E_c / (1 + \varphi)$ is based on the assumption that the concrete stress is approximately constant in time. To compensate for the gradual stress development, which occurs after t_2 in this case, the creep-ratio in the effective E-modulus expression is multiplied by a reduction factor, termed the aging coefficient X_{AEM}. The age adjusted effective E-modulus, $E_{AEM,}$ is then expressed as:

$$E_{AEM} = \frac{E_C(t_2)}{1 + X_{AEM} \times \phi(t_2, t_3)}$$

In which t_3 is the time (in days) when the crack risk is should be determined, t_2 the time at zero stress, $E_C(t_2)$ the E-modulus at t_2, and $\Phi(t_2\ t_3)$ the creep ratio representing the creep at t_3 for stress applied at t_2.. In [4] the following expression for the aging coefficient was used:

$$X_{AEM} = 0,69 + 0,005 \times t_2$$

It was not possible to find another expression or a modification of this equation which gave better agreement with the Nor-Crack test results. Finally the stress may be calculated as:

$$\sigma(t_3) = \varepsilon_0(t_2, t_3) \times E_{AEM} \times R$$

$$\sigma(t_3) = (\varepsilon_{AD}(t_2, t_3) + (T_3 - T_2) \times \alpha_T) \times \frac{E_C(t_2)}{1 + X_{AEM} \times \phi(t_2, t_3)} \times R$$

2.4 Verification

Within Nor-Crack the method was verified towards TSTM-tests (Temperature-Stress-Testing-Machine or stressrig) on a wide range of different concretes with varying content of silica fume, flyash and blast furnace slag [12]. The calculated versus experimental results are presented in figure 4. To characterize the deviation between theory and experiment, the standard deviation for the tensile stress at t_3 is calculated to 0,51 N/mm^2. Utilizing this information, an upper characteristic value of the tensile stress can be calculated as:

$$\sigma_{AEM,k} = \sigma_{AAEMM} + k \cdot 0{,}51 MPa$$

To achieve the value with 5% probability to be exceeded, k=1,645 should be used:

$$\sigma_{AEM,0,95} = \sigma_{AAEMM} + 0{,}84 MPa$$

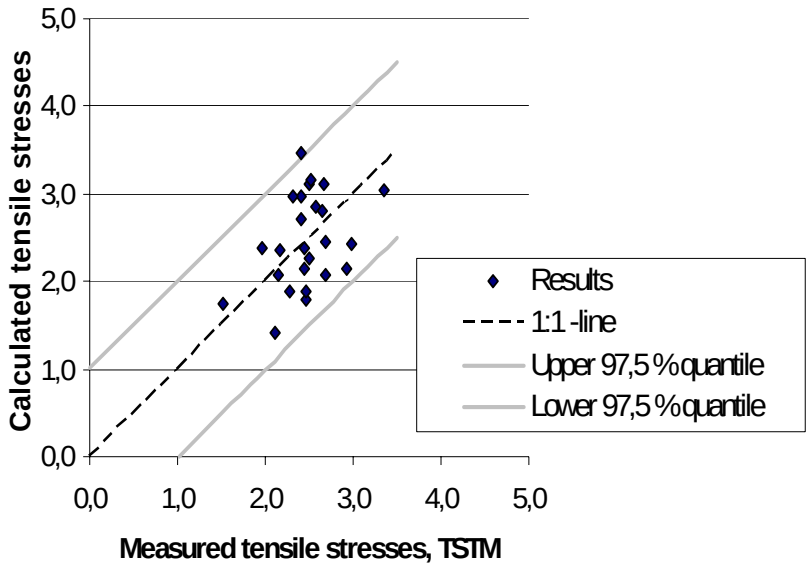

Figure 4. Tensile stresses after 13-17 days. Results from calculation by AEM versus TSTM-test results.

3 LINEAR VISCO-ELASTICITY FOR AGING MATERIALS: ADVANCED SOLUTION METHODS USED BY DIANA OR A VISUAL BASIC PROGRAM

The linear visco-elasticity for aging materials is probably the most suitable theory for early age crack prediction programs**.** A main advantage is that the entire time history of the structure may be simulated, and if finite element analysis is being used, both critical points of time and critical positions may be automatically determined. This theory has been frequently used for early age cracking problems by many researchers the last two decades, see f.i. [7,8,9]. In the present work the following compliance function, including the double power law for creep, and the modified CEB-equation for the E-modulus development [10], has been used:

$$J\left(t,t'_e\right)=\frac{1}{E\left(t'_e\right)}\left(1+\varphi\cdot\left(t'_e\right)^{-d}\left(t-t'_e\right)^{p}\right)$$

$$E_c\left(t_e\right)=E_c\left(28\right)\left\{\exp\left[s\cdot\left(1-\sqrt{\frac{28}{t_e-t_0}}\right)\right]\right\}^{n_E}$$

Figure 5 shows calculated versus experimental TSTM-results as presented in figure 4 for the simplified method. It is important that the model parameters were determined from independent test. Determination of the creep model parameters is described by Atrushi [8]. This means that no curve-fitting towards the experimental TSTM-results has been carried out. The standard deviation for the tensile stress after 13-15d is s = 0,34 N/mm^2.

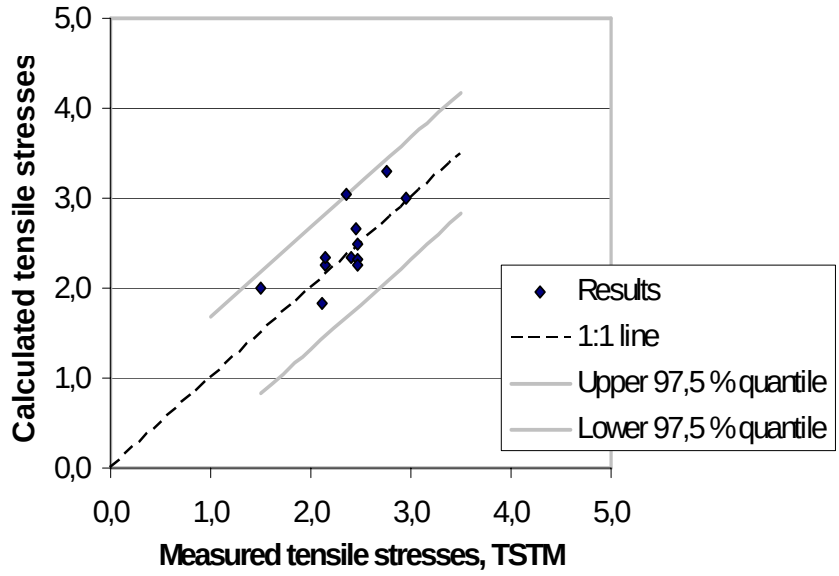

Figure 5 - Tensile stresses after 13-17 days. Results from calculations by linear viscoelasticity for aging materials versus TSTM-test results.

4 LINEAR VISCOELASTICITY FOR AGING MATERIALS: SIMPLIFIED SOLUTION BASED ON THE BURGER MODEL (4C TEMP&STRESS)

Several special-purpose finite element programs for analysing 2D temperature and 2D-2½D stress development in hardening concrete structures have been developed in recent years, e.g. CONSTRE, HACON, 4CTEMP&STRESS and HEAT2.5D [11]. In such programs usually only a slice (the cross section) of the structure is modeled, and while the temperature variations over the cross section can be quite accurately predicted, simplifications as the compensation plane method or the Navier-Bernoulli hypothesis (infinitely long structure assumptions), must be used to determine the principal stresses in the out of plane direction which usually are the main reason for cracking. Consequently, the adequate use of these programs requires knowledge of the total 3D structural response and the transformation into 2D-2½D models.

The physical interpretation and the basic equation of the creep model are illustrated in figure 6. For each new time-step the incremental creep strain may be calculated as a function of the current state of stress, and it is not necessary to take the entire stress history into account as it is when the general linear viscoelasticity is used.

A comprehensive evaluation towards the previously considered TSTM-test results has been carried out as part of the NOR-CRACK project [6], and some major results are summarized here. The solution of the Burger model was programmed in Excel, and the calculated versus experimental TSTM-results are presented in figure 7.

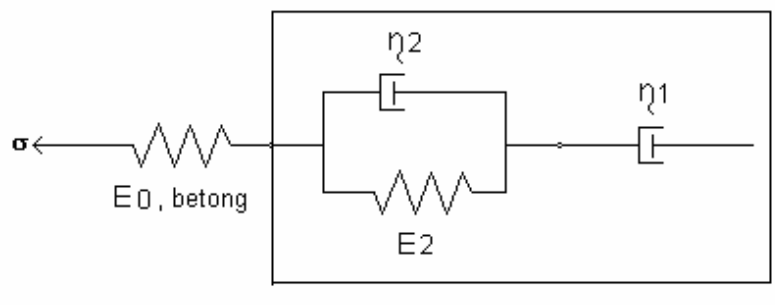

$$d\varepsilon_{kryp} = \left(\frac{d\sigma_0^1}{\eta_2^2} - \frac{E_2 \cdot d\sigma_0^1}{\eta_2^2} \right) \cdot dt + \left(\frac{d\sigma_0^1}{\eta_1^2} \right) dt$$

Figure 6 – The Burger Model

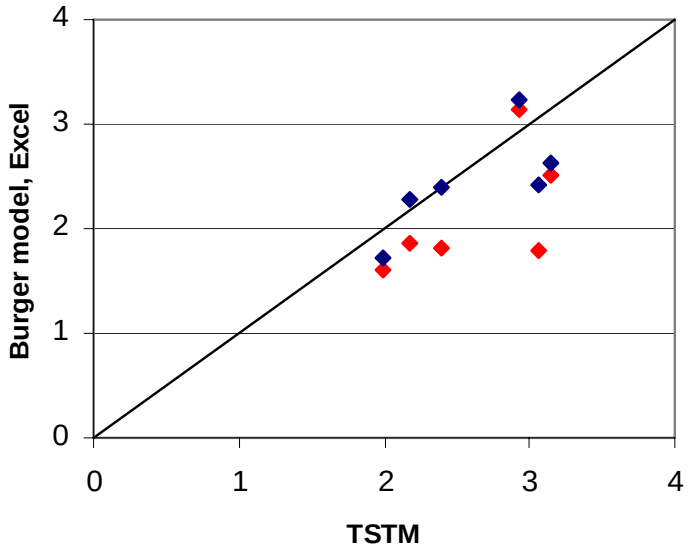

Figure 7 - Tensile stresses after 13-17 days. Results from calculations by the Burger model versus TSTM-test results.

In the analyses two sets of creep parameters have been used: The model parameters were either values determined by a specially designed test program on relevant Danish concretes, (reported by DTI and defined as default in the program) or model parameters determined from standard creep tests carried out at NTNU [9]. Comparing experimental TSTM results by theoretical values, the standard deviations for the two cases are 0,48 and 0,79 MPa, respectively. Our general conclusion, which confirms previous experience (Bosnjak [8]), may be stated as: The default values from DTI gave better agreement to the experimental behaviour than the ones determined from NTNU's creep tests, and should therefore be used. This is surprising, but it might be explained by the statement that the Burger model is unsuitable to describe creep under constant stress by model parameters which also are valid under variable stresses. It can also simply be stated that the model is too simple to describe creep under general stress histories.

5 CONCLUSIONS

For determination of the maximum tensile stress, the general solution based on linear visco-elasticity is in considerably better agreement with the TSTM results than the simplified solutions based on the Burger model, and the age-adjusted effective modulus method AEM (The standard deviations are 0,34 vs 0,48 and 0,51MPa, respectively).

An upper characteristic value of the calculated tensile stress can be calculated as:

$$\sigma_k = \sigma + k \cdot s$$

With 5% probablility to be exceeded, k=1,645 should be used, and based on the findings reported in this paper, we achieve the following expressions for the three investigated methods:

Age adjusted effective modulus method: $\sigma_{0,95} = \sigma + 0{,}84 MPa$

Burger model: $\sigma_{0,95} = \sigma + 0{,}79 MPa$

Linear visco-elasticity: $\sigma_{0,95} = \sigma + 0{,}56 MPa$

Furthermore should the calculated stresses be used in a crack-criterion as follows:

$$\sigma_{0,95} =\leq \quad \alpha \times f_{tk}$$

Where α in a range between 0,6 and 0,8 should be used.

In certain cases it can be worthwhile and economical to use the most advanced solution method. One should also remember that the linear visco-elasticity and finite element analysis makes it possible to simulate the entire stress history and to predict the critical time for cracking and the critical positions automatically.

REFERENCES

1. Kjellman O. and Olofsson J., *3D Structural Analysis of Crack Risk in Hardening Concrete Structure.* IPACS-report TG4/N2, 1999.

2. Kanstad, T., Bosnjak, D., Øverli, J.A., (2001) 3D Restraint Analyses of Typical Structures with Early Age Cracking Problems, IPACS-report, TULuleå Sweden. ISBN 91-89580-x.

3. Kanstad, T., Bosnjak, D., Øverli, J.A., (2001) Neural Network calculations of culvert wall by Diana -Verification, theoretical and practical background, IPACS-report, TULuleå, Sweden. ISBN 91-89580-61-3.

4. Nilsson, M. (2003) Restraint factors and partial Coeffisients for Crack Risk Analyses of Early Age Concrete Structures. Doctoral Thesis 2003.19. TU Luleå.

5. Larson, M. (2003) Thermal Crack Estimation in Early Age Concrete – Models and Methods for practical Application. Doctoral Thesis 2003.20. TU Luleå.

6. Hansen, F.B. Hansen F.B., Kanstad T. and Bjøntegaard Ø. (2005) Burger creep model (4C-Temp&Stress) and age adjusted effective E-modulus method (AEM) - Modelling for stress calculations. Preliminary report, NTNU, Department of Structural Engineering.

7. Emborg, M.(1989): Thermal Stresses in Concrete Structures at Early Ages. Doctoral Thesis 1989:73. TU Luleå.

8. Bosnjak, D. (2000) Self-induced Cracking Problems in Hardening Concrete Structures. Doctoral Thesis 2000:121. Department of Structural Engineering, NTNU.

9. Atrushi, D.S. (2003). Tensile and Compressive Creep of Early Age Concrete: Testing and Modelling. Doctoral Thesis 2003:17. Department of Structural Engineering, NTNU.

10 Kanstad T., Hammer T.A., Bjøntegaard Ø. and Sellevold E.J. (2003) Mechanical Properties of Young Concrete: Part II - Determination of Model Parameters and Test Programme Proposals, Materials and Structures (RILEM), Vol. 36, May 2003, pp 226-230

11 Larson, M. (2001): Comparison of programs Aimed for Computation of Thermal Stresses in Concrete Structures. IPACS-report, TULuleå, Sweden. ISBN 91-89580-58-3.

12 Bjøntegaard, Ø. (2006), The Nor-Crack Project 2001-2005: Project Information, Results and Materials Data Base. Experimental Data. Nordic miniseminar: Crack Risk Assessment of Hardening Concrete Structures. Held at NTNU in Trondheim, April 2005.

APPENDIX 4 The Nor-Crack project: Project information, results and materials data base

Paper

Bjøntegaard Ø. (2005) **The Nor-Crack project 2001-2005: Project information, results and materials data base**. Proc. of the Nordic workshop: Crack risk assessment of hardening concrete structures, Ed. by Bjøntegaard Ø. and Kanstad T., Trondheim, March 31 – April 1, The Nordic Concrete Federation, pp 8-16

Proc. of the Nordic workshop: Crack risk assessment of hardening concrete structures, Ed. by Bjøntegaard Ø. and Kanstad T., Trondheim, March 31 – April 1, Printed in 2006 by The Nordic Concrete Federation (www.tekna.no/NCF), pp 8-16

The Nor-Crack project 2001-2005: Project information, results and materials data base

Øyvind Bjøntegaard
Ph.D, Researcher
NTNU Department of Structural Engineering
N-7491 Trondheim
E-mail: oyvind.bjontegaard@ntnu.no

ABSTRACT

The Norwegian R&D project "NOR-CRACK" was carried out in the period 2001-2005. The paper gives project information, some overall results and shows the lay-out of a concrete materials database which is under development containing ready-to use input data for temperature- and stress simulations of hardening concrete structures. New experimental data have been generated and compositional parameters such as silica fume content, cement type, and low-heat 3-powder binder compositions have been investigated. 1D, 2D and 3D stress calculations have been performed and a simplified calculation method has been evaluated. Structural analyses have been compared to measurements from field tests. A guidelines report is under progress.

Key words: project information, hardening concrete, crack sensitivity, concrete composition, experimental tests, temperature- and stress simulations, materials database.

1. INTRODUCTION / PROJECT INFORMATION

The main aim of the project was to generate data for, and to perform, temperature- and stress simulations of hardening concrete structures, as well as to investigate properties on a more fundamental level such as early age creep, autogenous deformation and coefficient of thermal expansion (CTE). Various compositional parameters have been investigated in terms of their effect on cracking tendency. Silica fume (s) content, cement type and low heat concretes with fly-ash (FA) or blast furnish slag (BFS) have been the main variables. The investigated concretes had water-to-binder (w/b) ratios in the range 0.40-0.47. The main activities in the project are shown in the list below. The following chapters give some overall results from the project.

1. Materials testing
2. Modelling and stress calculations (simplified method, 1D, 2D and 3D)
3. Creation of a materials data base for “Norwegian concretes”
4. Field testing
5. Fundamental research (creep, coefficient of thermal expansion, autogenous deformation)
6. RILEM-committee work, including a Round Robin test program on autogenous deformation
7. Knowledge transfer (students, reports, articles)
8. Nordic mini-seminar

NTNU was project leader (Prof. T.Kanstad and Prof. E.J.Sellevold). Ph.D.-student J.Guomin, Postdoc K.T.Fosså and Postdoc Ø.Bjøntegaard were all project financed. Total budget was around 1 mill EURO, of which 65% was founded by The Norwegian Research Council. The remaining 35% was a combination of own research and financial support from the following project partners (active persons in parenthesis): The Norwegian Public Roads Administration (C.K.Larsen), Skanska Norge AS (S.Helland, S.Smeplass), Norcem AS (K.O.Kjellsen), Elkem ASA Materials (P.Fidjestøl), Fesil ASA (M.Carlsson).

2. EFFECT OF CONCRETE COMPOSITION: LAB. AND CALCULATIONS

2.1 Background: Experimental test conditions

All concretes referred to in the following were tested under both 20 ^{o}C isothermal and semi-adiabatic conditions (20 ^{o}C initial concrete temperature), while some concretes were tested also at other temperatures. The semi-adiabatic test conditions were found from temperature calculations of 0.6 - 1.0 m thich wall structures using hydration heat results for each given concrete as input.

2.2 Effect of silica fume (s)

Concretes with w/b=0.40, CEM I-52.5 LA, and with s-contents of 0, 5, 10 and 15% (of cement weight) have been tested with 20 ^{o}C and 30 ^{o}C initial concrete temperature and different maximum temperatures (1-3). The results show for the properties relevant for crack sensitivity that the concretes behave quite similar except for autogenous shrinkage and tensile strength - the "competition" between these two properties appears to be the most important in terms of crack sensitivity. Generally the autogenous shrinkage was increased with s-content (negative from a cracking perspective), but this was strongly temperature dependent and also counteracted by an increase in tensile strength (positive from a cracking perspective). For this reason no clear effect was found of 0-10% s content on the crack sensitivity for maximum curing temperatures of up to around 50 ^{o}C. Above 60 ^{o}C maximum the concretes with 10% and 15% tend to have increased crack sensitivity because autogenous shrinkage became very high. No significant difference in cracking tendency was found for the concretes with 0 and 5% s regardless of temperature history.

2.2 Effect of fly-ash (FA) and blast furnace slag (BFS)

Concretes with w/b=0.47 (5% s of cement weight) and with 40, 60 and 100% FA or BFS (of cement weight) were tested (5-7). For these concretes the results show that the given FA systematically reduces the crack sensitivity mainly, not surprising, due to reduced heat development, while the positive effect is not so pronounced for the given BFS. Fig. 1 shows direct tensile strength and E-modulus vs. adiabatic temperature rise for the concretes with varying FA- and BFS content, including a reference without FA/BFS (having the highest adiabatic temperature rise). The trend is a rather small decrease of tensile strength and stiffness with FA/BFS content, whereas the adiabatic temperature rise is significantly reduced. The results on autogenous shrinkage showed little influence of FA and BFS (when cured at semi-adiabatic temperatures realistic for a 1 m thick wall structure) whereas the CTE was somewhat reduced with FA- and BFS-content; most pronounced for FA.

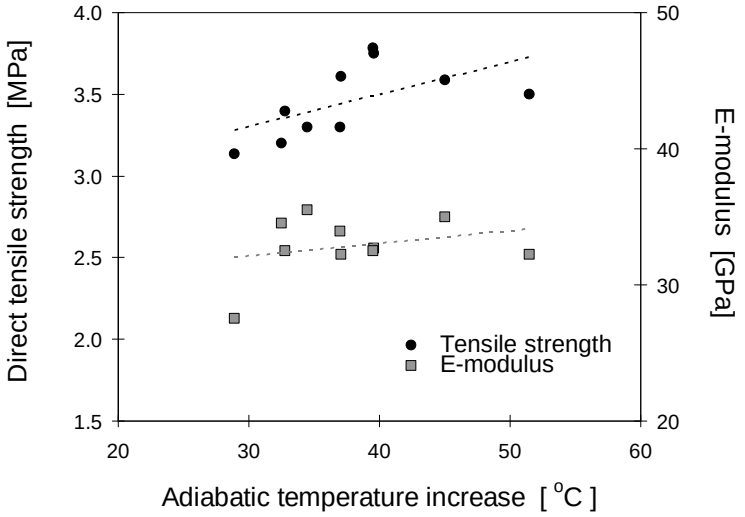

Fig. 1

Relation between adiabatic temperature rise and direct tensile strength and E-modulus. Concretes with varying FA- and BFS content.

3D-calculations (20 °C initial concrete temperature, 20 °C air temperature) were carried out for some of the concretes, among others for the reference (no FA/BFS) and the one with 60% FA. Fig.2 and 3 shows geometry/element net for the simulations. The results showed that the given FA-concrete had a crack index (ratio concrete stress to tensile strength) of 0.6-0.75 in the two structures, which is rather good considering the geometry (1 m thick walls) and the rather high degree of restraint (around 70%) from the bottom slabs. Calculated crack index for the reference concrete was 20-30% higher (. For the 60% FA concrete one case with 10 °C initial concrete temperature and 10 °C air temperature was (tested and) simulated. This condition reduced the crack index with 15-30% compared to the 20 °C case.

In the present test series with varying FA-content it is notable that that a *k*-factor of 1.0 was used when calculating the mass ratio (m = water / (cement + 2.0 x silica fume + *k* x FA), while the European standard EN-206-1 states that a *k*-factor of 0.4 shall be used. The consequence for practical use is that the w/b-ratio must be lowered significantly (w/b=0.36 for 60% FA) compared to a reference without FA (having w/b=0.47) to be within the same mass ratio class (here m=0.45). Low w/b generally leads to higher crack sensitivity, hence the advantageous behaviour of adding FA (mainly reducing heat with *k*=1.0) seen in the present test series will probably be smaller (if present at all) with the use of *k*=0.4. This issue should be explored

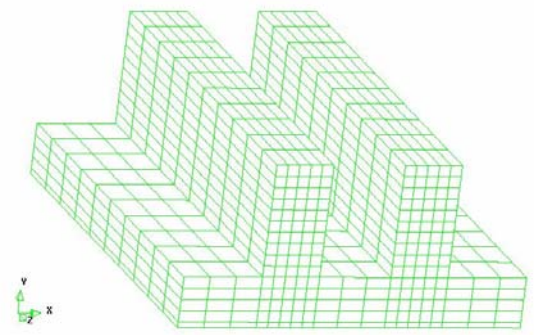

Fig. 2
Element net for a 3D-calculation of the double wall field tests (18)

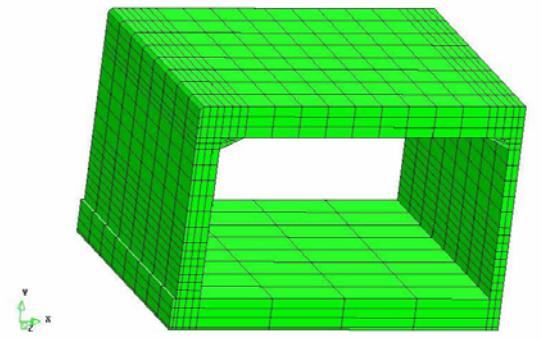

Fig. 3
Element net for a 3D calculation of a tunnel part (19)

further in the future. Moreover, in the on-going submerged tunnel project in Norway (to be placed outside the opera in Oslo) the descriptions set by the Norwegian Road Administration gives a *k*-factor of 0.7. This probably improves the chance of "getting out" potential beneficial effects of FA in terms of low crack sensitivity since the necessary w/b-ratio to satisfy the mass ratio class then becomes higher (w/b=0.41 for 60% FA).

2.3 Effect of cement type

Concretes with three different cement types and three different contents of FA in combination with one of the cement types were tested. The results are presently being analysed and the results will be reported in (4).

3. FUNDAMENTAL STUDIES

3.1 Coefficient of thermal expansion (CTE)

It is generally agreed that the CTE of hardened cement paste and concrete is strongly moisture dependent. This has been found also for the hardening phase (9, 17), hence the topic is very relevant for early restraint stress development since thermal dilation is the primary driving force in most cases. The issue has been dealt with in the project (21-23). Thermally induced deformations has been discussed in three categories:

A) Pure thermal dilation (immediate response)
B) Thermally induced relative humidity change (immediate response)
C) Thermally induced shrinkage or swelling (delayed/slow response)

Mechanism (A) is simply that cement paste (binder) and aggregate each has a CTE value which gives a certain CTE when interacting in concrete. Water saturated cement paste is generally found to have a CTE around 10-13 x $10^{-6}/^{o}$C.

Mechanism (B) has been known in principle, but was quantified recently (23), and it is a plausible explanation of the CTE moisture dependence. It is found that RH in partly saturated cement paste pore systems increases during a temperature increase (and vice versa) and that the change in RH pr. ^{o}C change in temperature (the %RH/^{o}C-factor) may be about 0.2%/^{o}C. The effect is not present for saturated systems. Furthermore, when studying shrinkage vs. RH curves it can be found that a shrinkage (or swelling) of around 10 x $10^{-6}/^{o}$C can be expected for a change in RH og 0.2%. Hence for a partly saturated cement paste the 10 x $10^{-6}/^{o}$C caused by the RH-effect will add to the pure CTE of 10 x $10^{-6}/^{o}$C. The result is that the CTE of cement paste may vary from around 10 x $10^{-6}/^{o}$C (saturated state) to around 20 x $10^{-6}/^{o}$C (semi-dry state). The moisture effect for concrete is less, but still significant. The consequence for hardening cement paste and concrete is an increased CTE over time for systems that self-desiccates (low w/b-ratios). Such behaviour has been shown several times in tests.

Mechanism (C) is considered to be slower than (A) and (B), since it involves transport of water. (C) is considered mainly responsible for the so-called "delayed deformations" and thereby for the fact that it is difficult to separate thermal- and autogenous deformations in the hardening phase, see (21-23) for more details.

3.2 Creep tests in tension and compression on FA- and BFS-concretes

Creep tests on FA- and BFS-concretes were performed as a part of an on-going Ph.D.-project (7). The present evaluation indicates that FA or BFS both influences the relation between compressive and tensile creep as well as the creep magnitude. The results show increased creep in the concretes containing FA or BFS. This then contributes to higher stress relaxation which is beneficial for reducing cracking risk, in addition to the more well-known and expected effect - the reduction in hydration heat. The Ph.D.-work will be concluded in 2006.

4. MATERIALS DATA BASE

The concretes presently incorporated in the materials database is given in *Table 1*. The table shows only part of the concretes that have been tested; other concrete results are not yet prepared for the format of the database. The data is generated during the present (1-7) and in previous projects (8-12). The following properties are determined experimentally: Activation energy, heat development, coefficient of thermal expansion, autogenous deformation, mechanical properties, creep and stress development in a Temperature-Stress testing machine.

The idea of the data base is that the user of a temperature/stress calculation program can get relevant input data according to a given w/b-ratio, strength, cement type etc. The data is then available on a printed page or from an Excel sheet by clicking on the link given in the right column in *Table 1*. An example of such page for the concrete denoted "Basic-5" is given in Fig.4. For the sake of user friendliness all data is on a single page. For some properties different sets of parameters for different models are given, as well as discrete data (to be used directly in programs/systems). For autogenous deformation (the two boxes at the right in Fig.4) the data for different maximum temperatures are given as well as for different initial temperatures of the concrete (if tested). The simple exponential functions in the material data base used to express autogenous *shrinkage* does not take into account the autogenous *expansion* that may occur in concrete during the cooling phase (after being through high curing temperatures) (9, 16, 17). However the model expresses the overall behaviour/magnitude of autogenous deformation. All data are given as functions of maturity (equivalent) time. Default values are put in for properties that are not covered by tests - this is then noted in the data sheet. Adequate references are also given (bottom in Fig.4). A separate data sheet only containing default (average) parameters will also be made for given concrete qualities.

Examples of models and parameters used are the Arrhenius constants (A and B) expressing the activation energy. For heat development parameters in the Freiesleben-Hansen equation (13) used in the program *4C-Temp&Stress* and the equation used in the Swedish program *ConTestPro* (14) are given. The coefficient of thermal expansion (CTE) is given as one (average) constant value even though the CTE will increase with time as the concrete self-desiccates (9, 16, 17), as already discussed. However, one constant CTE-value is very convenient for implementation in calculation programs[1]. A modified CEB-FIP 1990 Model Code (MC) equation is used to express the development of the mechanical properties, while the double power law expresses the creep behaviour (names of the default creep files in *4C-*

[1] Thermal dilation and autogenous deformation are measured simultaneously in tests performed with variable temperature, hence autogenous deformation is found by subtracting the thermal dilation from the total measured strain. The procedure then means that the possible inaccuracy in using a constant CTE is compensated by the autogenous deformation given in the data sheet (the sum of the two strain types gives the measured strain for the particular temperature history used in the test).

Temp&Stress are also given). Autogenous deformation is also expressed by the MC equation, as well as the equation used in *ConTestPro*.

5. FINAL COMMENTS / FUTURE WORK

The effects of compositional parameters such as FA and BFS have been investigated. Such low-heat concretes have not been used extensively in Norway up till now, but the development trend goes in this direction. This is likely to be positive from a hardening concrete cracking perspective (and for durability aspects more generally). The project has generated new knowledge, but much research is needed in the future as the low-heat concrete technology develops. This holds also for the development of blended cement types (CEM II and CEM III).

A guideline report compiling results and experience from the present and previous projects has started. The report will also include the presented materials data base for "Norwegian" concretes. The progress rate of the report is dependent on further financial support.

Fundamental research: The interaction/separation between thermal dilation and autogenous deformation during selected variable temperature histories has been investigated for some concretes. CTE has also been studied (theoretically/literature) for hardened cement past and concrete in order to understand the fundamental mechanisms behind its moisture dependence. However, many important questions remain unresolved, and further research could hopefully increase the knowledge also for hardening systems, for instance the effect of concrete/binder type, moisture level and time-development at different temperature regimes. Furthermore, autogenous deformation is rather unsystematically affected by the temperature history; both the rate and total magnitude may vary greatly for a given concrete. For stress simulations of structures, autogenous deformation input data should be determined experimentally at semi-adiabatic temperature(s) as close as possible to what is expected to occur in the field. The presented materials data base expresses autogenous deformation with a simple exponential function which is fitted to test results directly or interpolated between test results from different temperature histories. Note particularly that isothermal tests are not useful as basis for predicting autogenous deformation under variable temperatures.

Table 1 - Overview of concretes in the materials database

Concrete nickname	W/B-ratio	28-days strength (MPa)	Cement type	Pozzolanic addition [a)]	Air-entrainment	Aggregate	Link to data in Page / File
Basic-0 (REF)	0.40	72	CEM I-52.5 LA Norcem Anlegg	no	no	Årdal 0-16 mm	Page x / File
Basic-5	0.40	81	CEM I-52.5 LA Norcem Anlegg	4.8% s	no	Årdal 0-16 mm	Page x / File
Basic-10	0.40	85	CEM I-52.5 LA Norcem Anlegg	9.1% s	no	Årdal 0-16 mm	Page x / File
Basic-15	0.40	78	CEM I-52.5 LA Norcem Anlegg	13% s	no	Årdal 0-16 mm	Page x / File
REF-FA	0.40	67	CEM II/A-V-42.5 R Norcem Standard FA	no	no	Årdal 0-16 mm	Page x / File
REF-STD	0.40	63	CEM I-42.5 R Norcem Standard	no	no	Årdal 0-16 mm	Page x / File
Maridalen	0.42	72	CEM I-52.5 LA Norcem Anleggt	4.9% s	yes	Svelvik 0-24 mm	Page x / File
Södra Länken	0.42	60	CEM I-42.5 BV/SR/LA Degerh. Anläggningscem.	4.8% s	yes	Betongindustri 0-27 mm	Page x / File
Varehus SKI	0.50	66	Norcem STD + Norcem Anlegg	3.0% s	no	Vinterbro 0 - 22 mm	Page x / File
SVV 40% FA	0.465	47	CEM I-52.5 LA Norcem Anlegg	3.4% s, 28% FA	yes	Årdal 0-16 mm	Page x / File
SVV 60% FA	0.464	41	CEM I-52.5 LA Norcem Anlegg	3.0% s, 36% FA	yes	Årdal 0-16 mm	Page x / File

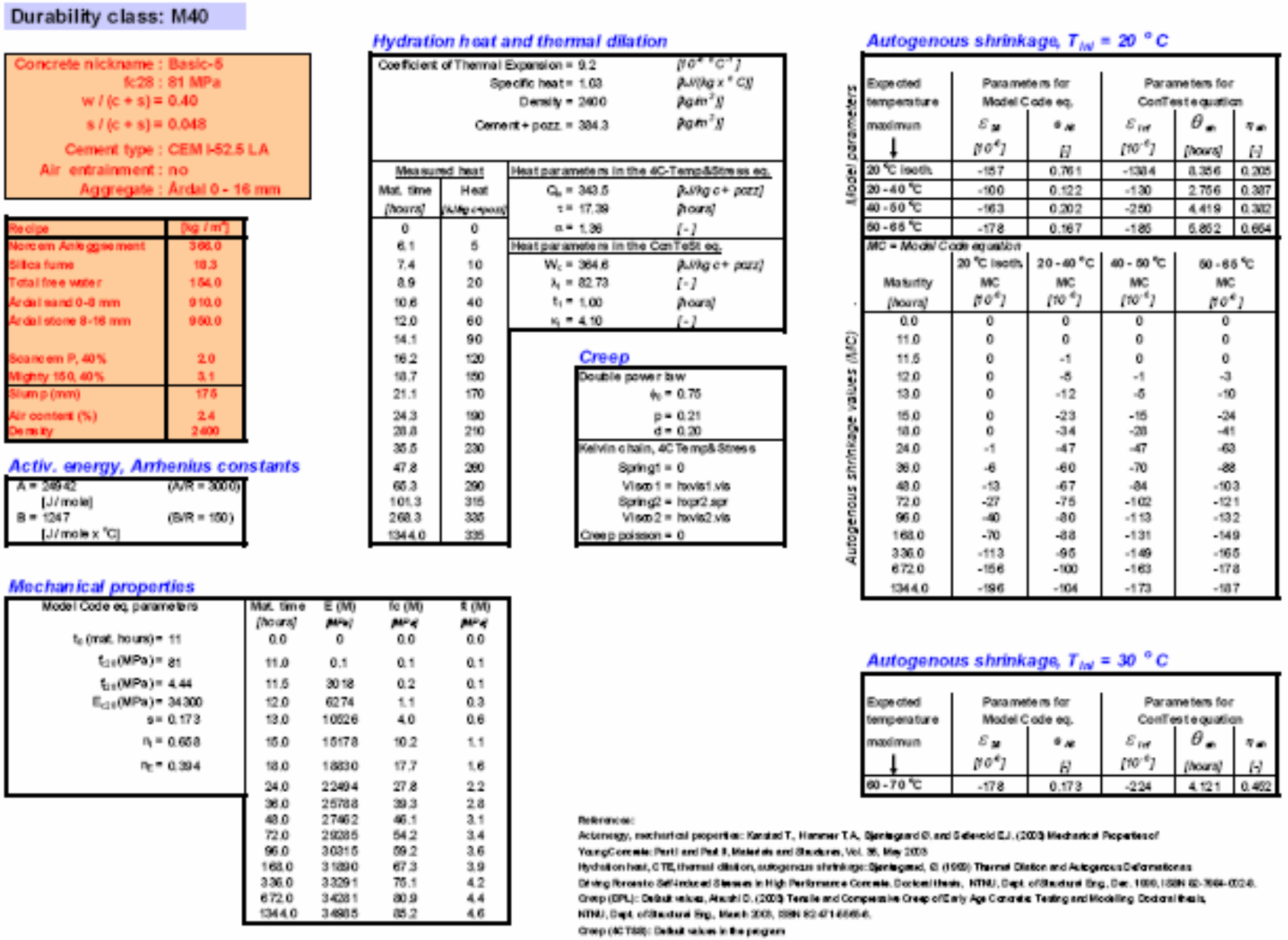

Durability class: M40

Concrete nickname : Basic-5
fc28 : 81 MPa
w / (c + s) = 0.40
s / (c + s) = 0.048
Cement type : CEM I-52.5 LA
Air entrainment : no
Aggregate : Årdal 0 - 16 mm

Recipe	[kg / m³]
Norcem Anleggcement	366.0
Silica fume	18.3
Total free water	154.0
Årdal sand 0-8 mm	910.0
Årdal stone 8-16 mm	950.0
Scancem P, 40%	2.0
Mighty 150, 40%	3.1
Slump (mm)	175
Air content (%)	2.4
Density	2400

Activ. energy, Arrhenius constants

A = 28942 [J / mole]	(A/R = 3500)
B = 1247 [J / mole x °C]	(B/R = 150)

Hydration heat and thermal dilation

Coefficient of Thermal Expansion =	9.2	[10⁻⁶ °C⁻¹]
Specific heat =	1.03	[kJ/(kg x °C)]
Density =	2400	[kg/m³)]
Cement + pozz. =	384.3	[kg/m³)]

Measured heat	
Mat. time [hours]	Heat [kJ/kg cement]
0	0
6.1	5
7.4	10
8.9	20
10.6	40
12.0	60
14.1	90
16.2	120
18.7	150
21.1	170
24.3	190
28.8	210
35.5	230
47.8	260
65.3	290
101.3	315
268.3	335
1344.0	335

Heat parameters in the 4C-Temp&Stress eq.		
Q_u =	343.5	[kJ/kg c+ pozz]
τ =	17.39	[hours]
α =	1.36	[-]
Heat parameters in the ConTeSt eq.		
W_c =	364.6	[kJ/kg c+ pozz]
λ_1 =	82.73	[-]
t_1 =	1.00	[hours]
η_1 =	4.10	[-]

Creep

Double power law	
ϕ_0 =	0.75
p =	0.21
d =	0.20
Kelvin chain, 4C Temp& Stress	
Spring1 =	0
Visco1 =	hsvis1.vis
Spring2 =	hspr2.spr
Visco2 =	hsvis2.vis
Creep poisson =	0

Autogenous shrinkage, T_{hd} = 20 °C

Model parameters

Expected temperature maximum ↓	Parameters for Model Code eq. ε_{sh} [10⁻⁶]	θ_{sh} [-]	Parameters for ConTest equation ε_{inf} [10⁻⁶]	θ_{sh} [hours]	η_{sh} [-]
20 °C isoth.	-157	0.761	-1384	8.356	0.205
20 - 40 °C	-100	0.122	-130	2.756	0.387
40 - 60 °C	-163	0.202	-250	4.419	0.302
60 - 65 °C	-178	0.167	-185	5.852	0.664

Autogenous shrinkage values (MC)

MC = Model Code equation

Maturity [hours]	20 °C isoth. MC [10⁻⁶]	20 - 40 °C MC [10⁻⁶]	40 - 60 °C MC [10⁻⁶]	60 - 65 °C MC [10⁻⁶]
0.0	0	0	0	0
11.0	0	0	0	0
11.5	0	-1	0	0
12.0	0	-5	-1	-3
13.0	0	-12	-5	-10
15.0	0	-23	-15	-24
18.0	0	-34	-28	-41
24.0	-1	-47	-47	-63
36.0	-6	-60	-70	-88
48.0	-13	-67	-84	-103
72.0	-27	-75	-102	-121
96.0	-40	-80	-113	-132
168.0	-70	-88	-131	-149
336.0	-113	-95	-149	-165
672.0	-156	-100	-163	-178
1344.0	-196	-104	-173	-187

Autogenous shrinkage, T_{hd} = 30 °C

Expected temperature maximum ↓	Parameters for Model Code eq. ε_{sh} [10⁻⁶]	θ_{sh} [-]	Parameters for ConTest equation ε_{inf} [10⁻⁶]	θ_{sh} [hours]	η_{sh} [-]
60 - 70 °C	-178	0.173	-224	4.121	0.462

Mechanical properties

Model Code eq. parameters
t_0 (mat. hours) = 11
f_{c0} (MPa) = 81
f_{ct0} (MPa) = 4.44
E_{c0} (MPa) = 34300
s = 0.173
η_1 = 0.658
η_E = 0.394

Mat. time [hours]	E (M) [MPa]	fc (M) [MPa]	ft (M) [MPa]
0.0	0	0.0	0.0
11.0	0.1	0.1	0.1
11.5	3018	0.2	0.1
12.0	6274	1.1	0.3
13.0	10526	4.0	0.6
15.0	15178	10.2	1.1
18.0	18830	17.7	1.6
24.0	22494	27.8	2.2
36.0	25788	39.3	2.8
48.0	27962	46.1	3.1
72.0	29285	54.2	3.4
96.0	30315	59.2	3.6
168.0	31890	67.3	3.9
336.0	33291	75.1	4.2
672.0	34281	80.9	4.4
1344.0	34985	85.2	4.6

References:
Actenergy, mechanical properties: Kanstad T., Hammer T.A., Bjøntegaard Ø. and Sellevold E.J. (2003) Mechanical Properties of Young Concrete: Part I and Part II, Materials and Structures, Vol. 36, May 2003
Hydration heat, CTE, thermal dilation, autogenous shrinkage: Bjøntegaard, Ø. (1999) Thermal Dilation and Autogenous Deformations as Driving Forces to Self-Induced Stresses in High Performance Concrete, Doctoral thesis, NTNU, Dept. of Structural Eng., Dec. 1999, ISBN 82-7984-0024.
Creep (DPL): Default values, Akutsi O. (2003) Tensile and Compressive Creep of Early Age Concrete: Testing and Modelling, Doctoral thesis, NTNU, Dept. of Structural Eng., March 2005, ISBN 82-471-6645-6.
Creep (4C TSS): Default values in the program

Fig. 4 Materials data base for the concrete denoted "Basic-5"

REFERENCES

1 Kanstad T., Bjøntegaard Ø., Sellevold E.J., Hammer T.A. and Fidjestøl P., "Effects of Silica Fume on Crack Sensitivity", *Concrete International*, 2001, vol. 23, No. 12, pp. 53-59

2 Bjøntegaard Ø. and Sellevold E.J. (2004) Effects of Silica Fume and Temperature on Autogenous Deformation of High Performance Concrete. ACI Special Publication SP 220 Autogenous Deformation in Concrete, Ed. Jensen O.M., Bentz D.P. and Lura P., ISBN 0-87031-143-3, pp. 125-134

3 Bjøntegaard Ø. and Sellevold E.J. (2004) Young high performance concrete with w/b=0.40 and varying silica fume content: Experimental test results and 1-dimensional restraint stress calculations. Evaluation of new results on hot climate conditions and previous results. NOR-CRACK report #3.1, Subtask 3 Parameter studies, STF22 A04616, ISBN 82-14-02588-5

4 Bjøntegaard Ø. and Kjellsen K.O. (2006) Experimental tests and 1D stress calculations on young high performance concrete with w/b=0.40. Effect of cement type and fly-ash. NOR-CRACK report #3.2, Subtask 3 Parameter studies, to be published in 2006

5 Bjøntegaard Ø. and Sellevold E.J. (2003) Bjørvika submerged tunnel - Determination of concrete properties relevant for cracking tendency in the hardening phase (in Norwegian). NTNU-report R-9-03, Dept. of Structural Engineering, pp.37

6 Bjøntegaard Ø. (2004). Bjørvika submerged tunnel, phase 2: Determination of concrete properties relevant for cracking tendency in the hardening phase. Experimental results for mixture A, B, C and D (in Norwegian). NTNU-report R-5-04, Dept. of Structural Engineering, pp.26

7 Guomin J., Bjøntegaard Ø. Atrushi D., Sellevold E.J. and Kanstad T. (2005) Compressive and tensile creep of early age concrete with mineral additives. Concreep7: Int. conf. on creep, shrinkage and durability of concrete and concrete structures, Nantes, France, pp. 369-374

8 Atrushi D. and Kanstad T. (2005) Comparison between creep in tension and compression at early age high performance concrete. Concreep7: Int. conf. on creep, shrinkage and durability of concrete and concrete structures, Nantes, France, pp. 435-440

9 Bjøntegaard, Ø. (1999) Thermal dilation and autogenous deformation as driving forces to self-induced stresses in high performance concrete. Doctoral thesis, NTNU Dept. of Structural Engineering, Dec. 1999, ISBN 82-7984-002-8.

10 Kanstad T., Hammer T.A, Bjøntegaard Ø. and Sellevold E.J. (1999) Mechanical properties of young concrete: Evaluation of test methods for tensile strength and modulus of elasticity. Determination of model parameters. SINTEF report no. STF22 A99762, Trondheim, Norway

11 Kanstad T., Hammer T.A., Bjøntegaard Ø. and Sellevold E.J. (2003) Mechanical Properties of Young Concrete: Part I - Experimental Results related to Test Methods and Temperature Effects, Materials and Structures, Vol. 36, May 2003, pp 218-225

12 Kanstad T., Hammer T.A., Bjøntegaard Ø. and Sellevold E.J. (2003) Mechanical Properties of Young Concrete: Part II - Determination of Model Parameters and Test Programme Proposals, Materials and Structures, Vol. 36, May 2003, pp 226-230

13 Pham K. (2002) Determination of stress generation and risk of cracking of concrete structures during the hardening phase. Master thesis, NTNU Dept. of Structural Engineering.

14 Freisleben Hansen, P. (1978) Hærdeteknologi-2, Dekrementmetoden. BKF-centralen (in Danish).

15 Jonasson J-E. (2000) Slipform Construction – Calculations for Assessing Protection Against Early Freezing. Swedish Cement and Concrete Institute, CBI Forskning/Research Fo 4.84, Stockholm, pp 70.

16 Bjøntegaard Ø. and Sellevold E.J. (2001) Interaction between Thermal Dilation and Autogenous Deformation in High Performance Concrete, Materials and Structures, Vol.34, June 2001, pp 266-272

17 Sellevold E.J. and Bjøntegaard Ø. (2005) Coefficient of Thermal Expansion of Cement Paste and Concrete: Mechanisms of Moisture Interaction. Concrete Science and Engineering, in press

18 Larsen C.L. (2004) Bjørvika submerged tunnel, Large scale field test with fly-ash concrete and SV-40 - Control station E6 (in Norwegian), Norwegian Public Roads - Road Directorate, assignment A-35 A, report nr. 10

19 Guomin J., Kanstad T. and Bjøntegaard Ø. (2004) Analysis of the SVV double wall field test related to the Bjørvika tunnel project. NTNU-rapport R-7-04, Institutt for Konstruksjonsteknikk.

20 Kanstad T. and Guomin J. (2004) Bjørvika submerged concrete tunnel, Phase 2: Evaluation of the risk of cracking in the hardening phase. NTNU-rapport R-6-04, Institutt for Konstruksjonsteknikk.

21 Sellevold E.J. and Bjøntegaard Ø. (2004) Coefficient of Thermal Expansion (CTE) of Hardening Concrete. Nordic Concrete Research, 1/2004, ISBN 82-91341-82-6, pp. 41-49

22 Sellevold E.J. and Bjøntegaard Ø. (2006) Coefficient of Thermal Expansion of Cement Paste and Concrete: Mechanisms of Moisture Interaction. Materials and Structures, in press

23 Radjy F., Sellevold E.J. and Hansen K.K., ‘Isosteric Vapor Pressure - Temperature Data for Water Sorption in Hardened Cement Paste: Enthalpy, Entropy and Sorption Isotherms at Different Temperatures’, Report BYG-DTU R-057, Techn. Univ. of Denmark, Lyngby, 2003. Available at http://www.byg.dtu.dk/publicering/rapporter/R-057.pdf

APPENDIX 5 Complete list of IPACS-reports

General reference to be included with report title and ISBN...
Published by Department of Civil & Mining Engineering, Division of Structural Engineering, Luleå University of Technology, 2001."

ISBN-number	Author(s)	Title	Subtask/Activity	
1-89580-80-X	Mats Emborg	Final Technical Report	T1	TASK 1
1-89580-10-9	Hans Hedlund and Jan-Erik Jonasson	Temperature effect on autogenous deformation. Measurements and modelling of thermal and moisture related deformation and stresses.	T2.4	TASK 2
1-89580-11-7	Alexander-W. Gutsch and Ferdinand S. Rostásy	Test Results and Modelling of Autogenous Deformations of Concrete at Early Age	T2.4	
1-89580-12-5	Matias Krauß, Karim Hariri and Ferdinand S. Rostásy	Non-Destructive Assessment of Mechanical Properties of Concrete at Very Early Age by US Techniques – Method, Results and Modelling	T2.1/T2.2	
1-89580-13-3	Matias Krauß, Ferdinand S. Rostásy and Alexander- W. Gutsch	Modelling of Degree of Hydration on Basis of Adiabatic Heat Release.	T2.1/T2.3	
1-89580-14-1	K. van Breugel, P. Lura	Deformational Behaviour and Self-induced Stresses in Hardening Concrete. Experimental studies on thermal and autogenous deformations, creep and relaxation of hardening concrete.	T2.4/T3.2	
1-89580-15-X	P. Lura and K. van Breugel	THERMAL PROPERTIES OF CONCRETE: SENSITIVITY STUDIES	T2.5	
1-89580-16-8	Gorden Allas and Klaas van Breugel	Numerical Simulation Model for Hydration and Microstructural Development of Cement-Based Materials. Prediction of adiabatic and isothermal hydration curves.	T2.1	
1-89580-17-6	K. van Breugel	Hydration of Cement-Based Systems. Aspects of hydration of cement-based systems and possibilities to quantify the evolution of hydration processes.	T2.1	
1-89580-18-4	Paolo Morabito	THERMAL PROPERTIES OF CONCRETE. Variations with the temperature and during the hydration phase.	T2.3	
1-89580-19-2	Paolo Morabito	APPARENT ACTIVATION ENERGY. An example of determination from adiabatic hydration tests.	T2.2	
1-89580-20-6	Øyvind Bjøntegaard and Erik J. Sellevold	Autogenous and Thermal Deformations	T2.4	
1-89580-21-4	Øyvind Bjøntegaard, Erik J. Sellevold, Terje Kanstad and Tor Arne Hammer	Measuring, modelling and 3D stress calculations of concrete in the early age - Compilation of four papers	T2.4	
1-89580-22-2	*Per Fidjestöl, Anne-Marit Tonnesland*	***Early age material behaviour***	T2.1	
1-89580-23-0	Knut Kjellsen	DEVELOPMENT OF AUTOGENEOUS DEFORMATION AND RH OF CEMENT PASTE WITH AND WITHOUT CSF	T2.1	
1-89580-24-9	Steinar Helland	NORWEGIAN STANDARDS ON ACTIVATION ENERGY AND HEAT RELEASE	T2.2	

1-89580-25-7	K. van Breugel	Heat of Hydration and Apparent Activation Energy of cement Past.	T2.2		
1-89580-26-5	*TU-Delft*	***Modelling thermal Properties of Concrete***	T2.3		
1-89580-27-3	Tu-Trondheim	Early age Deformations in Concrete as driving Forces to Cracking - How to measure and Model for use in Stress Calculations	T2.4		
1-89580-28-1	*Selmer*	Report from the RR-tests performed during Summer 1999	T2.5		
1-89580-35-4	Ferdinand S. Rostásy, Matias Krauß and Alexander-W. Gutsch	Computation of Stresses and Cracking Criteria for Early Age Concrete – Methods of iBMB –	T3/T4/T6		**TASK 3**
1-89580-36-2	Karim Hariri	FRACTURE MECHANICS BEHAVIOUR OF CONCRETE AT EARLY AGE	T3.1 & T6.3		
1-89580-37-0	Dr.ing K. van Breugel	Stress predictions in hardening concrete. The role of microstructural development	T3.4		
1-89580-38-9	Alexander-W. Gutsch	Viscoelastic behaviour of Early Age Concrete	T3.2		
1-89580-39-7	Alexander-W. Gutsch and Ferdinand S. Rostásy	Mechanical Models of the Stress-Strain Behaviour of Young Concrete in Axial Tension and Compression	T3.3		
1-89580-40-0	K. van Breugel	MODELLING OF STRENGTH DEVELOPMENT IN HARDENING CONCRETE. MICROSTRUCTURAL FEATURES AND ENGINEERING MODELS	T3.1		
1-89580-41-9	A. Cark, K. van Breugel	Estimation of Mechanical Properties of Concrete Using the Hydration Concept	T3.1		
1-89580-42-7	Morabito et al	Round Robin Testing Programme - Equipment, test methods, test results.	T3.4		
1-89580-43-5	D. Atrushi, O. Bjontegaard, T. Kanstad, E.J. Sellevold	Creep deformation in hardening concrete: Test method investigations and the effect of temperature	T3.2		
1-89580-44-3	G. Westman, S. Utsi, J-E. Jonasson	Evaluation of Creep Tests	T3.2		
1-89580-45-1	J-E. Jonasson, G. Westman	Conversion of creep data to relaxation data by the program RELAX	T3.2		
1-89580-46-X	*M. Emborg*	***Influence of concrete constituents - literature review***	T3.4		
1-89580-47-8	*J-E. Jonasson et al*	***LTU engineering creep model***	T3.2		
1-89580-48-6	E. Sellevold et al	Influence of Silica Fume on Cracking Risks	T3.4		

1-89580-49-4	T. Kanstad et al	Mechanical Properties, NORIPACS report	T3.1	
1-89580-50-8	*Westman, Emborg Hedlund, Bosnjak, Jonassonl*	***Influence of elasticity and creep on cracking risks***	T3.2	
1-89580-53-2	Ola Kjellman and Jan Olofsson	3D Structural Analysis of Crack Risk in Hardening Concrete Verification of an Engineering Method.	T4.2.	**TASK 4**
1-89580-54-0	Jan Olofsson and Mathias Uhlán	Round Robin Simulation - Ground Slab Examples	T4.2	
1-89580-55-9	Mathias Uhlán, Jan Olofsson and Hans Hedlund	Uddevalla Bridge Casting of Bottom Slab S5 - Evaluation of Temperature Development	T4.2	
1-89580-56-7	Mårten Larson	IMPROVED HAND CALCULATION METHOD.	T4.2	
1-89580-57-5	Mårten Larson	RESTRAINT FROM ADJOINING STRUCTURES. - Empirical, Analytical and Numerical Evaluation of Restraint Coefficients	T4.1	
1-89580-58-3	Mårten Larson	COMPARISON OF PROGRAMS AIMED FOR COMPUTATION OF THERMAL STRESSES IN CONCRETE STRUCTURES	T4. 2	
1-89580-59-1	F.S. Rostásy, A. -W. Gutsch and M. Krauß	ENGINEERING MODELS FOR THE ASSESSMENT OF RESTRAINT OF SLABS BY SOIL AND PILES DURING EARLY AGE OF CONCRETE	T4.1	
1-89580-60-5	Paolo Dalmagioni	Sluice gate in-situ experiment: Numerical evaluation of measurements	T4. 2	
1-89580-61-3	Terje Kanstad and Daniela Bosnjak	Neural Network Calculations of Culvert Walls by Diana, Verification, Theoretical and Practical Background	T4.2	
1-89580-62-1	P. Lura and K. van Breugel	STRESS PREDICTIONS IN THICK HARDENING CONCRETE SLAB	T4.2	
1-89580-63-X	P. Lura and K. van Breugel	NUMERICAL EVALUATION OF CRACKING RISK IN MASSIVE CELLAR WALLS CAST ON SLAB	T4.2	
1-89580-64-8	Jan Olofsson, Mathias Uhlán and Hans Hedlund	2D and 3D Restraint Analyses, Typical Structure – Wall-on-Slab	T4.1	
1-89580-65-6	Jan-Erik Jonasson and Hans Hedlund	Framework for Restraint Factors, Typical Cases 1 – 5 in IPACS Expert System	T4.1	
1-89580-66-4	Jan Olofsson, Mathias Uhlán and Hans Hedlund	Slab cast on rock ground. Model for restraint estimation	T4.1	
1-89580-67-2	Hans Hedlund and Jan	Restraint Analyses and Simplifications, Typical Structure –	T4.1	

	Olofsson	Wall-on-Wall			
1-89580-68-0	Martin Nilsson	Test of Wall Cast on Slab	T4.2		
1-89580-69-9	Martin Nilsson	Rotational Boundary Restraint Factor	T4.1		
1-89580-31-1	K. van Breugel and E.A.B Koenders	Solar Radiation.	T4.2		
1-89580-32-X	Kanstad T, Bosnjak D, Øverli A.	3D Restraint analysed of typical structures with early age cracking problems.	T4.2.		
1-89580-33-8	Kanstad T. and Bosnjak D.	The Maridal culvert field test. Numerical simulations of temperature...	T4.2		
1-89580-34-6	*Kanstad T and Bosnjak D*	***The Maridal culvert field test. Evaluation of field test results towards theoretical investigations.***	T4.2		
1-89580-79-6	Jan Olofsson, Hans Hedlund and Mathias Uhlán	Concrete cast on rock – Restraint evaluation	T4.1		
1-89580-71-0	M. Larsson	Crack Risk Estimations Compared with Field Observations...	T5.1.3		**TASK 5**
1-89580-72-9	G. Petkovic, R. Kompen, J. Hellum	Bond Failure Registrations on Wall-to-Slab Casting Joints	T5.2.4		
1-89580-73-7	E. Heimdal, T. Kanstad, R. Kompen	Maridal Culvert, Norway - Field Test I.	T5.1.1.		
1-89580-74-5	E. Heimdal, T. Kanstad, R. Kompen	Maridal Culvert, Norway - Field Test II.	T5.1.6		
1-89580-75-3	S. Helland, S. Smeplass	Concrete for the Maridal culvert - Round Robin Test	T5.1.6		
1-89580-76-1	P. Morabito	Sluice gate - Brembo river, Italy - Field test	T5.1.4		
1-89580-77-X	S. Smeplass	Evaluation of Crack Risk	T6.1.3		**TASK 6**
1-89580-88-5	Jan-Erik Jonasson and Hans Hedlund	Evaluation of Material Data from IPACS Data Base for Use in Program ConTeSt1	T6.2		
1-89580-89-3	Jan-Erik Jonasson and Hans Hedlund	Instructions and Users Guide for ConTeSt1	T6.3		
	Jan-Erik Jonasson, Martin				

1-89580-90-7	Nilsson, Mårten Larson and Hans Hedlund	Manual Method with Diagrams for Crack Risk Estimation and Restraint Curves	T6.2	
1-89580-91-5	Paolo Dalmagioni, Marco Lazzari, Rita Pellegrini	Final report of the TASK 6	T6.3	
1-89580-92-3	P. Dalmagioni	IPACS thermal solver: Users guide	T6.3	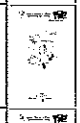
1-89580-93-1	P. Dalmagioni	The VERSIG mono-dimensional solver: theory and users' guide	T6.2	
1-89580-94-X	M. Lazzari	IPACS database. Users manual	T6.3	
1-89580-95-8	Paolo Dalmagioni, Marco Lazzari	Detailed design of an expert system for the management of concrete at early ages	T6.3	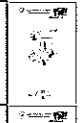
1-89580-96-6	Marco Lazzari, Paolo Dalmagioni	IPACS Expert System - users manual	T6.3	
1-89580-97-4	M. Lazzari	Short users guide to the material database	T6.3	
1-89580-98-2	M. Lazzari	State of the art report on expert systems in civil engineering	T6.3	
1-89580-99-0	Paolo Dalmagioni, Marco Lazzari	Specification and conceptual design of the IPACS Expert System	T6.3	

SINTEF Building and Infrastructure is the third largest building research institute in Europe. Our objective is to promote environmentally friendly, cost-effective products and solutions within the built environment. SINTEF Building and Infrastructure is Norway's leading provider of research-based knowledge to the construction sector. Through our activity in research and development, we have established a unique platform for disseminating knowledge throughout a large part of the construction industry.

COIN – Concrete Innovation Center is a Center for Research based Innovation (CRI) initiated by the Research Council of Norway. The vision of COIN is creation of more attractive concrete buildings and constructions. The primary goal is to fulfill this vision by bringing the development a major leap forward by long-term research in close alliances with the industry regarding advanced materials, efficient construction techniques and new design concepts combined with more environmentally friendly material production.